TOPICAL REVIEW

Polymer gel dosimetry

C Baldock[1,10], Y De Deene[2,10], S Doran[3], G Ibbott[4], A Jirasek[5],
M Lepage[6], K B McAuley[7], M Oldham[8] and L J Schreiner[9]

[1] Institute of Medical Physics, School of Physics, University of Sydney, Australia
[2] Radiotherapy and Nuclear Medicine, Ghent University Hospital, Belgium
[3] CRUK Clinical Magnetic Resonance Research Group, Institute of Cancer Research, Surrey, UK
[4] Radiation Physics, UT M D Anderson Cancer Center, Houston, TX, USA
[5] Department of Physics and Astronomy, University of Victoria, Victoria, BC, Canada
[6] Centre d'imagerie moléculaire de Sherbrooke, Département de médecine nucléaire et de radiobiologie, Université de Sherbrooke, Sherbrooke, QC, Canada
[7] Department of Chemical Engineering, Queen's University, Kingston, ON, Canada
[8] Department of Radiation Oncology, Duke University Medical Center, Durham, NC, USA
[9] Cancer Centre of South Eastern Ontario, Kingston, ON, Canada

E-mail: c.baldock@physics.usyd.edu.au and yves.dedeene@ugent.be

Abstract

Polymer gel dosimeters are fabricated from radiation sensitive chemicals which, upon irradiation, polymerize as a function of the absorbed radiation dose. These gel dosimeters, with the capacity to uniquely record the radiation dose distribution in three-dimensions (3D), have specific advantages when compared to one-dimensional dosimeters, such as ion chambers, and two-dimensional dosimeters, such as film. These advantages are particularly significant in dosimetry situations where steep dose gradients exist such as in intensity-modulated radiation therapy (IMRT) and stereotactic radiosurgery. Polymer gel dosimeters also have specific advantages for brachytherapy dosimetry. Potential dosimetry applications include those for low-energy x-rays, high-linear energy transfer (LET) and proton therapy, radionuclide and boron capture neutron therapy dosimetries. These 3D dosimeters are radiologically soft-tissue equivalent with properties that may be modified depending on the application. The 3D radiation dose distribution in polymer gel dosimeters may be imaged using magnetic resonance imaging (MRI), optical-computerized tomography (optical-CT), x-ray CT or ultrasound. The fundamental science underpinning polymer gel dosimetry is reviewed along with the various evaluation techniques. Clinical dosimetry applications of polymer gel dosimetry are also presented.

(Some figures in this article are in colour only in the electronic version)

---

[10] The authors of the article are listed in alphabetical order. The principal authors are Y De Deene and C Baldock, who contributed equally to the article.

1. Introduction

Polymer gel dosimeters are fabricated from radiation sensitive chemicals which, upon irradiation, polymerize as a function of the absorbed radiation dose. These dosimeters, which uniquely record the radiation dose distribution in three-dimensions (3D), have specific advantages when compared to one-dimensional dosimeters, such as ion chambers, and two-dimensional dosimeters, such as film. These advantages are particularly significant in dosimetry situations where steep dose gradients exist such as in intensity-modulated radiation therapy (IMRT) and stereotactic radiosurgery. Furthermore, polymer gel dosimeters have also specific advantages in brachytherapy dosimetry. Potential applications also exist in low-energy x-ray, high-linear energy transfer (LET) and proton therapy, radionuclide and boron capture neutron therapy dosimetries. These 3D dosimeters are radiologically soft-tissue equivalent with properties that may be modified depending on the application.

The use of radiation sensitive gels for the purposes of radiation dosimetry was first suggested by Day and Stein in 1950 when radiation was used to produce color changes in gels containing dyes such as methylene blue (Day and Stein 1950). In 1957 Andrews *et al* subsequently investigated depth doses using spectrophotometry and pH probe measurements of irradiated radiation sensitive gels containing chloral hydrate diffused throughout an agar gel (Andrews *et al* 1957). The use of radiation sensitive gels for the purposes of radiation dosimetry, as currently used, is as a result of the work undertaken by Gore *et al* in 1984 who showed the ferrous sulfate chemical dosimeter, initially developed by Fricke and Morse (1927), could be probed by nuclear magnetic relaxometry and hence by magnetic resonance imaging (MRI) (Gore *et al* 1984). It was subsequently shown that irradiated Fricke-type gel dosimeters did not retain a spatially stable dose distribution due to ion diffusion within the irradiated dosimeters (Olsson *et al* 1992). Fricke solutions with various gelling agents such as gelatin, agarose, sephadex and polyvinyl alcohol (PVA) were investigated. Chelating agents to reduce diffusion in Fricke gels, such as xylenol orange (XO), had only limited success (Baldock *et al* 2001a) and diffusion continued to be a significant problem in the advancement of gel dosimetry.

Polymer systems for the use of radiation dosimetry were first proposed as early as 1954, where Alexander *et al* (1954) discussed the effects of ionizing radiation on polymethylmethacrylate. Subsequently Hoecker *et al* investigated the dosimetry of radiation-induced polymerization in liquids (Hoecker and Watkins 1958), and Boni used polyacrylamide as a gamma dosimeter (Boni 1961).

In 1992, Kennan *et al* reported NMR longitudinal relaxation studies performed on an irradiated aqueous solution of N,N'-methylene-bis-acrylamide (Bis) and agarose, which showed that the relaxation rates increased with absorbed dose (Kennan *et al* 1992).

In 1992a new gel dosimetry formulation was proposed based on the polymerization of acrylamide (AAm) and Bis monomers infused in an aqueous agarose matrix (Maryanski *et al* 1992). This system was given the acronym BANANA due to the use of the chemical components (Bis, AAm, nitrous oxide and agarose). The BANANA polymer gel dosimeter did not have the diffusion problem associated with Fricke gels and was shown to have a relatively stable post-irradiation dose distribution. The polymerization consisted of the addition of monomers and of crosslinking of neighboring polymer chains induced by the free radicals resulting from water radiolysis. In 1994 Maryanski *et al* refined the formulation by replacing agarose with gelatin and gave the acronym BANG (consisting of Bis, AAm, nitrogen and aqueous gelatin), to the first in a series of new polymer gel formulations (Maryanski *et al* 1994b). This formulation was subsequently patented (Maryanski *et al* 1994a) and became commercially available through MGS Research Inc. as BANG®. Subsequently, to distinguish

in-house polymer gel formulations from the commercial product, PAG (Baldock *et al* 1998a) became the polymer gel dosimeter acronym of choice for most authors working in the field of gel dosimetry. Subsequently different compositions and formulations of polymer gel dosimeters were investigated (Pappas *et al* 1999, Lepage *et al* 2001a).

During this early period in the development of polymer gel dosimetry a number of studies were undertaken to investigate the clinical applications of PAG-type polymer gel dosimetry using MRI (Maryanski *et al* 1993, 1994b, Ibbott *et al* 1997, Oldham *et al* 1998, Low *et al* 1999). De Deene *et al* (1998a) undertook an investigation into the overall accuracy of an anthropomorphic polymer gel dosimetry phantom for the verification of conformal radiotherapy treatments. It was established that significant issues relating to the accuracy of this dosimetry technique were a result of oxygen inhibition in the polymer gel and MRI imaging artifacts. Authors continued to investigate clinical aspects of polymer gel dosimetry using MRI including conformal therapy, IMRT and IMAT (Cosgrove *et al* 2000, De Deene *et al* 2000c, Vergote *et al* 2003, Duthoy *et al* 2003, 2004, Love *et al* 2003, Vergote *et al* 2004a, Sandilos *et al* 2004), stereotactic radiosurgery (Ertl *et al* 2000, Grebe *et al* 2001, Pappas *et al* 2001, Audet *et al* 2002, Novotny *et al* 2002, Scheib and Gianolini 2002, Watanabe *et al* 2002, Papagiannis *et al* 2005, Karaiskos *et al* 2005), brachytherapy (Farajollahi *et al* 1999, Wuu *et al* 2003), low-energy x-rays (Boudou *et al* 2004), high-LET and proton therapy (Ramm *et al* 2000, Jirasek and Duzenli 2002, Heufelder *et al* 2003, Gustavsson *et al* 2004), boron capture neutron therapy (Farajollahi *et al* 2000, Gambarini *et al* 2004) and tissue inhomogeneities (Love *et al* 2003, Vergote *et al* 2003).

In 1996 Gore *et al* (1996) and Maryanski *et al* (1996) demonstrated the potential of optical-CT as an alternative imaging technique to MRI for PAG-type polymer gel dosimeters. This technique was further investigated by Oldham *et al* (2001, 2003) and Oldham and Kim (2004). In 2000 Hilts *et al* demonstrated the use of x-ray CT to image PAG-type gels and subsequently used x-ray CT to investigate stereotactic dose distributions. In 2002 Mather *et al* (2002b) demonstrated the use of ultrasound to image polymer gel dosimeters. In 2003 Rintoul *et al* (2003) demonstrated the use of Raman imaging to evaluate an electron depth dose in an irradiated PAG dosimeter.

Although polymer-type dosimeters did not have the diffusion limitations of Fricke-type gel dosimeters, there was another significant limitation to their use. Due to the nature of their free radical chemistry, polymer gel dosimeters were susceptible to atmospheric oxygen inhibiting the polymerization processes. As a result, these gel dosimeters had to be manufactured in an oxygen-free environment, for example in a glove box flushed with inert gas such nitrogen or argon (Baldock *et al* 1998a, De Deene *et al* 1998a).

A significant development in the field of gel dosimetry was reported by Fong *et al* (2001). This development was a new type of polymer gel dosimeter, known as MAGIC, in which atmospheric oxygen was bound in a metallo-organic complex thus removing the problem of oxygen inhibition and enabling polymer gels to be manufactured on the bench-top in the laboratory. These types of polymer gel dosimeters became known as the new class of *normoxic* gel dosimeters. The existing PAG dosimeters subsequently became known as *hypoxic* or *anoxic* gel dosimeters. The MAGIC polymer gel formulation consisted of methacrylic acid, ascorbic acid, gelatin and copper. The principle behind removing the problem of oxygen in the MAGIC gel is in the use of ascorbic acid, commonly known as vitamin C. Ascorbic acid binds free oxygen contained within the aqueous gelatin matrix into metallo-organic complexes in a process initiated by copper sulfate (De Deene *et al* 2002b). It was subsequently shown that other antioxidants could also be used in the manufacture of normoxic gels including tetrakis (hydroxymethyl) phosphonium chloride (THPC) (De Deene *et al* 2002a, Baldock 2006). Numerous authors subsequently published results of work
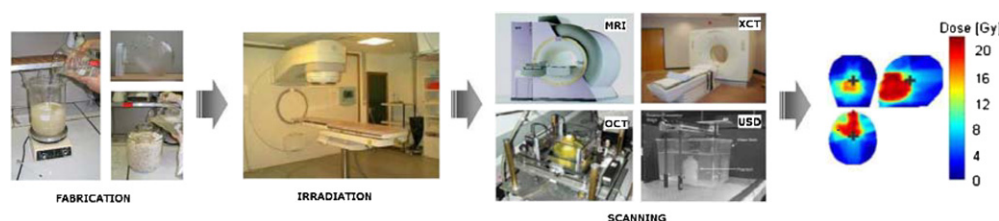
Figure 1. Gel dosimetry involves three major steps in order to obtain a dose distribution: (a) after fabrication the gel is poured into an (antropomorphically shaped) cast and into calibration vials; (b) the phantom is irradiated with a specific dose distribution and calibration samples are irradiated to known doses; (c) the irradiated gel dosimeter phantoms are scanned with an appropriate and optimized scanning technique (magnetic resonance imaging (MRI), optical computerized tomography (optical-CT), x-ray computerized tomography (x-ray CT) or ultrasound; (d) finally the data are used to produce an image of the irradiated dose distribution.

investigating different compositions and formulations of normoxic polymer gel dosimeters which have been summarized by Senden *et al* (2006).

With the introduction of normoxic gel dosimeters, MRI studies were undertaken to investigate their usefulness for IMRT (Gustavsson *et al* 2003), and radionuclide therapy (Courbon *et al* 2006, Gear *et al* 2006, Braun *et al* 2007, 2009).

There have been a limited number of previous reviews on polymer gel dosimetry (McJury *et al* 2000). For further reading on gel dosimetry see the proceedings of the DOSGEL conferences (DOSGEL 1999, 2001, 2004, 2006, 2008).

This current topical review comprehensively reviews the field of polymer gel dosimetry since its beginnings. The fundamental science underpinning the dosimetry technique is reviewed along with the various evaluation techniques and associated issues for the purposes of clinical dosimetry applications. In addition, areas of future potential developments are discussed.

2. Polymer gel dosimetry methodology

Polymer gel dosimetry involves three steps (figure 1): first, the radiation sensitive polymer gel is fabricated and poured into an antropomorphically shaped container and associated calibration vials, and left to set. Second, the antropomorphic phantom and associated vials are irradiated. Third, after polymerization the gel is scanned by use of a dedicated optimized imaging technique, and the acquired images are subsequently analyzed.

2.1. Fabrication

Polymer gel dosimeters are hydrogels in which vinyl monomers are dissolved. Water free radicals induce the polymerization of the monomers, such that monomers are converted to polymers. The amount of polymer produced is a function of the absorbed dose. The purpose of the gel matrix is to hold the polymer structures in place, preserving spatial information of the absorbed dose.

As previously mentioned, the fabrication process of the early polymer gel dosimeters was complicated by the fact that the oxygen concentration in the polymer gel dosimeters had to be reduced to less than 0.01 mg l^{-1}, a factor of approximately 1000 lower than normal atmospheric conditions. Oxygen is found to inhibit the radiation-induced polymerization

through the formation of peroxides. In 2001, Fong *et al* proposed the use of an anti-oxidant to scavenge the oxygen in the polymer gel dosimeter (Fong *et al* 2001).

Since the early polymer gel dosimeter formulations several other chemical compositions were studied. Different gelling agents and radiation sensitive monomers have been investigated. Some of the monomers used are summarized in table 4. However, to date, the dosimetric properties have been comprehensively investigated for only a few polymer gel compositions (De Deene *et al* 2006a). Apart from a measurable dose sensitivity, the polymer gel dosimeter phantom and calibration samples should be (i) stable in time and space, (ii) should be radiologically tissue equivalent, (iii) should be dose rate and energy independent with the effect of temperature and pressure on the gel negligible (De Deene *et al* 2004b). Other significant factors are the influence of temperature during fabrication (De Deene *et al* 2000d) and storage (De Deene *et al* 2007a). The manufacture of polymer gel dosimeters is known to have certain potential health hazards and risks associated with the chemicals used (Baldock and Watson 1999). More recently, less toxic gel dosimeter compositions have been proposed (Senden *et al* 2006).

2.2. Irradiation

Polymer gel dosimeters can be considered as chemical dosimeters that rely on a radiation-induced chemical reaction. The interaction of several types of radiation with polymer gel dosimeters has been studied. The most studied types of irradiation are gamma rays from cobalt sources and high-energy x-rays produced by clinical linear accelerators. No significant energy dependence was found for photon beam energies between 6 MV and 25 MV for most gel dosimeters (De Deene *et al* 2006a).

A second type of irradiation for which polymer gel dosimeters have been investigated are protons and heavy ions. However, due to saturation effects close to the proton track, the dosimetric response is less than found with x-rays. Further, the dose–response is dependent on LET and therefore varies along the proton track (Jirasek and Duzenli 2002).

2.3. Imaging

The dose information of an irradiated gel can be read out using different imaging techniques based on the specific physical change that has taken place in the irradiated gel. The three most-extensively used imaging techniques for polymer gel dosimetry are MRI, optical-CT and x-ray CT.

Any MRI contrast parameter that changes upon polymerization of the monomers in the gel is a potential candidate for mapping the dose distribution. The spin–lattice relaxation rate ($R_1 = 1/T_1$) has been found to change only slightly upon irradiation-induced polymerization (Maryanski *et al* 1993). The MRI property that has been used most often is the spin–spin relaxation rate ($R_2 = 1/T_2$) because of the large sensitivity and dynamic range of R_2 with respect to the radiation-induced polymerization as a function of absorbed dose. Important criteria are the accuracy and precision of the scanning technique. Imaging artifacts will decrease dosimetric accuracy. The dosimetric precision is determined by the sensitivity of the physical property determining the contrast in the scanned images, while the spatial precision is determined by the scanning technique. By calculating quantitative R_2 maps instead of using conventional T_2 weighted images, image inhomogeneities due to the inhomogeneous radio-frequency field (B_1 field) and external magnetic field (B_0 field) are filtered out to a large extent. An alternative contrast mechanism is magnetization transfer (MT) (Lepage *et al* 2002)

which has been found to be very useful in scanning low-density gel dosimeters (De Deene *et al* 2006b).

Due to the irradiated regions in polymer gel dosimeters becoming visibly opaque with absorbed dose, optical computerized tomography (optical-CT) of polymer gel dosimeters has been considered as an alternative to MRI. Several optical scanner types have been developed (Gore *et al* 1996, Oldham *et al* 2001, Doran *et al* 2001, Wuu *et al* 2003, Krstajic and Doran 2006, Sakhalkar and Oldham 2008, Van Doorn *et al* 2005) which rely on the principle of filtered back projection to reconstruct the cross-sectional image(s). Much recent optical-CT work has focused on non-scattering dosimeters (Sakhalkar and Oldham 2008).

X-ray computerized tomography (x-ray CT) is a third alternate imaging technology that enables readout of polymer gel dosimeters (Hilts *et al* 2000). X-ray CT is based on radiation-induced polymerization causing a change in the absorption coefficient of the irradiated polymer gel. The change in absorption coefficient is related to an associated change in mass density. The relative mass density change is in the order of 1 mg cm^{-3} Gy^{-1} (Trapp *et al* 2001a) and results in a change in CT number in the order of 1 Hounsfield unit per Gray for PAG dosimeters. Although signal-to-noise (SNR) is an important consideration in MRI and optical-CT, it is particularly significant in x-ray CT. In order to obtain a dose related image with a sufficiently high SNR in x-ray CT, image averaging of multiple acquisitions must be performed. In order to obtain x-ray CT images within a reasonable scanning time and with a sufficiently high SNR, different image filtering techniques have been proposed (Hilts and Duzenli 2004, Jirasek *et al* 2006b).

The change in density and viscosity in irradiated polymer gels also results in a change in the speed of sound (Mather *et al* 2002a, 2002b). An ultrasonic imaging system was developed to evaluate irradiated dose distributions (Mather and Baldock 2003a).

3. Fundamental principles of polymer gel dosimetry

3.1. Basic radiation chemistry mechanisms

The percentage water content of gel dosimeters is generally of the order of 90%. Experimental studies on numerous solutions of different compounds in water illustrate that the solute is often not being affected directly by the radiation but indirectly by some entities produced from water (Swallow 1973). Upon irradiation, water molecules are dissociated into several highly reactive radicals and ions (Spinks and Woods 1964, Magee and Chatterjee 1987) during a process termed 'radiolysis'.

The cluster size of radiolytic products and the types of species that are created within the first femtoseconds are dependent on the type of irradiation and the energy of the primary particles. In the case of x-rays, gamma rays and electrons, the radiolytic products appear in clusters called 'spurs' (figure 2). These pre-thermal events occur in a time period of 10^{-15} s to 10^{-14} s (Spinks and Woods 1964). For 6 MV photons the location of the radiolytic products is within 1 nm from the path of the incident ionizing particle at the point of creation. Because these events take place over a short time and spatial scale, the observation of these events is limited by intrinsic quantum uncertainties. From this moment onward, the probability that these reactive particles reach each other by Brownian motion and then react with one another increases with time. As a result, the radius of diffusing radiolytic products starts to grow. After 10^{-11} s a local thermal equilibrium in the recombination of reactive particles is reached. With an average diffusion coefficient of the reactive particles of 4×10^{-9} m^2 s^{-1} in water (Magee and Chatterjee 1987), it is estimated that after 10^{-11} s the root mean square displacement of the particles from the point of creation is 0.28 nm which is only one tenth of the intermolecular
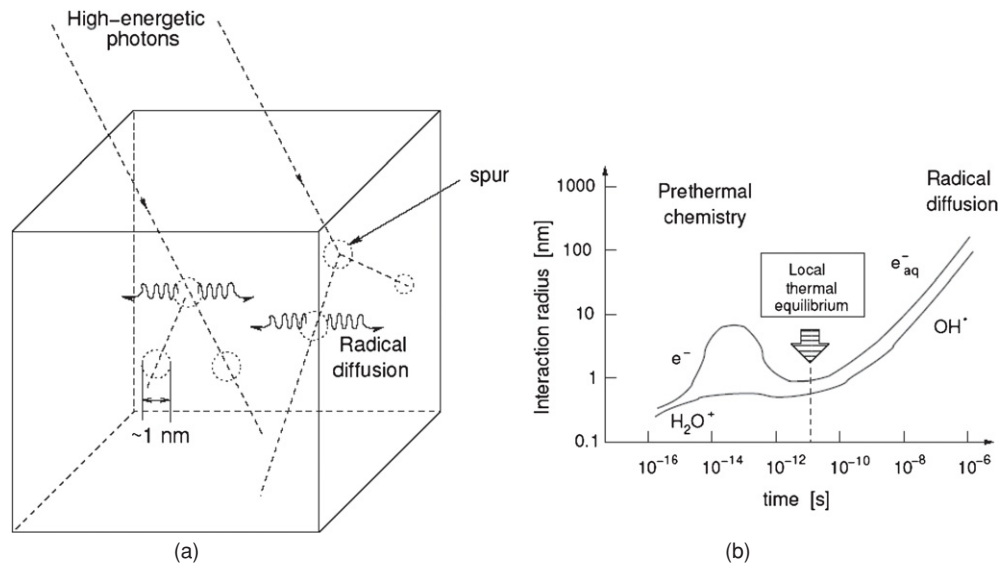
Figure 2. Radiation-induced radiolysis of water by high-energy x-rays occurs in 'spurs' (a). The radiolytic products diffuse from the site of creation while recombination processes take place (De Deene 2004b). Reproduced with permission.

Table 1. Radiochemical yields of intermediates (number of particles per 100 eV of absorbed energy) in the radiolysis of pure neutral water with hard x-rays, gamma-rays or fast electrons. $e_{\bar{a}q}^-$ is the hydrated electron (Spinks and Woods 1964).

Species	$e_{\bar{a}q}^-$	OH$^\bullet$	H$^\bullet$	H$_2$	H$_2$O$_2$	H$_3$O$^+$
G-value	2.7	2.7	0.55	0.45	0.71	2.7

distance of the monomers in a typical polymer gel dosimeter. As the molecular diffusion coefficient of water in the hydrogel is only 15% lower than in pure water (De Deene *et al* 2000d) it can be expected that the diffusion coefficient for the radiolytic products of water is of the same order of magnitude. After 10^{-8} s the root mean square displacement from the point of creation amounts to 9 nm. The predominant intermediates present after 10^{-8} s are listed in table 1 together with their radiochemical yields (G-values, i.e. number of particles per 100 eV primary energy) (Spinks and Woods 1964). These radiolytic products of water, particularly $e_{\bar{a}q}^-$, may react subsequently with the monomers. For example, the hydrated electron, $e_{\bar{a}q}^-$, reacts with the monomers by the formation of a radical anion that can be later neutralized by a proton (Panajkar *et al* 1995).

In summary, the decomposition of reactive intermediates (R$^\bullet$) can be written as a simplified reaction of which the dissociation rate (k_D) is proportional to the absorbed dose:

$$H_2O \xrightarrow{k_D} 2R^\bullet. \tag{1}$$

The radicals initiate the polymerization of monomers by reacting the monomer. The initiation step can be written as follows:

$$R^\bullet + M \xrightarrow{k_I} M_1^\bullet \tag{2}$$

Table 2. Initiation reaction rate constants, k_I, for different monomers that are used in gel dosimeters (in l mol^{-1} s^{-1}). The letters a–d give the reference in which the value is quoted. (a) Buxton *et al* (1988), (b) Panajkar *et al* (1995), (c) Safrani and Wojnarovits (1993), (d) Kozicki *et al* (2002), (e) Kozicki *et al* (2003).

Monomer	$e_{\bar{a}q}$	OH$^\bullet$	H$^\bullet$
AAm	2.2×10^{10} (a)	5.9×10^{9} (a)	3.1×10^{10} (a)
Bis	2.8×10^{10} (b)	? (e)	? (e)
Acrylic acid	2.4×10^{10} (a)	1.5×10^{9} (a)	3.3×10^{9} (a)
Methacrylic acid	1.9×10^{10} (a)	–	–
Hydroxyethylacrylate	7.5×10^{10} (c)	1.1×10^{10} (c)	–
N-Vinylpirolidone	1.6×10^{10} (a)	7.3×10^{9} (a)	–
Poly(ethyl glycol) diacrylate	1.7×10^{10} (d)	3.0×10^{10} (d)	–

Table 3. Rate constants for the propagation of various vinyl monomers in aqueous solution (in l mol^{-1} s^{-1}). The letters a–b give the reference in which the value is quoted. (a) Brandrup *et al* (1999), (b) Panajkar *et al* (1995).

Monomer	k_P (l mol^{-1} s^{-1})
AAm	2×10^{4} (a)
Bis	6×10^{6} (b)
Acrylic acid	1×10^{3} (a)
Methacrylic acid	1×10^{3} (a)
Hydroxyethylacrylate	–
N-Vinylpirolidone	–
Poly(ethyl glycol) diacrylate	–

with $k_I(n)$ the initiation reaction rate constant. The resulting radiochemical yield (G) factor for AAm and Bis is found to be 2.54×10^5 and 3.42×10^5 respectively and for the formation of polymer 5×10^5 (Lepage *et al* 2001d).

In table 2, some initiation reaction rate constants are given for several monomers used as constituents in the manufacture of typical gel dosimeters.

The growth of the polymer continues by chain propagation reactions in which the polymeric radicals react further by adding monomers or by adding pendant vinyl groups (resulting from Bis) that are present on other polymer chains. The general case in which a polymer radical with n monomer units reacts with a monomer or a dead polymer chain containing m monomer units is shown in equation (3):

$$M^\bullet_m + M_n \xrightarrow{k_T c(n,m)} M^\bullet_{n+m}. \tag{3}$$

Rate constants for the propagation reaction of various vinyl monomers in aqueous solution with monomers ($m = 1$) are listed in table 3.

Termination of the polymerization reaction occurs by the reaction of two radicals by either combination or disproportionation:

$$M^\bullet_m + M^\bullet_n \xrightarrow{k_T c(n,m)} M^\bullet_{m+n} \tag{4}$$

$$M^\bullet_m + M^\bullet_n \xrightarrow{k_T d(n,m)} M_m + M_n. \tag{5}$$

Note that primary radicals generated by water radiolysis can also react with growing polymer chains to induce termination:

$$R^\bullet + M_n^\bullet \xrightarrow{k_T c(o,m)} M_n \tag{6}$$

and that primary radicals can react with pendant vinyl groups on dead polymer chains to initiate additional polymerization reactions:

$$R^\bullet + M_n \xrightarrow{k_I(n)} M_n^\bullet. \tag{7}$$

In addition to termination reactions, the growing polymer-radical may also terminate by transfer of the radical group to other molecules (Whittaker *et al* 2001). Typical chain transfer constants $C_M = k_{\text{trans}}/k_P$ of radicals are of the order of 10^{-3} to 10^{-4} (Brandrup *et al* 1999):

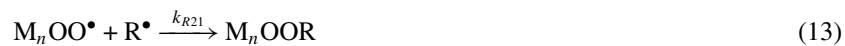$$M_m^\bullet + M_n \xrightarrow{k_{Trans}} M_m + M_n^\bullet. \tag{8}$$
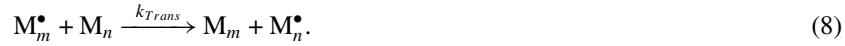
When crosslinker molecules such as Bis are consumed via propagation reactions (equation (3)), one vinyl group on the crosslinker polymerizes and the other becomes a pendant vinyl group along the polymer chain, which is available for later propagation reactions, which lead to the formation of crosslinks. Alternatively, depending on the geometry of the crosslinker molecule, the second vinyl group can sometimes be consumed immediately after polymerization of the first vinyl group, via a cyclization reaction (Okay *et al* 1995), thereby reducing the number of pendant vinyl groups available for crosslinking.

The radical site on the growing polymer can also undergo chain transfer to the gelatin biopolymer (Whittaker *et al* 2001). The polymeric gelatin radicals that are formed are slow to propagate with additional monomer, so that increasing gelatin concentration results in a reduction in the extent of polymerization (Lepage *et al* 2001c). The reaction coefficients of the hydrated electron, $e_{\bar{a}q}$, and the hydroxyl-radical,, with gelatin are respectively $6.4 \times 10^{10}\,\text{l mol}^{-1}\,\text{s}^{-1}$ and $9.1 \times 10^{10}\,\text{l mol}^{-1}\,\text{s}^{-1}$ (Buxton *et al* 1988).

Peroxide-radicals are created when oxygen is present in the gel:

$$R^\bullet + O_2 \xrightarrow{k_{o1}} ROO^\bullet \tag{9}$$

$$M_n^\bullet + O_2 \xrightarrow{k_{o2}} M_n OO^\bullet. \tag{10}$$

These peroxide-radicals will quickly react with other radicals leading to termination,

$$ROO^\bullet + R^\bullet \xrightarrow{k_{R11}} ROOR \tag{11}$$

$$ROO^\bullet + M_n^\bullet \xrightarrow{k_{R12}} ROOM_n \tag{12}$$

$$M_n OO^\bullet + R^\bullet \xrightarrow{k_{R21}} M_n OOR \tag{13}$$

$$M_n OO^\bullet + M_m^\bullet \xrightarrow{k_{R22}} M_n OOM_m. \tag{14}$$

The viscosity within the precipitated polymer microgels is very high, hindering termination by mutual interaction of the growing chains (equation (6)) but has less effect on the propagation reaction (equation (3)) because diffusion of the small monomer molecules is not affected significantly by the increased viscosity (Kim and Hamielec 1984). As a result, the rate of polymerization increases with high conversions (Swallow 1973). This effect of auto-acceleration is also called the gel effect or Trommsdorff effect (Chernyshev *et al* 1997). It has been reported that in systems in which the polymer precipitates from the solution by the creation of a heterogeneous gel system, the increase of viscosity takes place very rapidly even
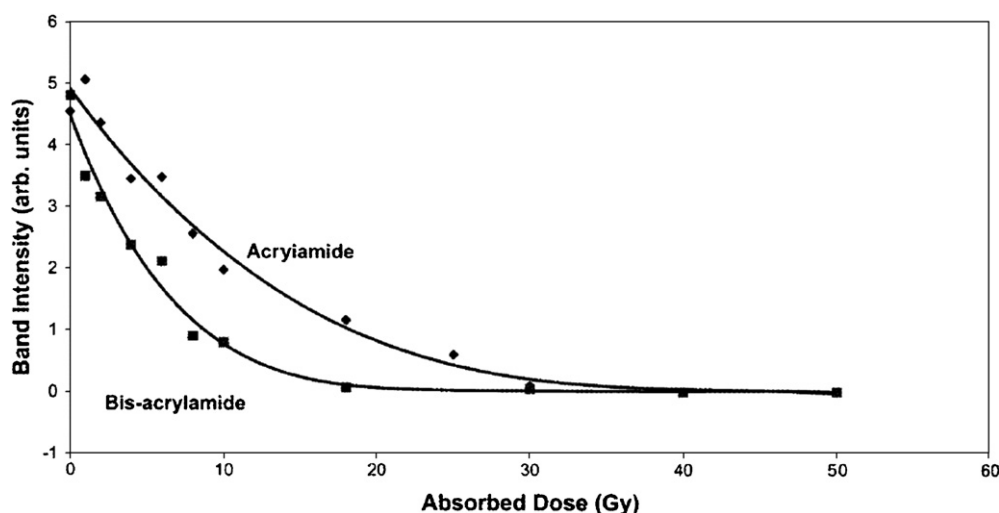
Figure 3. Consumption of AAm and Bis in a PAG as measured by Raman spectroscopy (Baldock *et al* 1998b). Reproduced with permission.

at low conversions (Chapiro 1962). This effect has also been illustrated through mathematical models of dispersion radical polymerization kinetics (Chernyshev *et al* 1997). The lower termination rate may also be responsible for the increasing size of the polymer microgels with increasing dose, as has been observed by optical turbidity spectra (Maryanski *et al* 1996).

   To date it is not known if the nonlinear response in the low-dose region (seen from 0 to 1 Gy) (De Deene *et al* 2000d) of most polymer gel systems is a reflection of this sudden change or if it is due to inhibitors (such as oxygen) in the gel. Note that although most of the dose–R_2 plots of polymer gel dosimeters are fitted against a linear or mono-exponential fit, it can be seen that for most polymer gel systems the dose–R_2 sensitivity up to 1 Gy is less than in the higher dose range (2–10 Gy).

   With polymer gel dosimeters in which crosslinking copolymerization occurs (such as the aqueous AAm/Bis gel system) the kinetic models as mentioned in equations (2)–(13) become more complicated due to the differences in reactivity of the two comonomers (Baldock *et al* 1998b, Lepage *et al* 2001d, Jirasek *et al* 2001a) (figure 3) and the change in the reaction rate coefficients during the growth of the copolymer-network. The different reaction rates of the comonomers lead to a shift in the instantaneous relative comonomer concentration (Baselga *et al* 1988, 1989). The reaction rates of the growing copolymer chains are not only dependent on the number of monomer units but also on the crosslinking density and the shape of the polymer structures (Tobita and Hamielec 1992).

   According to Baselga *et al* (1989), in the crosslinking copolymerization of an AAm/Bis aqueous solution, three different reaction steps can be observed: a pre-gelation, gelation and post-gelation step. In the pre-gelation step, no microgel has precipitated, and the polymer molecules are rich in Bis, because Bis has a higher reactivity than AAm due to its two vinyl groups. During gelation, microparticles precipitate due to crosslinking reactions. As the copolymerization proceeds, the concentration of unreacted Bis falls more quickly than the concentration of AAm. The precipitated copolymer microgels that form later contain less reacted Bis than the microgels that form earlier, and have lower crosslink density. The post-gelation phase is characterized by slow crosslinking, due to the low mobility of pendant vinyl
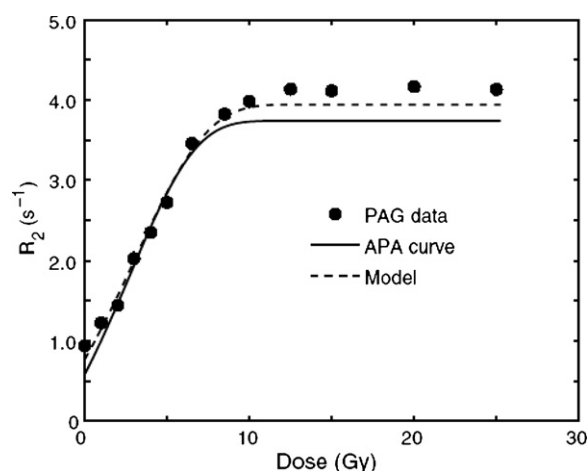
Figure 4. Dose–R2 response of both a (6%T/50%C) PAG and a corresponding AAm/Bis aqueous solution (APA). The dashed line corresponds to a spin–compartment model in the fast-exchange limit (Babic and Schreiner 2006). Reproduced with permission.

groups (from Bis) along the polymer chains and steric hindrance (Tobita and Hamielec 1992, De Deene *et al* 2000d) and reorganization of the polymer networks (Lepage *et al* 2001d).

From figure 4 it can be seen that the gelatin has a small moderating effect upon the reaction kinetics. It is noted that the dose–R_2 response in AAm/Bis-solution is in contrast with previous published assumptions of a step response in the R_1–dose response indicating a go/no-go reaction at about 15 Gy (Maryanski *et al* 1993).

Some studies have been performed on PAG dosimeters and aqueous solutions with different ratios of AAm and Bis. From FT Raman spectroscopy studies it is seen that the relative content of AAm and Bis has a significant influence on the consumption rate of both monomers (Jirasek and Duzenli 2001b). This results in a difference in dose sensitivity of gels with different compositions. Previously, it was reported that the dose sensitivity of PAG dosimeters is maximum for equal amounts (in weight) of monomer (AAm) and crosslinker (Bis) (Maryanski *et al* 1997). The solubility of the crosslinker Bis in the gel is limited to approximately 3% in weight relative to the total weight of the gel (w/w). The solubility of the crosslinker in gel can be further increased by the addition of co-solvents (Koeva *et al* 2008). This finding appeared to be independent of scanning temperature. It was also found that the saturation R_2 (the R_2 for very high doses) increases with increasing crosslinker fraction. In the study performed by Maryanski *et al* (1997), it was assumed that the dependence of dose sensitivity on crosslinker fraction reflected two opposing tendencies: an increase in sensitivity with crosslinker content up to 50%C (%C is the relative content of crosslinker with respect to the total amount of comonomer in percentages of weight) due to greater NMR relaxivity of more crosslinked (rigid) polymer, whereas a decrease in sensitivity with increase in crosslinker content beyond 50%C might be caused by lower reactivity of the crosslinker (Bis). The latter explanation has been contradicted by several studies using FT-Raman vibrational spectroscopy in which it was found that the consumption rate of the Bis crosslinker monomer is twice as large as the AAm monomer (Baldock *et al* 1998b, Jirasek *et al* 2001a, Lepage *et al* 2001d, Rintoul *et al* 2003). The difference in consumption rate of comonomers may explain that the relative fraction of monomer and crosslinker changes with dose. Thus the polymer structures created at small doses differ from the structures created at larger doses. It has been

proposed that the change in viscosity by structures rich in AAm and a higher incidence of comonomer reacting with itself at high crosslinker (Bis) concentrations, which is slowed by steric hindrance, explains the dose sensitivity versus crosslinker concentration (Jirasek and Duzenli 2001b). These reactions have also been described in previous works on crosslinked polyacrylamide gels (Gelfi and Righetti 1981a, 1981b, Baselga *et al* 1988, 1989, Tobita and Hamielec 1990, 1992).

Although no hard evidence has been published for methacrylic acid based polymer gel dosimeters to date, it is assumed that in these polymer gel dosimeters the methacrylic acid polymer chains react with the gelatin in a process called 'graft polymerization' (Stejskal *et al* 1988, Keles *et al* 1999). This assumption is based on the observation of physical properties of polymer gel dosimeters irradiated to different doses such as the completely different characteristics of ultrasonic speed and elasticity modulus (Mather *et al* 2002a), the different characteristics of restricted molecular self-diffusion of the water molecules, the melting temperature of both gels, the chemical stability of the gels (De Deene *et al* 2002b) and the dose–R_2 response curves obtained for different irradiation temperatures.

A comprehensive model describing the reaction kinetics in PAG was developed and numerically solved by Fuxman *et al* (2003). In this model two phases were considered. One phase is the aqueous phase that consists of monomers and linear polymer dissolved in water. Crosslinked polymer chains precipitate from the aqueous phase into a polymer phase. In this model, all the above-mentioned kinetic reaction mechanisms (except with oxygen) are incorporated. Pseudo-empirical models have been applied to model the effect of growing polymer on the diffusion-controlled rate coefficients. However, the diffusivity of the monomer within the precipitated polymer remains unknown. Although some of the rate coefficients had to be adjusted, the model was able to predict phenomenologically the behavior of the gel dosimeter response with respect to gelatin concentration, monomer concentration and dose rate. The model also predicted temperature changes in irradiated PAG (Salomons *et al* 2002) and has also been extended to describe the reactions that take place at the edge of a non-uniform dose distribution (De Deene *et al* 2002a, Fuxman *et al* 2005).

3.2. The structure of polymer gel dosimeters

The structure of the gel dosimeters before irradiation can be determined from basic calculations regarding the amount of gelatin and monomers that are present and from other studies on gelatin gels. The gelation of aqueous gelatin solutions is governed by the growth of a 3D network of biopolymer chains. The junctions of the network matrix result from renaturing of collagen. The collagen unit (tropocollagen) is a rod of approximately 280 nm in length made of three polypeptide chains, each one being twisted into a left-handed helix and all three wrapped into a super-right-handed helix (Ward 1977) (figure 5).

The gelation process of aqueous gelatin solutions has been investigated by the observation of different physico-chemical properties such as by use of viscosimetry (Huang and Sorensen 1996), atomic force spectroscopy (Mackie *et al* 1998), dye fluorescence (Bozena 1999), dielectric measurements (Bohidar *et al* 1998) and polarimetry and MR relaxometry (Maquet *et al* 1986). Models have been developed to describe the sol–gel transition of gelatin gels (Daoud 1987, Del Gado *et al* 1998). All of these studies demonstrate that the gelation occurs quickly during the first minutes after quenching the sol–gel at temperatures below 35 °C with a much slower progression after the first hours. No equilibrium is found even after a week. This has also been observed as one source of chemical instability in several gel dosimeters that results in a drift in the offset of the dose–R_2 response curves (De Deene *et al* 2000d, 2002b). Through FT Raman spectroscopy, it has been found that the anti-oxidant, THPC, may
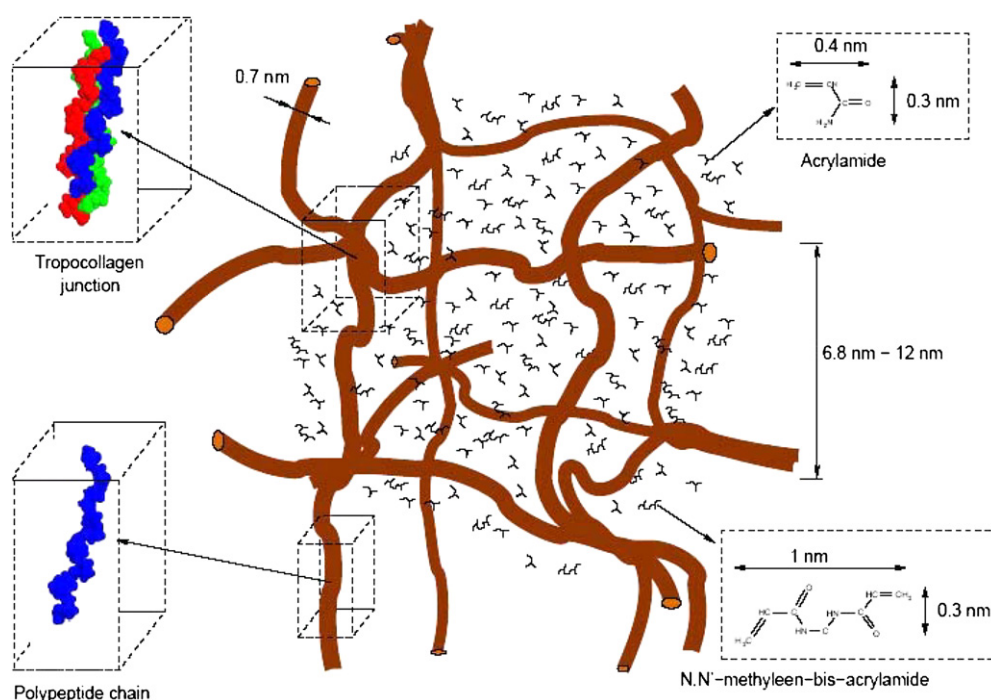
Figure 5. Representation of the microscopic structure of an unirradiated (6%T/50%C) polymer gel based on stoichiometric calculations.

crosslink gelatin polymers (Jirasek *et al* 2006a). It is believed that the irreversible change in gel structure may have an effect on the polymerization kinetics.

The distance between the gelatin biopolymer chains will be randomly distributed. However, to obtain an idea about the size of the network structure, a cubic topology has been considered. In this case an order of magnitude of the size of the vacant spaces within the gelatin network can be determined. Based upon the dimensions of the gelatin helices (Ward 1977) it is found that the mazes measure in the order of 7 nm to 12 nm for a 6% (w/w) gelatin gel.

The size of the monomers is in the order of a few ångstroms (for AAm 0.4 nm by 3 nm, for Bis 10 nm by 3 nm). The average intermolecular distance of the monomers in an un-irradiated dosimeter gel can be calculated from the molecular weight and the molecular weight fraction. For a (6%T, 50%C) PAG the average intermolecular distance is 2.0 nm for the AAm monomers and 2.5 nm for the Bis crosslinker. The average molecular distance between the water molecules is in the order of 0.39 nm (Narten *et al* 1967). Since the spacing between the gelatin structures is large compared to the sizes of monomer and water molecules, the gelatin has little influence on the diffusivities of these small molecules.

Upon irradiation, different polymer structures are created in the gel. Due to the high amount of crosslinker in the case of a PAG, the polyacrylamide network can be seen as microgel particles embedded in the gelatin hydrogel. It has been mentioned previously that the size of the polymer structures differs with dose. As a result, the polymer chain density in the irradiated PAG dosimeters can be expected to be far from uniform (Jirasek and Duzenli 2001b) (figure 6).
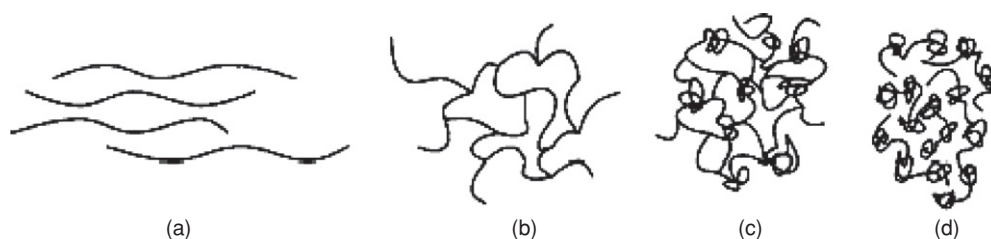
Figure 6. Progression in polymer structure as a function of initial crosslinker concentration: (a) a gel solely composed of monomer (AAm). Long, linear chains are formed with no crosslinks; (b) gel composed of low initial Bis fraction. The predominant gel formation is an ordered, crosslinked network; (c) gel composed of high initial Bis fraction. Gels begin to form a larger number of knots; (d) a gel composed solely of crosslinker (Bis). The predominant structures are knots, loops and doublets which together form beads (Jirasek and Duzenli 2001b). Reproduced with permission.

Several studies on polyacrylamide gels have shown large heterogeneities (domains of high and low gel density) in highly crosslinked gels (Gelfi and Righetti 1981a, Weiss and Silberberg 1977, Nieto *et al* 1987, Baselga *et al* 1987, 1989).

4. Evaluation of polymer gel dosimeters

4.1. Magnetic resonance response mechanisms

From the structural and chemical studies, it can be concluded that the extent of the resulting polymerization reaction is a function of dose. To understand the effect of radiation-induced polymerization on the magnetic resonance relaxation rates R_1 and R_2, different proton pools can be considered (i.e. ensembles of protons that can be considered as belonging to molecules that experience the same chemical environment). Three major groups of proton pools can be considered in a polymer gel dosimeter (Lepage *et al* 2001c): (1) the proton pool of free and quasi-free protons (denoted as mobile, *mob*). These are the protons from free water molecules and unreacted monomers; (2) the proton pool of a growing poly-acrylamide network (*poly*) and of water molecules bound to the macromolecules and (3) the proton pool of the gelatin matrix (*gela*) and of the water molecules associated with the gelatin. It is noted that in order to study other phenomena in more detail, a subdivision of these proton pools can be considered as well. In a study of the chemical stability of polymer gel dosimeters the third pool is subdivided in two pools (De Deene *et al* 2000d).

According to the theory of Bloembergen *et al* (1948), also referred to as the BPP-theory and further extended by Woessner (1962), the spin–spin relaxation of the different proton pools is governed by the rate of molecular 'tumbling' and Brownian motion of the molecules that contain these protons. This results in a change of the efficiency of dipolar coupling between neighboring protons and results in a change in the diphase rate of the spin–magnetic dipole moments. As this is directly correlated with the spin–spin relaxation, it can be expected that the relaxation rate of the proton pools is inversely correlated with the mobility of the protons within these pools. The different proton pools are thus characterized by different relaxation rates.

If the lifetimes of protons in the various environments are long compared to the characteristic correlation times of the environments, each environment has intrinsic relaxation rates that are independent of the specific lifetime value ($R_{2,\text{mob}}$, $R_{2,\text{poly}}$, $R_{2,\text{gela}}$). Further, if the lifetimes are long compared to these relaxation times, the NMR signal is the same as

the sum of the signals from isolated, non-exchanging environments. When this happens, the relaxation curves are multi-exponential, with the coefficient and R_2 of each exponential term being determined by the relevant population fraction and NMR properties of each different pool respectively. This is the slow exchange case. Alternatively, when these lifetimes are short compared to the relaxation times but still long compared to the correlation times (the rapid exchange limit), the observed relaxation curve will be mono-exponential with a relaxation rate that is the weighted average of the relaxation rates of the different proton pools in the entire sample (Zimmerman and Brittin 1957):

$$R_2 = f_{\text{mob}} \cdot R_{2,\text{mob}} + f_{\text{poly}} \cdot R_{2,\text{poly}} + f_{\text{gela}} \cdot R_{2,\text{gela}} \qquad (15)$$

with f_{mob}, f_{poly} and f_{gela} the relative fractions of protons in the mobile, polymer and gelatin pool, respectively.

For R_2 MRI measurements that have been performed on polymer gel dosimeters, the condition of fast exchange is fulfilled. Before irradiation, the second proton pool is empty while the first proton pool is at its maximum. Upon irradiation, the second proton pool starts to grow at the cost of the first proton pool.
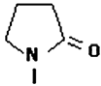
The mobility of monomers is relatively high and thus the mobility of water molecules bound to the monomers by hydrogen bridges is also high. However, upon irradiation of the gel dosimeters, the molecular mobility is significantly reduced. As the mobility of the bound water molecules is reduced, spin–spin relaxation is more effective, which is observed by an increase in R_2. Alternatively, exchange of water protons with fast relaxing polymer protons will increase R_2.

A comparison of the change in R_2 of gel dosimeters consisting of different monomers suggests that the change in relaxation rate cannot be explained by the BPP-theory solely. In table 4, the R_2-dose sensitivity of a number of different gel dosimeter formulations is listed.

The simple model of fast exchange is a good overall representation of the system but the exact values of the relaxation rate are modulated by the rate of exchange of magnetization between the pools. From studies in which different water pools are selectively inverted (Edzes and Samulski 1978), it is seen that cross-relaxation can occur between the different proton pools, for example between protons of the polymer with protons of mobile water (Ceckler et al 1992, Gochberg et al 1998). The exchange of magnetization may occur by proton chemical exchange between bound water and free water and by magnetization transfer between non-exchangeable macromolecular protons and bound water. It has been shown that magnetization transfer can also be mediated by chemical exchange interactions (Kennan et al 1996). It is shown that both chemical exchange and magnetization transfer are influenced by the pH of the system. As a result of the different interactions between the different proton pools, the relaxation rates of the different pools ($R_{2,\text{mob}}$, $R_{2,\text{poly}}$, $R_{2,\text{gela}}$) as they occur in equation (15) are not only determined by the mobility of the molecules but also by the exchange rates of protons. As some monomers have acidic or alkaline functional groups, the overall R_2 relaxation rate also depends on the pH of the gel (Gochberg et al 1998).

From table 4 it can be seen that the dose sensitivity of the different monomers is influenced by the functional group. The functional group determines both the polymerization rate of the monomers (inversely related to the half-dose value $D_{1/2}$ (Lepage et al 2001d)) and the efficiency of cross-relaxation. The hydroxyl and amino groups serve as hydrogen bonding sites (Ceckler et al 1992). The hydroxyl-group seems to be more efficient than the amino-group in the exchange of magnetization. However, it is seen that the reaction rate of AAm in the PAG is much higher than of acrylic acid. As a result, the dose sensitivity of both monomers is nearly the same but the dose-range of the AAc gel is larger than for the AAm based gel. Although the alkyl-group (in MAc and HEMA) does not have a large influence on the cross-relaxation

Table 4. MRI dose sensitivity of different gel dosimeters (from Lepage *et al* (2001a)).

Monomer	$D_{1/2}$ (Gy)	$\delta R_2/\delta D$ (s^{-1} Gy^{-1})	R_{2sat}–R_{20} (s^{-1})	Functional group
AAm/Bis	5.5 ($\pm$0.1)	0.33 ($\pm$0.1)	4.2 ($\pm$0.4)	
Acrylic acid (AAc)	31.2 ($\pm$0.1)	0.358 ($\pm$0.006)	10.6 ($\pm$0.4)	
Methacrylic acid (Mac)	12.5 ($\pm$0.1)	1.19 ($\pm$0.05)	18.4 ($\pm$0.4)	
1-Vinyl-2-pyrrolidone (VP)	23.6 ($\pm$0.1)	0.082 ($\pm$0.004)	13.7 ($\pm$0.4)	
2-Hydroxyethyl-acrylate (HEA)	5.5 ($\pm$0.1)	0.498 ($\pm$0.003)	4.2 ($\pm$0.4)	
2-Hydroxyethyl-methacrylate (HEMA)	41.6 ($\pm$0.1)	0.046 ($\pm$0.002)	4.9 ($\pm$0.4)	
N-Iso-propylacrylamide (NIPAM)/Bis (Bis)	20 ($\pm$0.1)	0.14 ($\pm$0.01)	5.2 ($\pm$0.4)	

efficiency it alters the polymerization rate of the monomers significantly. Studies have been undertaken to investigate the relative significance of the various components of the chemical components (De Deene *et al* 2002a, Venning *et al* 2005a, 2005b, Hurley *et al* 2005).

Magnetization transfer between different proton pools can be used directly to evaluate the polymer gel dosimeters (Lepage *et al* 2002). More recently, the magnetization transfer proportion was also proposed (Whitney *et al* 2008).

4.2. Magnetic resonance imaging considerations

Imaging parameters such as echo time (TE), repetition time (TR) and flip angle (FA) have a large influence on the contrast in diagnostic MR images. The most commonly used MR contrast for polymer gel dosimetry is the spin–spin relaxation rate R_2. Whereas T_2-weighted images are used in the clinic, a collection of these images are used to calculate R_2 maps. Although theoretically, the use of T_1- or T_2- weighted images is not excluded, it is found that main magnetic field (B_0) (De Deene *et al* 2001a) radio-frequency field (B_1) (De Deene *et al* 2000b) inhomogeneities have a detrimental impact on the accuracy of the dose reading. These effects are largely compensated by the use of quantitative R_2 maps as these effects are in first order proportional to the signal intensity.
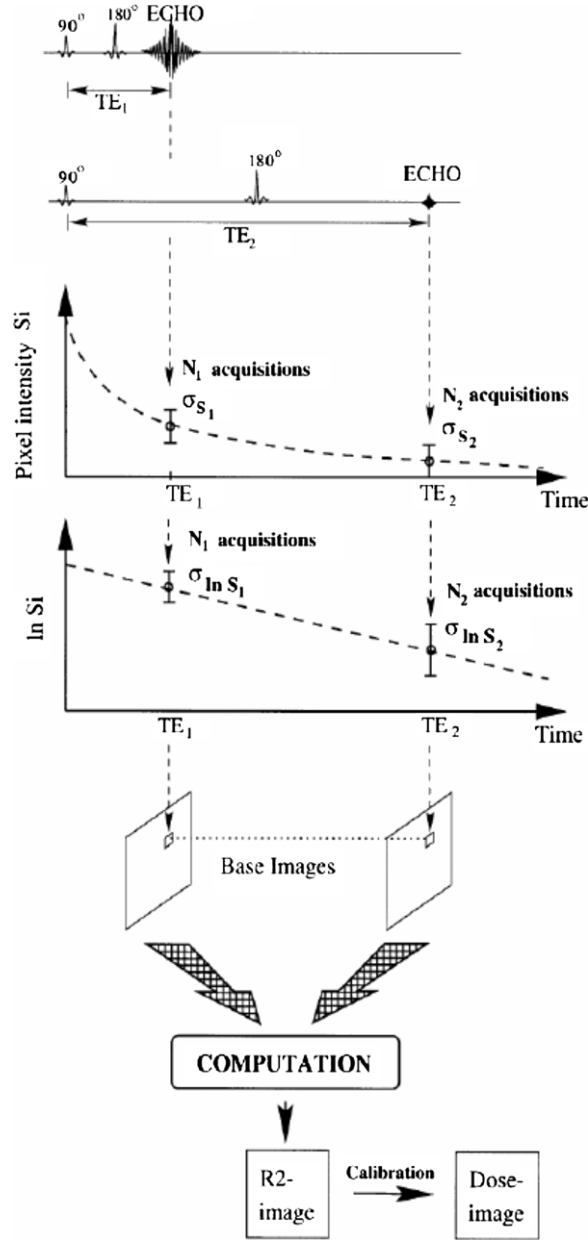
Figure 7. Construction of an R2- and dose-images using a two points single spin–echo sequence (De Deene *et al* 1998b). Reproduced with permission.

To obtain quantitative R_2 maps, different imaging sequences can be used. The most simple sequence is a conventional single spin–echo sequence. By changing the TE, the T_2 weighting in the base images can be varied. The R_2 value in each pixel can be acquired from two differently T_2 weighted images (figure 7) according to

$$R_2(i, j) = \frac{1}{TE_2 - TE_1} \ln \left[\frac{S_1(i, j)}{S_2(i, j)} \right].$$
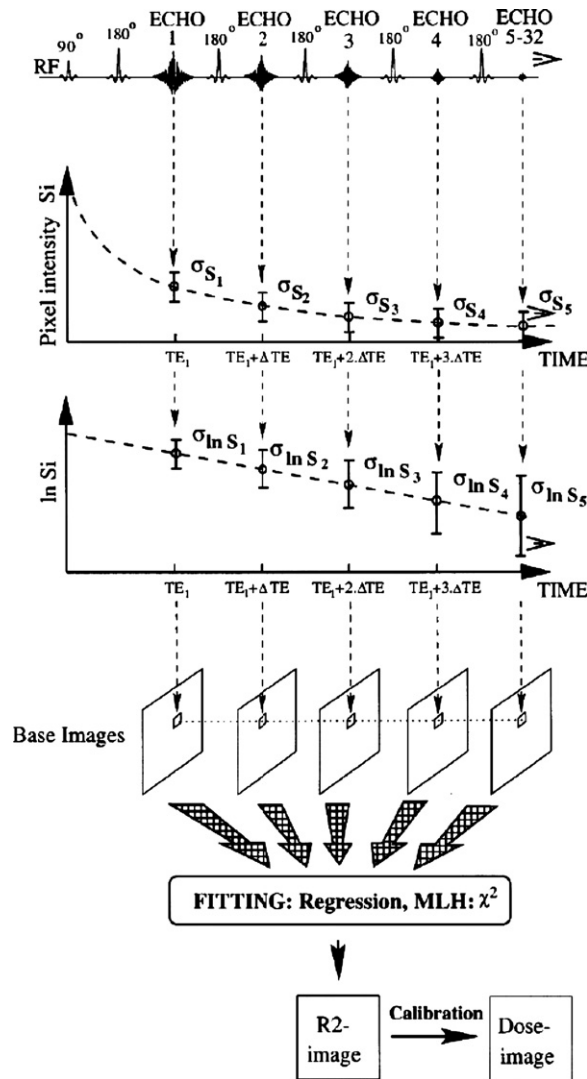(16)

Figure 8. Construction of $R2$- and dose-images using a multiple spin–echo sequence (De Deene *et al* 1998b). Reproduced with permission.

From a signal-to-noise point of view, it is more optimal to use a multiple spin–echo sequence. In a multiple spin–echo sequence, several different T_2 weighted images are acquired during the same repetition period. The R_2 value in each pixel can be obtained by fitting an exponential decay curve to corresponding pixel values in the base images (figure 8).

There have been attempts to increase the imaging time by making use of 'turbo' or 'fast' spin–echo sequences (Bausert *et al* 2000, Bankamp and Schad 2003). In these imaging sequences, more than one echo is used for constructing a base image. The number of echoes used within the same base image is called the 'turbo factor'. It should be noted however that the increase in scanning time results in a smaller number of base images and is thus at the cost of signal-to-noise ratio.
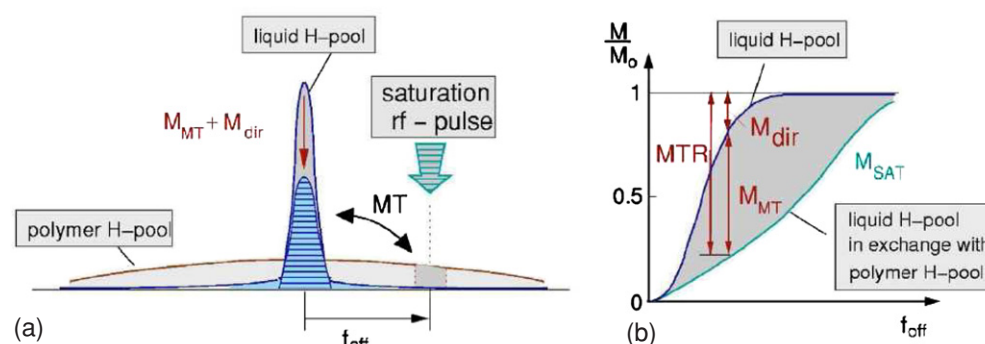
Figure 9. (a) Principle of magnetization transfer imaging. The polymer proton pool has a short $T2$ and thus covers a broader frequency line shape than the free water proton pool. By use of off-resonance saturation rf pulses part of the polymer protons is saturated. Because of magnetization transfer, polymer protons are exchanged with the water protons resulting in a decrease in longitudinal magnetization. (b) The observed relative signal decrease (MTR) is due to both direct saturation of the water protons (Mdir) and to magnetization transfer between the water proton pool and the polymer proton pool (MMT) (De Deene *et al* 2006a). Reproduced with permission.

Magnetization transfer is another contrast that can be used to acquire quantitative dose-related images (Lepage *et al* 2002). MT contrast is achieved by applying one or several off-resonance radio-frequency (rf) pulses. The off-resonance rf-pulses will decrease the magnetization of the macromolecular pool. Due to transfer of magnetization or exchange of protons between the macromolecular pool and the free water pool there will be a decrease in signal of the water protons.

In magnetization transfer, the signal decrease is proportional to the amount of saturated macromolecular protons (figure 9). The efficiency of the magnetization transfer also depends on the molecular side groups to which the macromolecular protons belong (Gochberg *et al* 1998, 2001, Lepage *et al* 2002). Magnetization transfer imaging has proven to be very useful for scanning low-density gel foam dosimeters (De Deene *et al* 2006b).

4.3. Optical-CT

Gore *et al* (1996) introduced a new method of 3D dosimetry using optical computed tomography, or optical-CT, to scan polymer gel dosimeters. Unirradiated gel is virtually transparent to visible light, but irradiated gel becomes increasingly opaque as the number density of radiation-induced polymer micro-particles increased (figure 10(a)). The localized variation in dose-dependent attenuation of the gel lent itself to 3D imaging by optical-CT, a technique analogous to x-ray CT, except utilizing visible light instead of x-rays. In a companion paper, Maryanski *et al* (1996) presented the optical properties of BANG polymer gels. The primary mechanism of optical contrast was identified as light scattering, because of an observed absence of absorption bands (figure 10(b)) in the turbidity spectra of gels irradiated to different doses. Negligible light absorption was reported. Measurements of the refractive index of gels irradiated to different doses revealed increasing refractive index with increasing dose. Both light-scatter and light-refraction therefore represent potential sources of artifacts in optical-CT dosimetry, as discussed further below. The authors also estimated the maximum particle sizes to be in the approximate range 400–700 nm, varying systematically
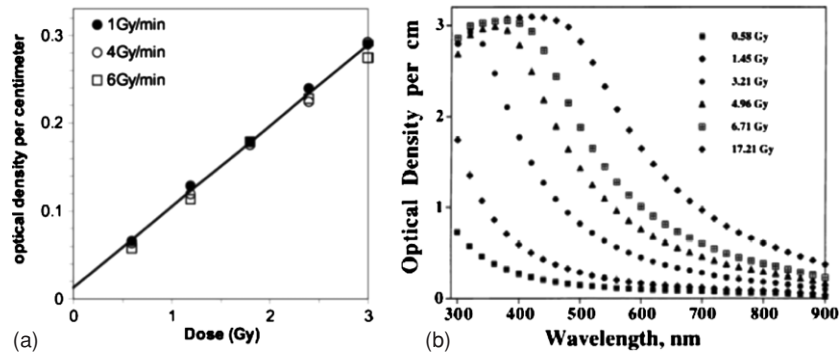
Figure 10. (a) Dose response of a polymer gel, as derived from an imaging measurement (Wuu and Xu 2006); (b) Optical density of a polymer gel at a variety of doses, demonstrating the lack of absorption bands (Maryanski *et al* 1996). Reproduced with permission.

as a function of crosslinker fraction. The Gore and Maryanski papers stimulated interest in the potential for high resolution 3D dosimetry by optical-CT. Prior to these works MR imaging had been the sole modality for imaging the dose in polymer gels (Maryanski *et al* 1993, 1994a). A question arose as to the relative merits of these imaging methods. Oldham *et al* (2001) showed that optical-CT could provide a low cost and attractive alternative to MRI scanning of polymer gels for many applications. It is noted that MRI gel dosimetry retains unique abilities enabling imaging of arbitrarily shaped gel dosimeters in phantoms containing opaque features or inhomogeneities.

4.3.1. Technique and theory of optical-CT. The technique and theory of optical-CT are similar to that for x-ray CT. Briefly, the raw data for the optical-CT technique are optical projections obtained either by a laser scanning across the sample, detected by a photoreceiver, or by broad incoherent light beam passing through the sample and imaged using a pixelated detector (usually a charge-coupled device (CCD), but potentially a complementary metal oxide semiconductor (CMOS) detector). Beer's law relates the measured signal intensity I to the signal in the absence of the sample I_0 by

$$I = I_0 \exp\left[-\int_{\text{ray-path}} \mu(s)\,\mathrm{d}s \right] \tag{17}$$

where μ is a quantity known as the optical attenuation coefficient and s is a distance along the selected ray-path through the sample. Under appropriate circumstances, changes in μ are proportional to the absorbed dose (or can at least be related by a calibration curve) and it is μ that we wish to extract from our measurement, in a spatially resolved fashion.

   If projections are obtained with the sample positioned at a range of rotation angles (typical of the order several hundred), then the mathematical procedure of filtered back-projection may be used to reconstruct 3D images of μ and, hence, by appropriate calibration, dose.

   For further information on the CT technique itself, see either Doran (2008), which deals specifically with optical-CT, or an x-ray CT text such as Hsieh (2003).

4.3.2. Optical-CT scanning systems. As implied above, there are two broad classes of optical-CT instrument, based on scanned laser beams and pixelated detectors. The original optical-CT design, described by Gore *et al* (1996) and illustrated in figure 11(a), was similar in design to first-generation x-ray CT scanners. First-generation systems consist of a laser
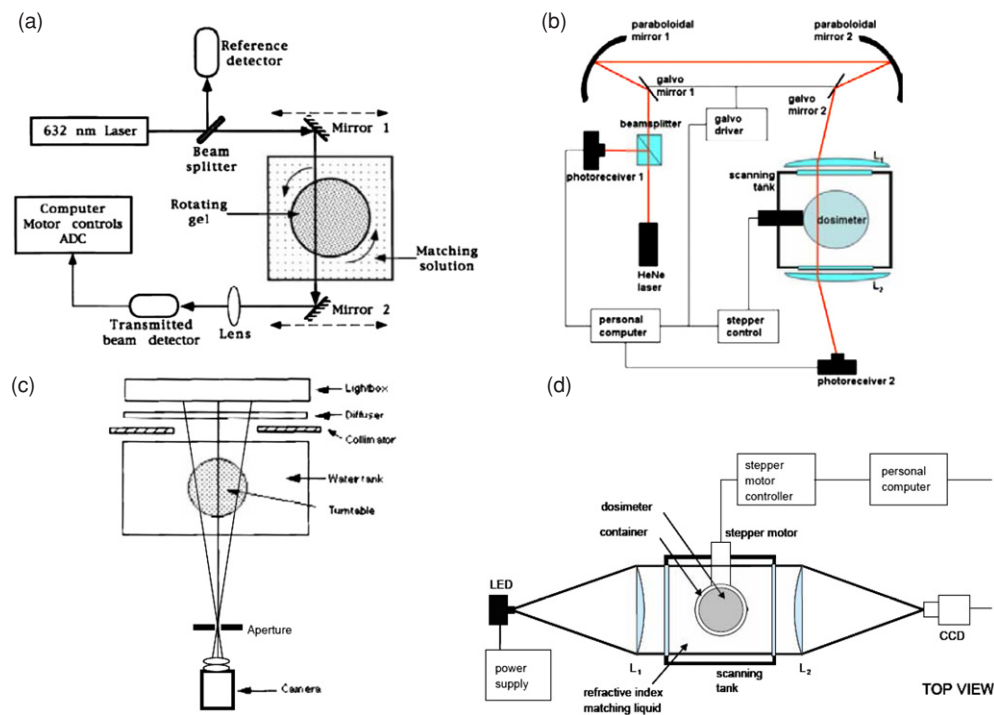
Figure 11. Schematic diagram of the different types of optical CT scanners: (a) first-generation laser system (Gore *et al* 1996); (b) fast laser scanner (Krstajic *et al* 2007); (c) cone-beam CCD scanner (Wolodzko *et al* 1999); (d) parallel-beam CCD scanner (Krstajic *et al* 2006). Reproduced with permission.

beam and a photo-detector that are mechanically coupled and are translated synchronously, by a stepper motor, in a lateral direction with respect to the phantom. Each full scan of the laser across the sample corresponds to a 1D optical projection and, after each such acquisition, the sample under study is rotated by a small angular increment. In order to avoid artifacts that are related to differences in refractive index between the gel itself, the gel container wall and the surrounding air, the phantom is mounted in a square bath containing an index-matched fluid. A further refinement is the addition to the matching liquid of a dye of similar absorption properties to the gel. This allows the most efficient use of the dynamic range of the detector (Xu *et al* 2003) and can increase the signal-to-noise in both the projections and the final reconstructed images. Since the development of this first optical scanner, several groups have published variations on the basic design (Oldham *et al* 2001, Islam *et al* 2003, Kelly *et al* 1998, Xu and Wuu 2004). Developments of Gore's original apparatus have been commercialized and marketed by MGS Inc. (Madison, Connecticut, USA) under the name 'OCTOPUS'. Results obtained using this type of scanner, as shown in figure 12(a) (Wuu and Xu 2006). While first-generation systems are most efficient at removing contaminant light, a major disadvantage is their slow scanning speed. A typical performance parameter for the original OCTOPUS system is found in Islam *et al* (2003), where slices of 128 × 128 pixels were acquired at a rate of 12 min per slice. True-3D scans, with isotropic high resolution and a large field-of-view in the slice direction, take many hours. More recently, improved imaging times of order 5 min per slice have been demonstrated using an improved version
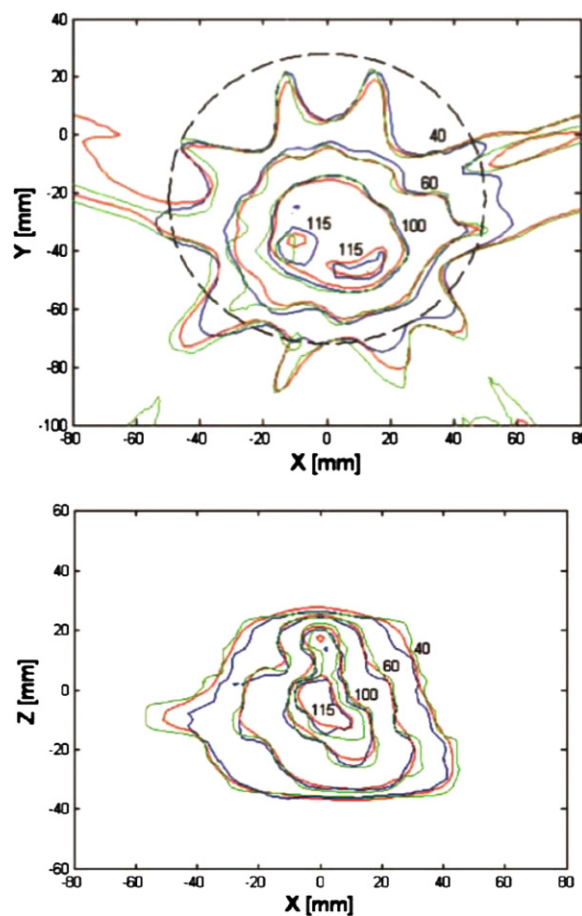
Figure 12. Examples of optical CT imaging using a laser system: (a) comparison of dose distributions in the central axial plane, with isodose lines at 40%, 60%, 100% and 115%, from treatment planning calculations (red), gel measurement (blue) and EDR2 measurements (green) (Wuu and Xu 2006); (b) same phantom as (a), results from sagittal plane 2 cm left of central plane. Reproduced with permission.

of OCTOPUS scanner (Lopatiuk-Tirpak *et al* 2008), but there is a limit as to how far this technology can be pushed and a full 3D scan still took many hours.

A number of groups have thus tried to modify the laser design in such a way as to eliminate the mechanical translation of the beam, which is the rate limiting step. Wuu *et al* (2003) introduced a design in which the laser was reflected by a rotating mirror, which allowed the beam to be scanned very rapidly across the sample in a single dimension. Van Doorn *et al* (2005) and Conklin *et al* (2006) have also demonstrated the feasibility of a rotating mirror approach. Perhaps the most sophisticated fast laser scanner built so far was introduced by Krstajic and Doran (2007) and makes use of ideas drawn from confocal microscopy. Instead of using simple rotating mirrors, this instrument manipulates the laser beam using a pair of galvanometer-controlled mirrors—see figure 11(b). This allows the beam to be scanned in 2D, with the potential of extremely rapid isotropic 3D imaging. Very few quantitative data have yet been published for any of the fast laser scanners and it is at present difficult to predict how successful they will be.

The fastest scanners reported to date use pixelated area detectors to acquire a complete 2D projection in the same time as a traditional laser scanner obtains a 1D projection, leading to dramatically reduced scan times of a few minutes instead of many hours. A cone-beam configuration was proposed by Wolodzko *et al* (1999) (figure 11(c)) and a similar device is marketed as a research tool by Modus Medical devices Inc. (London, Ontario, Canada) under the name *Vista*. Work has been published using the *Vista* system (Bosi *et al* 2007, 2009a, 2009b). A parallel beam configuration was proposed by Doran *et al* (2001) and later refined to include telecentric optics to minimize sensitivity to scattered light (Krstajic and Doran 2006, 2007, Sakhalkar and Oldham 2008)—see figure 11(d).

High quality results using both geometries have been obtained using absorbing dosimeters (e.g. PRESAGE^{TM} (Doran and Krstajic 2006, Wai *et al* 2008, Sakhalkar *et al* 2009) and Fricke gels (Babic and Schreiner 2006). However, the utility of these scanners for imaging polymer gels, where the optical contrast is generated by light scattering, is limited (see section 4.3.3).

4.3.3. Artifacts and characterization of Optical-CT performance. The vast majority of optical-CT dosimetry of polymer gels has involved the first-generation laser scanning systems described above. In-depth characterization of the potential artifacts and performance of these systems was presented in Oldham *et al* (2003), Oldham and Kim (2004) and Xu and Wuu (2004). Using 'needle phantom' experiments, geometrical distortion was found to be negligible (<0.25 mm) when the water-bath was well matched to the refractive index of the gel and was not significantly affected by radiation-induced refractive and scattering changes in the gel, or extreme geometries. When the water bath was poorly matched, a radial compression distortion was observed the magnitude of which was linear with increasing refractive index of the water bath fluid. Kelly *et al* (1998) examined the accuracy of optical-CT reconstructed attenuation coefficients in the absence of scatter, and found excellent agreement with independent measurement. The accuracy of optical-CT reconstruction and the influence of varying reconstruction parameters were also investigated.

Two of the most significant sources of artifacts in optical-CT imaging arise from reflection and refraction of light at the walls of the dosimeter. Early attempts to minimize these effects were suggested by Gore *et al* (1996), which involved limiting the range of projection data to exclude regions close to the edges of the flask. This method can give useful results if the radiation does not extend beyond about 90% of the diameter of the flask. For many radiation deliveries this is not the case as beams impinge on the flask in an axial manner. Several correction techniques to minimize refractive wall artifacts have since been proposed (Kelly *et al* 1998, Doran *et al* 2001, Oldham and Kim 2004). One method involves taking ratios of post- and pre-irradiation projection data of the same gel phantom, to eliminate common artifacts (e.g. due to refraction at the container walls, or from bubbles or specks of dirt) present in both scans. The subsequent reconstructed image reveals (ideally) only those changes in optical attenuation that were induced by the radiation. This method can improve significantly results close to the container walls, but is limited by the amount of information that can be retrieved where the transmitted light approaches zero. For a more in-depth discussion, refer to Kelly *et al* (1998) and Oldham and Kim (2004).

The source of radiation-induced optical contrast in polymer-gels is the presence of light-scattering particles, and the challenge of performing accurate optical-CT dosimetry in the presence of scatter was immediately acknowledged (Gore *et al* 1996). The presence of scattered radiation is also a well known problem in x-ray CT. Early reports of potential scatter artifacts were reported in Xu *et al* (2003) and Islam *et al* (2003), who both noted a cross-shaped artifact that appeared in optical-CT images of a high-dose square-field irradiation—see
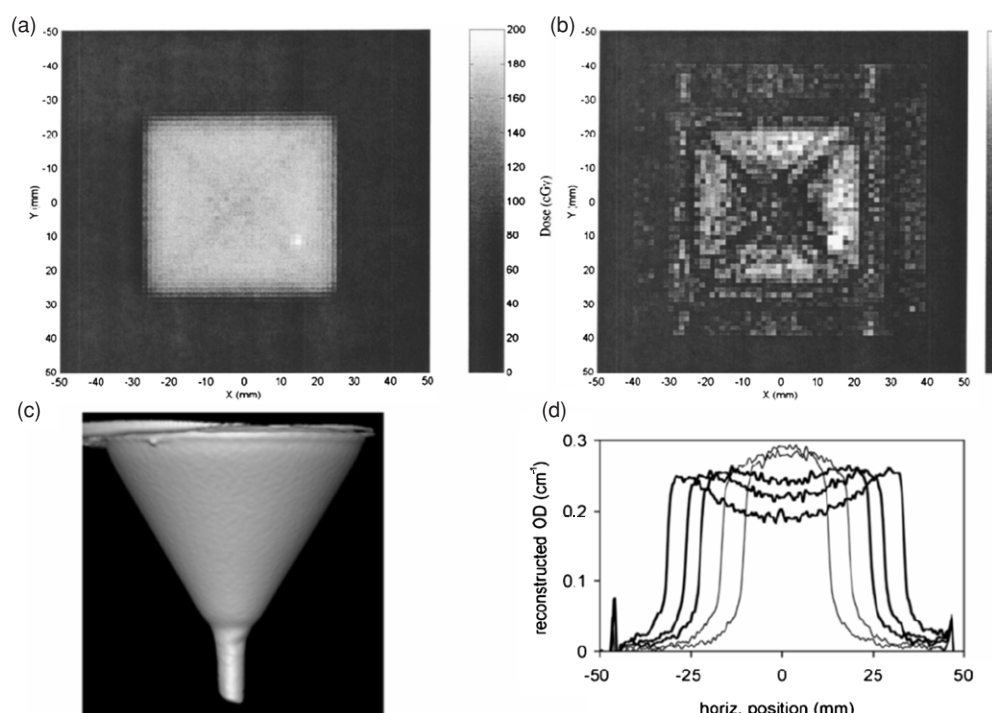
Figure 13. Examples of the effect of scatter in optical CT imaging: (a) square field image with diagonal cross artifact and (b) gamma map highlighting cross artifact (Islam *et al* 2003); (c) rendered optical CT image of a 'funnel phantom' and (d) profiles of reconstructed optical density across funnel phantom, showing both under- and over-estimation of the parameter (Bosi *et al* 2007, 2009b). Reproduced with permission.

figure 13(a). The cross artifact was confirmed to arise from light scattering in optical-CT Monte Carlo simulations performed by Oldham and reviewed (Oldham 2006) Light scattering in polymer gels was approximated by standard Mie scattering with monodispersive particles of radius 475 nm. Scatter artifacts have also been shown to systematically influence the magnitude of reconstructed attenuation coefficients to a significant degree ($>10\%$) (Oldham and Kim 2004). The situation is even more serious in the case of CCD imaging, where Bosi *et al* (2007, 2009a, 2009b) have reported large measurement errors in optical density ($\sim30\%$) in the presence of scattering—see figure 13(b).

The magnitude of these artifacts can be reduced by reducing the number-density of scattering sources, which translates to reducing the dose delivered to the gel. An uncomfortable trade-off thus occurs for any optical-CT dosimeter where scattering is the primary source of contrast. Despite these issues several groups have reported very successful 3D dosimetry verifications for laser optical-CT (Xu and Wuu 2004, Wuu and Xu 2006, Oldham *et al* 2005) indicating that workable low-scatter regimes are feasible. Work on CCD systems is at an earlier stage, but there are good anecdotal indications that scatter correction will be possible. The challenge for polymer optical-CT dosimetry is to determine the effect of scatter on the reconstructed dose in non-uniformly irradiated gel samples, without knowing the geometry *a priori*.

4.3.4. Optical-CT of non-scattering dosimeters. A dosimeter material that exhibits optical contrast through light absorbance rather than light scattering would have a clear advantage for the optical-CT approach as it would negate the scattering artifacts illustrated above. Several such materials now exist, and although these are not polymer gels, a brief discussion is warranted due to the active nature of this research area.

The first optical-CT dosimetry of a non-scattering gel was proposed by Tarte and van Doorn (1993, 1995) and subsequently by Kelly *et al* (1998), using a Fricke gel (agarose or gelatin doped with ferrous ions and the indicator xylenol orange), which exhibited a radiochromic color change. Promising performance was reported with the single limitation that the radiochromic distribution gradually diffused through the gel placing strict restrictions on the time available for imaging. However, the ready availability of an optical-CT scanner near the irradiation facility would likely remove this constraint in situations where the dose delivery itself was not too lengthy. The disadvantage of diffusion (Baldock *et al* 2001a) may also be outweighed by the speed of response of the Fricke system, which does not require time for a polymerization reaction to occur. High-quality results in a clinical situation have been demonstrated (Babic and Schreiner 2006) using Fricke gels.

PRESAGE is a polyurethane material doped with leucodyes that can be tailored to exhibit a peak radiochromic response at around 630 nm (the red HeNe laser wavelength). A number of potential advantages accrue including insensitivity to oxygen; strongly reduced diffusion; radiation-induced light absorption rather than scattering, and a solid texture amenable to machining to a variety of shapes and sizes, without the requirement of an external container. Detailed analysis of the PRESAGE/optical-CT dosimetry system has confirmed exceptional potential for 3D dosimetry (Krstajic and Doran 2007).

Exciting preliminary results for a number of other candidate gel systems were discussed at the DOSGEL 2008 meeting and the interested reader should refer to the proceedings of this conference (DOSGEL 2008) for further details.

Further details on the historical development and principles of optical-CT 3D dosimetry may be found in the previous reviews by and Oldham (2006) and Doran (2008).

4.4. X-ray CT

4.4.1. X-ray CT response mechanisms. Upon irradiation, a small change in the linear attenuation coefficient of polymer gel dosimeters enables the use of x-ray CT to be used as a scanning technique, as shown in figure 14 (Hilts *et al* 2000).

The change in linear attenuation coefficient is mainly attributed to a change in electron density originating from the expulsion of water in the polymer clusters (Trapp *et al* 2002, Brindha *et al* 2004). CT images are expressed as CT numbers (N_{CT}), in Hounsfield units (H). N_{CT} are measures of the linear attenuation coefficient of the sample (μ) relative to that of water (μ_w):

$$N_{CT} = 1000 \cdot \frac{\mu - \mu_w}{\mu_w}. \tag{18}$$

Density is, in theory, the sole gel parameter affecting μ (and therefore N_{CT}). Hence, changes in irradiated gel density (ΔN_{CT}) are directly proportional to a change in gel density ($\Delta \rho_{gel}$):

$$\Delta \rho_{gel} = K \Delta N_{CT} \tag{19}$$

where K is a function of un-irradiated gel density. For PAG gel, $K \approx 1$ and ΔN_{CT} in H is numerically equivalent to gel density change in kg m^{-3}.

Trapp *et al* (2001a) have made direct measurements of the change in PAG linear attenuation coefficient (μ), as well as PAG density, with dose. Their results proved that a change in μ
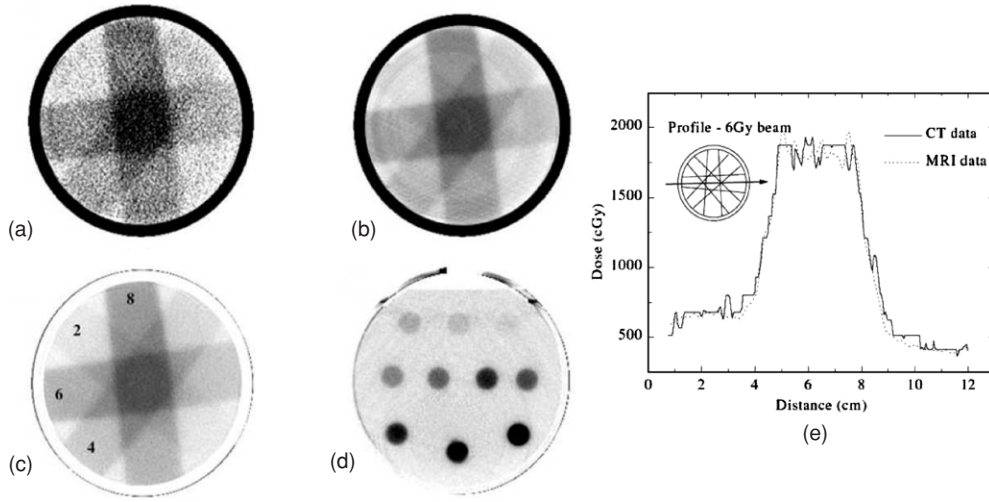
Figure 14. (a) X-ray CT images of PAG irradiated with four 3×3 cm^2 10 MV photon beams (doses in Gy at the depth of maximum dose) (a)–(c) and parallel opposed, 2 cm diameter, circular 6 MV photon beams (d). A preliminary CT image is shown in (a) and a noise reduced (by averaging) CT image in (b). Note the ring and beam hardening artifacts in (b). Images in (c) and (d) are the optimized images resulting from image averaging and background subtraction with the images acquired from an unirradiated blank gel. The dose profile along the axis of the 6 Gy beam path corresponding to the dose image of (c) is shown in (e) in comparison with a profile obtained in an MR acquired dose image (Hilts *et al* 2000). Reproduced with permission.

with dose accounts for the observed ΔN_{CT} in CT images of irradiated PAG (figure 15). Figure 15(b) illustrates the linear relationship between changes in PAG μ and density. Mather *et al* (2002a) also measured changes in gel density with dose for PAG, as well as the normoxic methacrylic acid based MAGIC gel. Their results indicate a smaller change in density with dose for the MAGIC than the PAG gels.

No mass is added to polymer gels through irradiation. Hence, the observed change in density is due to either a redistribution of mass within the system, or to a change in gel volume. A volumetric decrease would be required to account for the increase in gel density with dose, as seen above. There exists a potential loss of spatial integrity in polymer gels due to radiation-induced decrease in volume. Trapp *et al* (2001b) provided a qualitative calculation to show that four times the currently observed PAG density change is allowable before spatial distortions exceed 2 mm, the spatial resolution limit set by the International Commission on Radiation Units and Measurements (ICRU 1987).

A model has been developed to aid in understanding the density change observed in irradiated polymer gel (Hilts *et al* 2004). The model describes the density change as a function of the amount of polymer formed and an intrinsic density change that occurs when monomer is converted to polymer:

$$\Delta \rho_{\text{gel}} = \%T_{0Gy}(1 - f_m)\Delta_{\text{polymer}} \tag{20}$$

where $\Delta \rho_{\text{gel}}$ is the gel density change, $\%T_{0\text{Gy}}$ is the total monomer fraction in an unirradiated gel, f_m is the fraction of monomer remaining at a given dose, and $\Delta \rho_{\text{polymer}}$ is the intrinsic gel density change per unit dose. Combined with experimental investigations of PAG gel performed using CT and Raman spectroscopy, the model revealed two properties of PAG density change. The first is that the intrinsic density change ($\Delta \rho_{\text{polymer}}$) occurring per weight fraction monomer converted to polymer depends on the fraction of monomer that is the
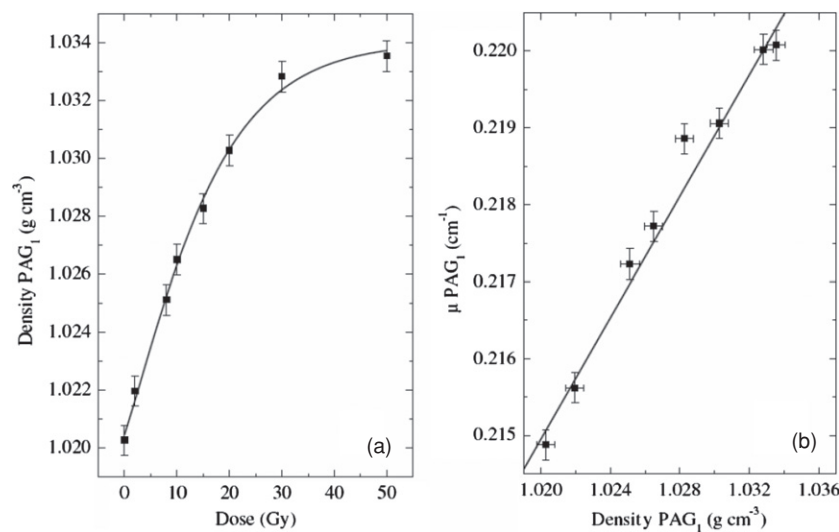
Figure 15. (a) Density of PAG as a function of dose. (b) Linear attenuation coefficient (μ) of PAG as a function of density (Trapp *et al* 2002). Reproduced with permission.

bis-acrylamide crosslinker (%C). Since %C affects the structure of the formed polymer, it is likely that PAG density change depends on this polymer structure. The second property is that the total PAG density change ($\Delta\rho_{gel}$) is linearly related to the total fraction of monomer in the system (%T). This highlights increasing %T as a potential method for improving contrast in CT gel images.

X-ray CT imaging of polymer gel dosimeters typically produces low-contrast images due to the low sensitivity (i.e. minute density changes with dose) of the technique. Table 5 lists the dose sensitivities of x-ray CT polymer gel dosimetry as measured by several research groups. The dose response for a standard PAG (6%T, 50%C) is mono-exponential with a saturation dose of $\sim$25 Gy. The sensitivity of the 'quasi-linear' low-dose region (0 to 8 or 10 Gy) ranges from 0.71 ± 0.02 to 0.86 ± 0.04 HGy^{-1}. Trapp *et al* (2001a) found slight decrease in gel dose–response sensitivity with gelatin concentration. Furthermore, they found that use of agarose in place of gelatin produced a significantly more sensitive, although less predictable, dose response. Hilts *et al* (2004), as described above, determined that the increase in gel dose response sensitivity with %T is linear (doubling %T will double sensitivity). Furthermore, PAG %C was found to have significant effect on CT dose response. Mid-range %C gels exhibit sensitive, exponential responses while low and high %C gels exhibiting weak, highly linear responses.

The CT dose response of three normoxic gels has also been studied: MAGIC, MAGAT and PAGAT. All three gels have mono-exponential CT dose responses with quasi-linear regions at lower doses. Hill *et al* (see table 5) showed that MAGIC gel exhibits a CT dose response significantly less sensitive than traditional PAG gel, but with a larger dose range. MAGAT gel has a CT dose response similar to traditional PAG gel both in terms of sensitivity and dose range. In contrast, PAGAT gels exhibit a lowered dose response than traditional anoxic PAG gel, as illustrated by Brindha *et al* (2004) and Jirasek *et al* (2009) (dose response sensitivities: 0.34 ± 0.01 HGy^{-1} and 0.36 ± 0.04 HGy^{-1} over regions of 0 to 10 and 16 Gy, respectively).

Table 5. CT dose response data for studied polymer gel dosimeters (Hilts 2006).

Polymer gel[a]	Sensitivity (H Gy^{-1})	Linear D_{max} (Gy)	Reported dose resolution (Gy)[b]	Calc. relative dose resolution (%)[c]	Reference
PAG	0.86 ± 0.04	8		10.0	Hilts et al (2000)
	0.71 ± 0.02	10	1.0	12.5	Trapp et al (2001)
	0.83 ± 0.03	8		10.2	Hilts et al (2005)
PAG (12%T)	1.43 ± 0.05	10	1.1	4.8	Trapp et al (2001a)
PAG (agarose)	1.2 ± 0.1	8	2.4	7.0	Trapp et al (2001a)
PAG (0%C)	0.226 ± 0.006	20		15.0	Hilts et al (2005)
PAG (70%C)	0.241 ± 0.005	20		14.1	Hilts et al (2005)
PAG (100%C, 3%T)	0.039 ± 0.002	>100		17.5	Hilts et al (2005)
PAGAT	0.31 ± 0.03	15		14.6	Brindha et al (2004)
	0.70 ± 0.03	–			Venning et al (2004)
	0.36 ± 0.04	16		11.8	Jirasek et al (2009)
MAGAT	0.85 ± 0.08	10		7.9	Brindha et al (2004)
MAGIC	0.38 ± 0.07	60	1.3	3.0	Hill et al (2005a)

[a] All gel formulations are standard (6%T, 50%C—where applicable) except for parameters in parentheses.
[b] Dose resolution (absolute, Gy), 95% confidence (Hill et al 2005a, Trapp et al 2001a).
[c] Relative (%) dose resolution, 95% confidence, calculated using uncertainty in $N_{CT} = 0.3$ H for all gels. Actual dose resolution may vary depending on the image noise in a particular situation.

4.4.2. X-ray CT imaging considerations. The low CT dose sensitivity of polymer gel dosimeters implies that in order to enable the use of x-ray CT for radiation dosimetry purposes, several imaging averages have to be taken for each slice. The SNR is proportional to $\sqrt{N}$ where N is the number of averages. It has been shown that typically between 16 and 32 image averages provide a reasonable trade-off between SNR improvement and imaging time and tube load (Hilts et al 2005).

The parameters used for CT imaging do not affect the sensitivity of the dose response. The only imaging factor with this potential, tube voltage (μ, depends on beam energy), has been shown to have no effect for both PAG and MAGIC gels. However, actual N_{CT} values for polymer gel can vary with x-ray tube temperature and it is recommended to warm-up a CT scanner before using it for gel dosimetry.

Apart from the inferior dose resolution of the CT gel dosimetry technique, this scanning method is found to have favourable characteristics in terms of intra-batch reproducibility and temperature insensitivity with a change in dose sensitivity of only 4 mH Gy^{-1} $^{\circ}$C^{-1} recorded for a PAG dosimeter (Hilts et al 2000). CT imaging technique can, however, have a dramatic effect on image noise and, therefore, the achievable dose resolution of CT polymer gel systems. Reconstruction algorithm has the largest single effect on image noise. For example, the 'edge' algorithm on a GE scanner can produce images ~5 times noisier than the 'standard' algorithms. Table 6 lists the quantitative effects on image noise of selectable imaging parameters (voltage (in kV), current (in mA), slice scan time, and slice thickness), number of image averages (NAX) and pixel dimension as achieved via binning pixels post-imaging. In summary, the tube voltage has the largest effect on image noise. Field of view (FOV) is another parameter selectable on many CT scanners and increasing FOV is found to increase image noise. CT

Table 6. Factors affecting CT image noise (Hilts 2006).

Factors affecting image noise (symbol)	Relationship with image noise (σN_{CT})
Phantom diameter (d)	$\sigma N_{CT} \propto e^d$
Tube voltage (kV)	$\sigma N_{CT} \propto (kV)^{-1.4}$
Tube current (mA)	$\sigma N_{CT} \propto (mA)^{-0.5}$
Slice scan time (mA)	$\sigma N_{CT} \propto s^{-0.5}$
Number of averages (NAX)	$\sigma N_{CT} \propto (NAX)^{-0.5}$
Pixel dimension (w)	$\sigma N_{CT} \propto e^w$ (or $w)^{-0.65}$
Slice thickness (h)	$\sigma N_{CT} \propto h^{-0.5}$

imaging parameters affect image noise independently of one another. Hence, the noise level resulting from any imaging protocol can be deduced from a single noise measurement (given known imaging parameters) through application of the relationships given in table 6.

In selecting CT imaging protocol, one must consider requirements for dose resolution (and therefore image noise), imaging time and spatial resolution. A compromise exists between achieving low noise (high CT scanning technique, large slice thickness and pixel size) and both high spatial resolution (thin slices and small pixel size) and short imaging times (fewer slices imaged, reduced load on the x-ray tube). The following general recommendations can be made.

- Use a standard or low noise reconstruction algorithm.
- Maximize voltage before increasing current, time or NAX. This is because voltage, current and NAX all affect load on the x-ray tube equally, but the voltage has the greatest affect on image noise.
- Maximize slice thickness and use a smooth reconstruction algorithm when imaging uniform dose calibration vials as spatial resolution is not important.

As an additional step, a background subtraction procedure is recommended to remove artifacts from the images. This procedure was introduced with the feasibility of CT for gel read-out and has been used with continued success since, in various forms, by all groups performing CT gel dosimetry.

X-ray CT dose in imaged polymer gel dosimeters. X-ray CT imaging of polymer gel dosimeters delivers dose to the gel, potentially creating further polymerization within the gel. This effect has been studied recently using a combination of CT dose measurements (with an ionization chamber), CT imaging and Raman spectroscopic measurements (Baxter *et al* 2007). The CT-dose-induced change in CT number for a range of imaging protocols and gel container sizes is shown in table 7. This study was performed for a PAG gel manufactured with THPC as antioxidant, with a reported gel sensitivity of 0.36 ± 0.03 H Gy^{-1}. Induced ΔN_{CT} for all imaging protocols remains below the minimum detectable ΔN_{CT} of 0.2 H. For imaging protocols requiring large image averages (e.g. 64 averages) per slice, the ΔN_{CT} can exceed the minimum detectable limit (e.g. 0.5 H). Currently, this study has been performed for only one type of gel (normoxic PAG). Recent efforts in the development of gels with increased sensitivity for CT imaging (Koeva *et al* 2009) may alter these results.

X-ray CT post-processing. Several post-processing noise reduction methods have been proposed to increase the SNR in the dose images (Hilts *et al* 2004, Jirasek *et al* 2006b, Hilts and Jirasek 2008). Figure 16 illustrates the ability of image filters to positively affect image quality in x-ray CT polymer gel dosimetry.
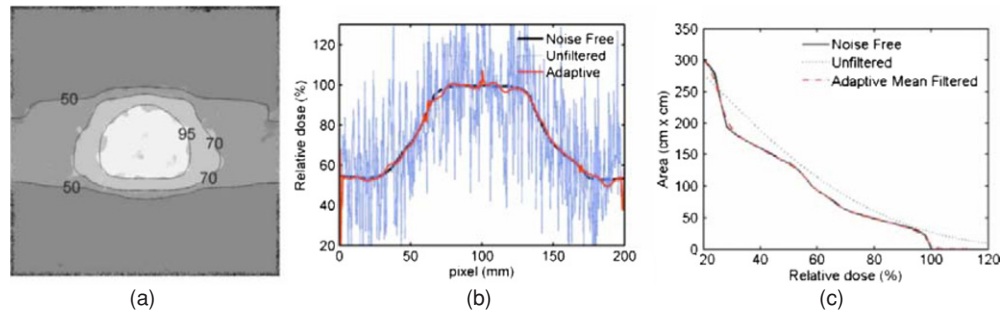
Figure 16. Adapative mean filtering ($K = 11$, $n = 2$) for synthetic 'gel' image (conformal prostate). (a) Noise free image with filtered image contour overlay, (b) profiles through noise-free, filtered and unfiltered images, and (c) dose area histograms of noise-free, filtered and unfiltered images (Hilts and Jirasek 2008). Reproduced with permission.

Table 7. CT dose and induced σN_{CT} for a range of imaging protocols (Baxter *et al* 2007).

| Imaging protocol	Phantom	kVp	mAs	Slice (mm)	Dose/image (cGy)	No of image averages	ΔN_{CT}
Volumetric (CTDI)	16 cm diam. (center)	120	200	2	3.38 ± 0.14	16	0.105 ± 0.001
				5	3.4 ± 0.1	16	0.105 ± 0.001
				10	3.4 ± 0.1	16	0.107 ± 0.001
	16 cm diam. (edge)	140	200	2	3.5 ± 0.1	16	0.109 ± 0.001
				5	3.5 ± 0.1	16	0.110 ± 0.001
				10	3.6 ± 0.1	16	0.111 ± 0.001
	16 cm diam. (center)	140	200	2	4.4 ± 0.2	16	0.136 ± 0.002
				5	4.4 ± 0.2	16	0.136 ± 0.002
				10	4.5 ± 0.2	16	0.138 ± 0.002
	16 cm diam. (edge)	140	200	2	4.5 ± 0.2	16	0.139 ± 0.002
				5	4.5 ± 0.2	16	0.139 ± 0.002
				10	4.6 ± 0.2	16	0.141 ± 0.002
Single slice (PD)	16 cm diam. (center)	120	200	2	0.70 ± 0.05	32	0.0430 ± 0.0002
				5	0.91 ± 0.06	32	0.0560 ± 0.0004
				10	1.07 ± 0.07	32	0.066 ± 0.001
	16 cm diam. (edge)	120	200	2	1.6 ± 0.1	32	0.099 ± 0.001
				5	1.7 ± 0.1	32	0.107 ± 0.001
				10	2.1 ± 0.2	32	0.133 ± 0.002
	16 cm diam. (center)	140	200	2	0.83 ± 0.06	32	0.0510 ± 0.0003
				5	1.07 ± 0.07	32	0.066 ± 0.001
				10	1.23 ± 0.09	32	0.076 ± 0.001
	16 cm diam. (edge)	140	200	2	1.5 ± 0.1	32	0.095 ± 0.001
				5	2.0 ± 0.1	32	0.125 ± 0.002
				10	2.1 ± 0.2	32	0.130 ± 0.002
Calibration (PD)	Calibration gel vials	140		10	2.3 ± 0.2	16	0.0720 ± 0.0001
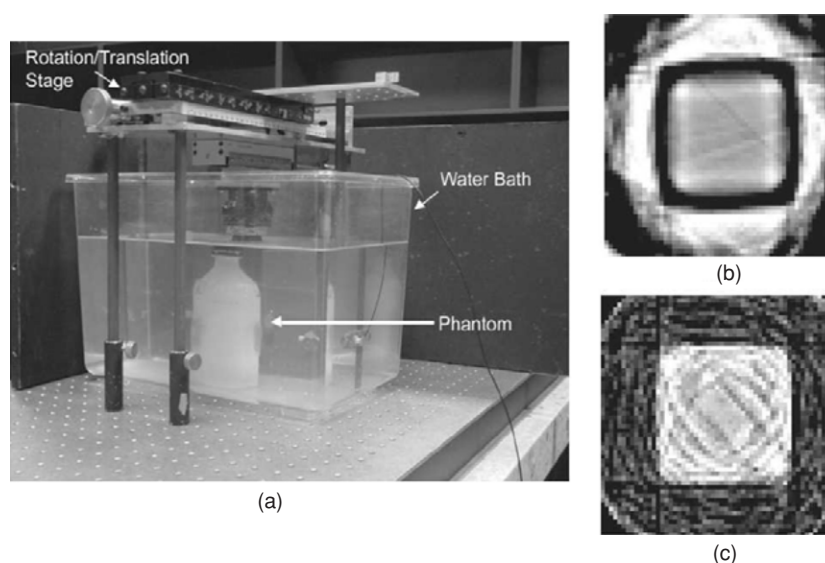
Figure 17. (a) Ultrasound tomography system. Transmission (b) and time-of-flight image (c) of a PAG irradiated with a 4×4 cm^2 square photon beam. Scan lines are acquired at a translational resolution of 1 mm and a rotational resolution of $2°$ with a total rotation of $360°$. The reconstructed image resolution was 1.45×1.45 mm^2 (Mather and Baldock 2003). Reproduced with permission.

4.5. Ultrasound evaluation

It was found that ultrasonic properties such as the acoustic speed of propagation, ultrasonic absorption and ultrasonic attenuation change with radiation-induced polarization in polymer gel dosimeters (Mather *et al* 2002b, 2003a). Changes in ultrasonic speed to absorbed dose for PAG and MAGIC gel dosimeters are related to both changes in the elastic modulus on absorbed dose and on changes in mass density. For PAG the changes in mass density with absorbed dose were the predominant factor (Mather *et al* 2002a). The changes in ultrasonic properties with absorbed dose enable the use of ultrasound imaging. The ultrasonic absorption may be correlated with relaxation mechanisms active over a broad range of ultrasound frequencies such as interactions between water and polymer via hydrogen bonding and proton transfer and relaxation associated with motion of polymer side groups (Mather *et al* 2003b, Crescenti *et al* 2007). A prototype tomographic ultrasound system is constructed that consists of a translation and rotation table onto which the phantom is suspended, an ultrasound transducer and a needle hydrophone (Mather and Baldock 2003). The phantom and ultrasound components are immersed in a water bath to avoid attenuation in air (see figure 17). Ultrasonic pulses are transmitted by the transducer and received by the needle hydrophone. From the time difference and amplitude difference of the transmitted and received pulses, a time-of-flight (TOF) and transmission signal can be derived. By rotating and translating the phantom with respect to the transducer and hydrophone several tomographic projections are obtained. From these tomographic projections, TOF and transmission images can be produced by filtered back projection.

The image quality of the TOF image is better than that of the transmission image, although the contrast between the unirradiated and irradiated part is higher in the transmission image. Artifacts in the transmission image are predominantly due to an acoustic impedance mismatch
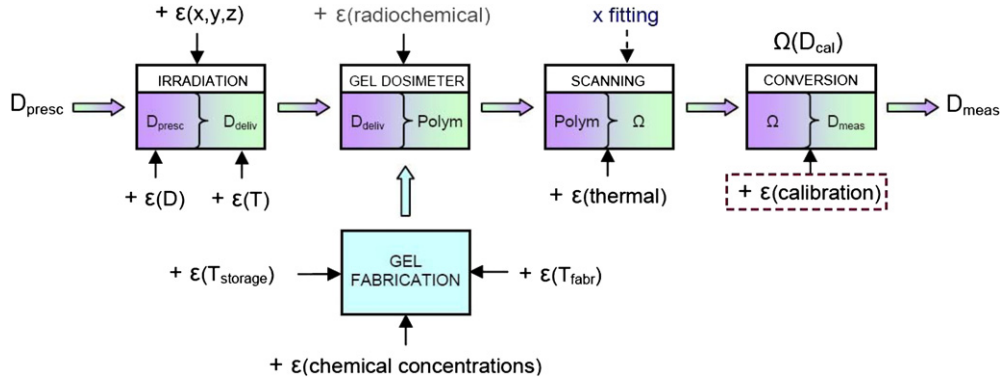
Figure 18. Gel dosimetry is performed in different stages. At each stage errors can add, leading to a decrease in the overall precision and accuracy (De Deene 2006). Reproduced with permission.

between water and gel phantom. There is much room for improvement of image quality by matching the acoustic properties of the matching fluid, by the use of more sophisticated acoustics components and improvements in the alignment of the system.

5. Accuracy and precision of polymer gel dosimetry

5.1. Sources of error

In the case of 3D gel dosimetry, both dosimetric and spatial accuracy and precision need to be considered as in the final result of a gel dosimetry experiment (and any radiation treatment), the spatial and dosimetric dimensions are interrelated. In the measured spatial dose distribution (the result of a 3D gel dosimetry experiment), it is theoretically impossible to extract both dosimetric and spatial errors. To encompass both spatial and dosimetric performance in one parameter the gamma-index was introduced (Low *et al* 1998). The gamma-index is defined as a metric given by the equation

$$\gamma = \sqrt{\frac{(\vec{r} - \vec{r}_2)^2}{\text{DTA}_a^2} + \frac{(D - D_r)^2}{\text{DD}_a}} \qquad (21)$$

with $\vec{r}$ and $\vec{r}_2$ the position vectors of a point in the experimental dose distribution and the nearest point with the same dose value in the reference dose distribution, respectively. The dose values at the position $\vec{r}$ in the experimental dose distribution and reference dose distribution are given by D and D_r, respectively. The acceptance criteria in spatial position and dose are given, respectively, by DTA_a and DD_a. By plotting the gamma-index on a pixel-by-pixel base a gamma map is obtained. Other dose distribution comparisons are performed on the basis of maximum allowed dose differences (Jiang *et al* 2006).

Various sources can lead to a loss in both accuracy and precision at different levels of the measurement process (see table 8). To evaluate the performance of a 3D gel dosimeter, the accuracy and precision can be evaluated at different stages of the gel dosimetry experiment (figure 18).

The prescribed dose distribution as obtained from the radiation treatment planning system (D_{presc}) is delivered by the irradiation facility (Linac, Gamma Knife, afterloader, etc) to the gel dosimeter resulting in a delivered dose distribution (D_{deliv}). The gel dosimeter is read out

Table 8. Factors influencing the precision and accuracy in 3D gel dosimetry under conditions of good practice.

	Precision		Accuracy	
	Dosimetric	Spatial	Dosimetric	Spatial
Fabrication	Dose sensitivity of the gel dosimeter	Spatial variations in manufacturing temperature	Discrepancies between calibration vials and phantoms Chemical stability spatial stability	Volumetric contraction of the gel dosimeter
Radiation	Stochastic variation in the delivered dose Variations in the temperature during irradiation	Variations in phantom positioning Spatial temperature variations in combination with temperature sensitive dose response	Positioning error of the calibration phantom Dose-rate-dependent response	Phantom positioning error
	Variations in the temperature during irradiation Reproducibility of calibration phantom positioning Radiochemical noise	Spatial temperature variations in combination with temperature	Dose-rate-dependent response Energy-dependent response Temperature dependence Tissue equivalence Recipient wall effects	
Imaging	Stochastic noise	Voxel size/shape (resolution)	Voxel shape (bandwidth) imaging artifacts Temperature during scanning	Imaging artifacts

by use of a non-invasive imaging technique (MRI, optical-CT, x-ray CT, ultrasound, etc). The result is a parametric map (Ω) that reflects the absorbed dose distribution. The parametric map displaying a physical quantity (R_1, R_2, MT, optical density, CT numbers, speed of sound, etc) is converted to a dose map by use of a calibration curve ($\Omega(D)$) that is obtained by passing through all of the above-mentioned stages but starting with a known dose or dose distribution ($D_{presc} = D_{cal}$)

When a gel dosimetry experiment is repeated many times, there will be stochastic deviations in both radiation output ($\varepsilon(D)$) and spatial errors ($\varepsilon(x, y, z)$) that may result in both spatial and dosimetric deviations in the resulting dose distribution. The magnitude of the positioning deviations will depend on the robustness of the positioning operation. Sophisticated methods to accurately position the gel dosimeters apply stereotactic frames and fiducial markers (Meeks *et al* 1999). Note that any positioning error during the irradiation of calibration phantoms may also give rise to dosimetric errors in the final dose distribution. It has been shown that in some gel dosimeters the dose response depends on the temperature of the gel dosimeter during irradiation and thus temperature variations may introduce dose variations ($\varepsilon(T)$) (Salomons *et al* 2002).

The response of the gel dosimeter is susceptible to variations in different parameters during fabrication of the gel (De Deene 2006). Differences in the temperature treatment during ($\varepsilon(T_{fabr})$) and after ($\varepsilon(T_{storage})$) fabrication of the gel dosimeter as well as variations in the concentration of the chemical components ($\varepsilon(\text{chemical concentrations})$) may result in differences in the dose response. Most of these deviations are compensated by using calibration phantoms that are constructed from the same manufactured batch of gel. However, it may be difficult to keep the temperature history after fabrication ($\varepsilon(T_{storage})$) similar for both the gel dosimeter phantom and the calibration vials because of the differences in phantom size (Dumas *et al* 2006, De Deene *et al* 2007a).

Upon irradiation, a complex set of radiation-induced chemical reactions take place. On a molecular level, these reactions are stochastic in nature ($\varepsilon(\text{radiochemical})$). In most gel dosimetry applications the voxel size is several orders of magnitude larger than the molecular size. As a result, this intrinsic radiochemical noise contribution can be neglected.

After irradiation, the gel dosimeter is scanned. During scanning, detector (thermal) noise ($\varepsilon(\text{thermal})$) will add to the measurements. The processing (fitting) of acquired data may have a large influence on the amplification of the noise parameter. For example, in quantitative R_2 MRI it is found that a least-square fit will amplify the thermal noise in the base images to a larger extent than a chi-square based minimization (De Deene *et al* 1998b). Imaging artifacts may result in systematic errors. Imaging artifacts can result in both dosimetric errors and in geometrical distortions.

To convert the measured physical quantity (R_2, MT, OD, CT) to dose a calibration procedure is performed. The calibration phantom has been subjected to the same pathway as the 3D gel dosimetry phantom. As a result, the calibration dose–response curve will also be susceptible to the same error sources. After calibration, the calibration error ($\varepsilon(\text{calibration})$) will add to the overall dose error.

5.2. Precision

Theoretically, the overall precision of the gel dosimeter would be measured by performing a reproducibility study of several 3D gel dosimetry experiments. Such a study would also include inter-operator variability. Due to the infinite number of different radiation treatment configurations, such a study is not feasible.

The overall dosimetric precision is governed by variations in the several operations that take place in the dosimetry experiment. The first step in a gel dosimetry experiment is weighing the chemicals. Stochastic variations in the weighing will result in variations in the measured dose-related value (R_2, MT, OD, CT) as the dose–response is determined by the chemical composition highlighting that the calibration samples should come from the same manufactured batch of polymer gel as the phantom. It is found that other manufacturing conditions may also have an influence on the dose–response such as the temperature during fabrication (De Deene 2006). Stochastic variations in the controlled temperature will therefore also lead to variations in the measured dose-related value. Also during irradiation there are different sources of stochastic variable contributions that determine the overall dosimetric precision such as variations in the dose delivery, variations in the temperature during irradiation and stochastic variations in the positioning of the calibration phantoms. Any form of scanning of the gel dosimeter will introduce thermal detector noise. The noise contribution is determined by some scan parameters. Often, the scan parameters can be optimized in order to achieve an optimal parameter of precision.

The concept of dose-resolution was introduced to evaluate the intrinsic dosimetric precision in terms of dose sensitivity and scanning signal-to-noise (SNR) (Baldock *et al* 2001b). The dose resolution, written as D_Δ^p, is defined as the minimal detectable dose difference within a given level of confidence, p. The dose resolution is related to the standard deviation on dose σ_D by the equation

$$D_\Delta^p = k_p \cdot \sqrt{2} \cdot \sigma_D \tag{22}$$

with k_p the coverage factor for a coincidence interval p. For a 95% confidence level the dose resolution becomes $D_\Delta^{95\%} = 2.77 \cdot \sigma_D$. In most radiation dosimetry experiments, gel dosimeters are used as relative dosimeters in the sense that the dosimeter is exposed to the same treatment as the patient but with a different total radiation dose. The total dose delivered to the dosimeter is scaled to cover the active dose range of the dosimeter. In this context, it is preferable to use the concept of dose resolution relative to the operating dose range, here defined as relative dose resolution $D_{\Delta\%}^p$:

$$D_{\Delta\%}^p = \frac{D_\Delta^p}{(D_{\max} - D_{\min})} = \sqrt{2} \cdot k_p \cdot \frac{\sigma_D}{(D_{\max} - D_{\min})}. \tag{23}$$

If the dose maps are derived from quantitative MRI-R_2 maps, it can be shown that the relative dose resolution $\left(D_{\Delta\%}^p\right)$ is equal to the relative R_2 resolution $\left(R_{2\,\Delta\%}^p\right)$ which is defined in a similar way:

$$D_{\Delta\%}^p = \sqrt{2} \cdot k_p \cdot \frac{\sigma_D}{(D_{\max} - D_{\min})} = \sqrt{2} \cdot k_p \cdot \frac{\sigma R_2}{(R_{2\,\max} - R_{2\,\min})} = R_{2\,\Delta\%}^p. \tag{24}$$

It should be noted that dose resolution does not include stochastic variations in chemical concentrations, in dose delivery or in the calibration procedure. For that reason, dose resolution can be considered as an intrinsic lower limit of dosimetric precision.

It is a misconception that the dose resolution is a parameter that is only related to the gel dosimeter formulation. Actually, the dose resolution is dependent on both the dosimeter itself *and* the signal acquisition system and strategy. In some publications, the concept of dose resolution has been used as the criterion to compare different types of gel dosimeters for a given set of scanning parameters. It should be recalled that the conclusions may differ if different scanning parameters were used. The concept of dose resolution however is very practical in assisting the optimization of the MRI sequence in terms of intrinsic precision (De Deene and Baldock 2002). In optimizing the MRI sequence, it is also important to take into account the number of slices that are required for the 3D dosimetry application. Depending on the MRI facilities three different optimization strategies can be followed.

5.2.1. Using a single spin–echo sequence. It can be shown mathematically that if one has only access to a single spin–echo sequence, a two-point(s) (two different echo times) method is preferred (De Deene *et al* 1998b). For two given echo times, for a specific R_2 value and for a signal-to-noise ratio (SNR) in the first base image, the relative dose resolution $D^p_{\Delta\%}$ can be calculated. The SNR in the first base image is a scanner-related parameter that depends mainly on the magnetic field strength, the receiver bandwidth, the radio-frequency coil and to a smaller extent on the electro-magnetic properties of the phantom and on the echo time corresponding with the first image. It is found that in this two-point(s) approach the optimum time interval between both echo times is

$$(T_E - T_E)_{\text{opt}} = 1 \times 10^9 T_2. \tag{25}$$

This equation applies for a single value of T_2 or for polymer gel dosimeters with a narrow range of T_2 values centered around this T_2 value. The optimum TE interval (and acquisition fraction) for a broader range of T_2 values can be derived from tables 1 and 2 in De Deene and Baldock (2002).

5.2.2. Using a multiple spin–echo sequence with a fixed number of echoes. Quantitative R_2 images can also be calculated from different T_2-weighted images acquired with a multiple-echo sequence. The quantitative R_2-image is obtained by fitting a mono-exponential decay-function to the pixel intensities of corresponding pixels in the T_2-weighted images. A multiple spin–echo sequence is preferred over a single spin–echo sequence because several differently T_2-weighted images are acquired within the same measurement time increasing the overall signal-to-noise ratio in the calculated R_2-images. A multiple spin–echo sequence is available on many MRI scanners with the number of available echoes 'hard-coded' in the sequence. In this case, it is advisable to optimize the TE interval. The TE interval is defined as the time interval between the first and the last echo in the multiple spin–echo acquisition window. The optimal TE interval can be derived (figure 9 in De Deene *et al* (1998b)). It is also found that the optimization also depends on the fitting algorithm that is used to derive the R_2 value. For more than seven echoes and using a chi-square minimization fitting algorithm, the optimal TE interval is approximately two times the T_2 value of the sample. To a good approximation this also applies to the median R_2 for a phantom containing a range of R_2 values.

5.2.3. Using a multiple spin–echo sequence with an arbitrary number of echoes. This is the optimal approach from the perspective of optimization of the dosimetric precision when more slices are acquired. The reasoning behind this is that within an optimal TE recording period it is preferable to acquire as many echoes as possible. To optimize this sequence, the TE spacing is taken as short as possible without introducing any artifacts, thereby optimizing the number of echoes. Most often, there is an upper threshold on the available echoes in the multiple spin–echo sequence. When the recommended (optimal) number of echoes exceeds the number of available echoes, the TE spacing is increased to cover the optimal TE interval. Table 5 in De Deene and Baldock (2002) provides the optimal number of echoes for a gel with a certain R_2 range ($R_{2,\text{min}}$, $R_{2,\text{max}}$). The number of echoes is limited by the minimal inter-echo time spacing which is determined by machine related characteristics such as the maximum gradient strength, sampling rate and SAR considerations. In practice, it is also advisable to check for imaging artifacts (uniformity, dose errors and geometrical distortions) while decreasing the inter-echo time spacing. Then, if more than one slice is acquired, the time interval between the end of the TE recording period and the repetition time can be used to scan another slice. Above a certain number of slices, not all slices can be recorded within the chosen repetition
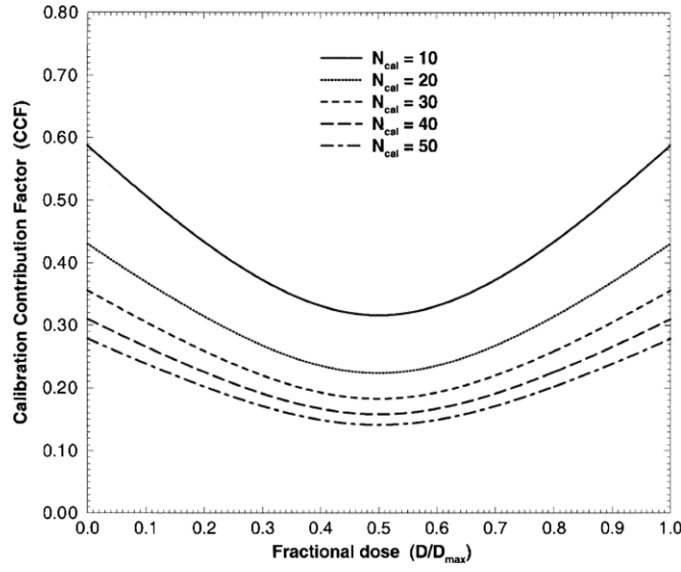
Figure 19. The calibration contribution factor (CCF) as a function of dose for various numbers of calibration points (N_{cal}). The values on the abscissa are relative to the maximum dose D_{max} in the calibration plot (De Deene *et al* 1998b). Reproduced with permission.

time. In that case, the repetition time should be extended to cover exactly the time needed to acquire all slices.

In order to make an equitable comparison between different imaging modalities, a parameter of intrinsic dosimetric precision on readout (IP_D) can be defined which is independent of spatial resolution and measurement time:

$$IP_D = \frac{1}{D^p_{\Delta\%} \cdot \Delta V \cdot \sqrt{t_{\text{meas}}}}. \tag{26}$$

The dose–R_2 curve is used to calibrate the R_2 map. The uncertainty σ^*_D on the estimated dose value D^* extracted from the fitted linear dose–R_2 plot with equation $R_2 = R_{2_0} + \alpha \cdot D$ is given by

$$\sigma^*_D = \frac{\sigma_c}{\alpha} \sqrt{\frac{(D^* - \bar{D})^2}{\sum_{i=1}^{N_{cal}} (D_i - \bar{D})^2}} = \frac{1}{N_{cal}} \tag{27}$$

with σ_c the standard deviation on R_2 in the calibration points (De Deene *et al* 1998b). This value is derived from the standard deviation in a region of interest of the calibration vials σ_{ROI}. If N_{ROI} is the number of points in the region of interest, the standard deviation on the calibration point is given by $\frac{\sigma_{\text{ROI}}}{\sqrt{N_{\text{ROI}}}}$. The value $\bar{D}$ is the mean dose of all dose values in the calibration plot $\left(\bar{D} = \frac{1}{N_{\text{calc}}} \sum_{i=1}^{N_{\text{calc}}} D_i\right)$ with D_i the dose in the calibration point with index i and N_{cal} the number of calibration plots.

The square root in equation (27) is named the calibration contribution factor (CCF). The CCF for an equally dose-spaced calibration plot is shown in figure 19.

5.3. Accuracy

The problem in evaluating the final accuracy of the dose maps obtained in a gel dosimetry experiment is that there is no 3D 'gold standard' with which to compare. The most reasonable strategy is to compare doses obtained with gel dosimetry with doses obtained by the 'most reliable' dosimetry techniques that apply to a certain spatial dimension. As such, dose profiles of a single photon or electron field can be compared with dose profiles obtained with an ionization chamber or diamond detector (De Deene *et al* 1998a, Haraldsson *et al* 2000). In two dimensions, gel dosimetry can be compared with film dosimetry (De Deene *et al* 1998a, 2000c, Pappas *et al* 2001). Most comparisons have been made with treatment plans (Ibbott *et al* 1997, Oldham *et al* 1998, Meeks *et al* 1999, De Deene *et al* 2000c, Cosgrove *et al* 2000, Ramm *et al* 2000, Grebe *et al* 2001). The verification of the treatment plan can be seen as the most important application of gel dosimetry in radiotherapy quality assurance so far. Factors that have an influence on the accuracy are listed in table 8. These factors can be classified in two categories: (1) dosimetric factors cause deviations between the measured dose and the described dose and (2) spatial deviations cause deviations in the spatial distribution of the delivered dose. In terms of the chemical processes within the gel dosimeter, inaccuracies arise from differences in dose–response between calibration phantoms and the dose verification phantom, from chemical instabilities and from the loss of spatial integrity.

When the radiation is delivered, other factors may have an influence on the inaccuracy such as a positioning error of the calibration phantom, a dose rate-dependent response, an energy-dependent response, a temperature-dependent response, tissue non-equivalence and recipient wall effects. During scanning, dose inaccuracies originate from the imaging voxel shape, dose-related imaging artifacts and a scanning temperature-dependent response. Spatial inaccuracies are attributed to a volume change of the gel dosimeter at the chemical level, a phantom positioning error during radiation and imaging artifacts during scanning. Controlling all these factors may largely increase the accuracy of the gel dosimetry experiment.

Scanning a homogeneous gel phantom will reveal any non-uniformities (De Deene *et al* 2000c). Subsequent corrections may be applied (Lepage *et al* 2001e, De Deene *et al* 2000b).

5.3.1. Sources of dosimetric inaccuracy.

Differences in dose response between calibration phantoms and the dose verification phantom. Several groups have observed dose deviations between calibration vials and larger phantoms originating from the same batch of gel with different potential causes being hypothesized for this phenomenon. In a Monte Carlo study by Michael *et al* (2000) it was shown that the effect of backscatter was negligible. In a recent study by De Deene *et al* (2007a) it is shown that the post-manufacturing temperature history of the gel dosimeter has a significant influence on the dose response. In many groups, the gel dosimeter phantom and calibration vials are placed in a fridge after fabrication. As the cooling rate of small calibration vials and a generally larger gel dosimeter phantom may differ significantly, the dose response may be different and a systematic error may be induced.

It was also found that dose deviations were not very reproducible. These findings point in the direction of a physico-chemical factor during fabrication such as thermal history (cooling rate) of the gel dosimeters after fabrication or traces of oxygen that adhere to the wall of the containers. Typically, in test tubes (13 mm diameter), polymer gel is solid within 10 min while the polymer gel in large phantoms (3–5 l) solidifies only after several hours when stored in the fridge. To date no external calibration has been performed with optical-CT. For x-ray CT

an external calibration has been applied (Audet *et al* 2002) but the effect on the dosimetric accuracy was not explored further.

Chemical instabilities. Two kinds of chemical instabilities have been observed in polymer gel dosimeters (De Deene *et al* 2000d, 2002b). One affects the slope of the dose–R_2 plot and is related to post-irradiation polymerization of the comonomer/polymer aggregates (Lepage *et al* 2001e). It is observed that for PAG-type gel dosimeters, the post-irradiation polymerization only lasts 12 h after irradiation. The other instability affects the intercept of the dose–R_2 plot, lasts for up to 30 days and is related to the gelation process of gelatin. The chemical instability depends on the polymer gel composition (De Deene *et al* 2002b). In order to minimize systematic errors it is advisable to scan the gel dosimeter phantom together with the corresponding calibration vials.

Loss of spatial integrity. Loss of spatial integrity may be a consequence of the diffusion of the active components or oxygen in the gel dosimeter. An extreme case is the Fricke gel in which the diffusion of ferric and ferrous ions results in a blurring of the measured dose distribution over time (Olsson *et al* 1990, Harris *et al* 1996, Kron *et al* 1997, Baldock *et al* 2001a). But also in polymer gel dosimeters the diffusion of monomers during irradiation at very high dose gradients and high doses (De Deene *et al* 2001a) and in the first hours after irradiation (Maryanski *et al* 1994b, De Deene *et al* 2002b) can have an influence on the measured dose distribution. A model that describes the creation of overshoots in the measured dose distribution near steep dose gradients and high-dose regions was introduced (De Deene *et al* 2001a). The model was later extended to incorporate the combined effect of diffusion and post-irradiation polymerization (Vergote *et al* 2004b). In this model, unreacted monomer diffusing from a non-irradiated region reacts with large polymer radicals in the irradiated region in the first hours post-irradiation.

Positioning error of the calibration phantom. A positioning error of the calibration phantom may lead to an error in the presumed absorbed dose in the calibration phantom. This will result in an erroneous calibration curve and will eventually result in a systematic dose error in the dose distribution. The presumed dose to the calibration phantom is most often the result of an independent measurement with a standard quality assurance dosimeter (ionization chamber). Any error in the independent measurement will also contribute to the overall error in the calibration curve.

Dose-rate-dependent dose–response. It is seen that in certain polymer gel dosimeters the dose–response is also dose rate dependent. This may be the result of competing radiation-induced chemical reactions. This effect is more pronounced in a normoxic THP-based methacrylic acid (MAc) gel dosimeter than in PAG dosimeters (De Deene *et al* 2006a, Bayreder *et al* 2006, Karlsson *et al* 2007). This effect should not be underestimated as it may lead to a depth-dependent dose–response. A dose-rate dependence may be detrimental for a dosimeter. Nevertheless, the dose-rate dependence has not been documented for many gel dosimeter systems.

Energy-dependent dose–response. Only a slight energy-dependence has been found in a few polymer gel dosimeters for photon energies of 6 MV and 25 MV (Novotny *et al* 2001, De Deene *et al* 2006a). Although this may not have a strong influence on the dose distribution obtained with external radiotherapy, it may be a concern for brachytherapy applications. In many papers that report on brachytherapy verifications with gel dosimetry, a dose–response
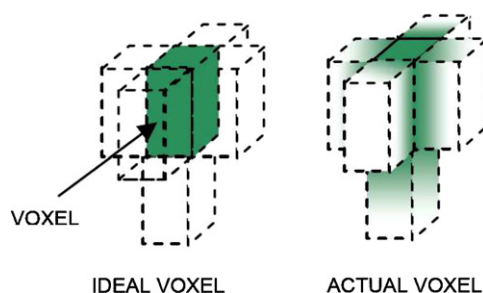
Figure 20. Schematic representation of an ideal voxel shape without any outer voxel contribution (left) and an actual voxel with spread of signal to neighboring voxels.

calibration plot is obtained with high-energy photons. However, until now, no extensive study has been performed to investigate independently the energy-dependence down to these photon energies. A difference in dose–response for low-energy ionizing radiation as compared to the high-energy ionization will lead to a systematic dose error in the measured dose distribution.

Temperature-dependent dose–response during radiation. It was found that in some polymer gel dosimeters the temperature during irradiation has an influence on the dose–response (De Deene *et al* 2006a). This is likely due to a temperature-dependent change in the diffusion coefficient of the monomers in the gel matrix and a change in the chemical reaction kinetics.

Tissue non-equivalence. When using a dosimeter in the therapeutic energy range, the most important parameters to consider for radiological water equivalence are the relative electron and mass densities. For high-energy photon irradiation, most polymer gel dosimeters can be considered as soft tissue equivalent (Keall and Baldock 1999, Venning *et al* 2005c, De Deene *et al* 2006a, Brown *et al* 2008). However, at low energies, some deviations may occur. At low photon energies such as in ^{125}I and ^{103}Pd brachytherapy, dose corrections in the order of 5% are required. However, it is found that the required dose corrections for polymer gel dosimeters are still an order of magnitude lower than for a LiF TLD detector-solid water phantom (Pantelis *et al* 2004).

Recipient wall-effects. To avoid permeation of oxygen through the recipient's wall, Barex® (Baldock *et al* 1996) or glass are often used as phantom materials. It should be noted that some glass may contain heavy metals. These specific glass materials may result in a stronger attenuation of the incident beam and may also result in beam hardening (Michael *et al* 2000). Some caution is therefore advised in selecting cast materials.

Imaging voxel shape. The dose-related parametric map is constituted of 3D voxels. The signal that is plotted in these voxels originates from a set of measurements. In most measurements, there are also outer-voxel signal contributions (figure 20).

The voxel shape is also defined through the point-spread-function (PSF). The convolution of the point-spread-function with the theoretical (block shaped) voxel gives the voxel shape. In MRI, the voxel shape is determined by the receiver bandwidth and the slice profile which is determined by the radiofrequency pulse envelope (De Deene 2004a). The imaging voxel shape is very important if it comes to high-resolution applications such as with point sources in brachytherapy and high-LET irradiation.
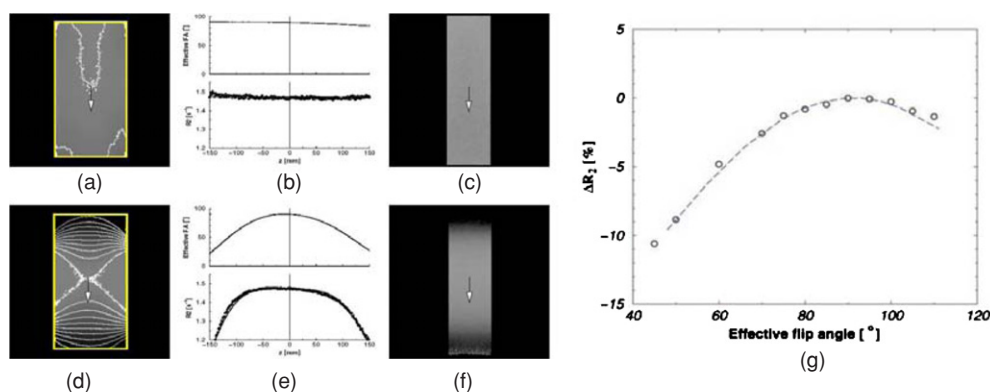
Figure 21. $B1$ field map (effective flip angle) acquired with the body coil (a) and with the head coil (d). $R2$ images of a blank unirradiated polymer gel dosimeter acquired with the body coil and head coil are shown in (c) and (f) showing the effect of the inhomogeneous $B1$ field for the head coil. The field-of-view (FOV) is 320×320 mm^2. Corresponding longitudinal profiles through the center are also shown (b and e). The plot in figure (g) gives the relation between the change in $R2$ and the flip angle for a nominal flip angle of $90°$ (De Deene *et al* 2000b). Reproduced with permission.

Dosimetric imaging artifacts. Imaging artifacts may degrade the dose value in each voxel. Dosimetric imaging artifacts can be machine-related or object-related. Machine-related artifacts originate from imperfections in the scanning device while object-related artifacts originate from the dosimeter itself. The most-important machine-related MRI artifacts are attributed to eddy currents, stimulated echoes, B_1 field inhomogeneity, imperfect slice profiles and standing waves (figure 21).

These machine-related artifacts may depend on the dosimeter shape and make it difficult to make general statements on the accuracy of the dosimeter. A larger phantom or a phantom with sharp edges may perform differently than a smaller cylindrical or spherical shaped phantom. Standing waves can severely deteriorate the dose distribution in dosimeters with specific shapes and spatial dimensions but may be almost completely absent if the dosimeter phantom has a slightly different shape. Object-related MRI artifacts are mainly attributed to a temperature drift during scanning or molecular self-diffusion. For a more detailed overview of different MRI artifacts and compensation strategies we refer to the DOSGEL 2004 proceedings (De Deene 2004a).

In optical-CT, dosimetric artifacts are related to reflection and absorption by the recipient walls, inhomogenities in refractive index, off-axis positioning of the recipient, variation of the laser output and photo-detector and light scattering by both impurities in the matching fluid, container and by the polymer (Oldham and Kim 2004, Xu and Wuu 2004, Bosi *et al* 2007, 2009a) (figure 13).

In x-ray CT imaging, dosimetric artifacts may originate from ring and beam hardening of the containers (Hilts *et al* 2000). Many dosimetric imaging artifacts in x-ray CT can be compensated by image subtraction.

Scanning temperature-dependent response. It has been shown that the NMR spin–spin relaxation rate (R_2) of polymer gel dosimeters is temperature dependent. Temperature coefficients of the R_2–dose response have been published for PAG dosimeters (Maryanski *et al* 1997, De Deene *et al* 1998a), for acrylic acid based gel dosimeters (Spevacek *et al*

Table 9. Approximate time for a typical 3D gel dosimetry experiment.

Process	Time
Fabrication	1 h
Storage	5–20 h
Irradiation/treatment	1 h
Stabilization	10 h
Scanning MRI	10 h
Optical CT	20 min–4 h
X-rat CT	1–2 h
Image processing	1–5 h

2001) and for methacrylic acid based normoxic gel dosimeters (De Deene *et al* 2006a). The temperature coefficient of the x-ray CT dose sensitivity was found to be $4 \times 10^{-3}\,\mathrm{H\,Gy^{-1}\,{}^{\circ}C^{-1}}$ or 0.5% $^{\circ}\mathrm{C}^{-1}$. While it can be expected that the temperature dependence of the optical properties of 3D dosimeters and other NMR properties such as magnetization transfer is not as high as for R_2, no temperature coefficients have been communicated so far.

5.3.2. Sources of spatial inaccuracy. *Volumetric changes of the gel dosimeter.* Upon gelling, the polymer gel dosimeter may contract which may result in a physical geometrical deformation. However, until now, no significant contraction has been reported that would lead to measurable deformations of the dose distribution. Upon irradiation, some additional contraction may be expected as an increase in density has been reported for different polymer gel dosimeters (Trapp *et al* 2001a, 2001b, Hilts *et al* 2004).

Phantom positioning error. Any deviation in the position of the phantom with respect to the presumed position will lead to both a dose error and a geometrical error in the dose distribution. The positioning error can be minimized by using special registration devices such as stereotactic frames (Ibbott *et al* 1997, Grebe *et al* 2001) and an infrared light-emitting diode optical tracking system (Meeks *et al* 1999).

Imaging artifacts that cause spatial deformations. Imaging artifacts may also deform the image space. In MRI, geometrical distortions originate from deviations in the magnetic field distribution of the scanner during excitation or signal acquisition. These deviations in the magnetic field may arise from machine related sources such as eddy currents, main magnetic field inhomogeneities and gradient nonlinearity and from phantom related sources such as susceptibility differences and chemical shifts (De Deene 2004a). Different strategies have been proposed to compensate for these artifacts (see De Deene 2004a and references herein).

6. Applications of polymer gel dosimetry

The aim of gel dosimetry in clinical practice is to provide an integrated dose distribution in 3D in anthropomorphic phantoms. To date, however, gel dosimetry has been a rather time-consuming technology that requires several actions from the medical physicist.

The complete process of a polymer gel dosimetry experiment may take upward of 45 h (table 9).

With the use of an anti-oxidant the fabrication time is approximately 1 h. After fabrication, the volumetric gel phantom and calibration samples have to be cooled to room temperature slowly in order to obtain the same dose response for both volumetric gel phantom and calibration tubes. The gels should be stored in a large water reservoir for approximately 20 h. It can be expected that this time can be reduced by use of a controlled cooling system and by the use of other chemical compositions. The actual irradiation of the gel dosimeter takes about 1 h and includes setting up the irradiation experiment and irradiation of both the volumetric gel phantoms and calibration tubes. In order to stabilize the post-irradiation polymerization process a period of 10 h should be left between irradiation and scanning. When MRI is used to read out the gels, the gel phantoms should be stored in the scanner room so that the gel phantom temperature also equilibrates to the scanner temperature. The MRI scanning period for a complete 3D dosimetry experiment is strongly dependent on the required spatial resolution and dosimetric precision but is typically in the order of 10 h. In order to compensate for temporal chemical instability during scanning, calibration vials and volumetric gel dosimeter phantom should be scanned together. It is difficult to provide data for optical and x-ray CT scanning as no thorough comparison has been made with MRI for comparable resolution and SNR to date. A qualitative comparison was made of optical-CT to MRI (Oldham *et al* 2001), however, as the MRI pulse sequence used was not optimized, useful comparative conclusions are limited. Depending on the purpose of the gel dosimetry experiment, the post-processing step takes from 1 to 5 h. A first step in the post-processing is the extraction of the dose–response curve obtained from the calibration phantoms and calibrating toward a 3D dose distribution. Eventually, the 3D gel dose distribution can be compared with dose distributions obtained with other dosimetry techniques.

Further research in gel composition and further optimization in cooling may help in reducing the storage times significantly.

6.1. Conformal radiotherapy

Because of the relatively long processing time to acquire a 3D dose distribution and high cost, gel dosimetry should not be considered as a routine dosimeter to check all conformal radiotherapy patient treatments. However, gel dosimetry should be used as a dosimetric tool to verify dose distributions obtained with treatment planning of class solutions (De Wagter 2004).

When enough correspondence is obtained between the experimentally obtained gel dose distribution and the treatment planning dose distribution, there is confidence that the computed dose distribution reflects the actual dose distribution. For IMRT treatment verification, gel dosimetry should be used initially with subsequent use of other dosimetry techniques in cases where non-acceptable discrepancies are found (figure 22).

Gel dosimetry is considered to have an important role in benchmarking the performance of new treatment techniques and in the regular QA of IMRT (Schreiner 2006). There are three major motivations to use gel dosimetry for regular QA (De Deene 2002). First, there is the possibility of discrepancies between calculated dose distributions and actual given dose as not all scatter contributions may be taken into account in the computation algorithm or the shape and output factors of small beams may differ substantially from the calculated ones. Second is that machine failures or drifts may not always be picked up by conventional 1D or 2D dosimeters. Third is that gel dosimetry can provide information on setup errors. The gel dosimeter goes through every stage of the IMRT treatment in the same way as the patient. The phantom may be scanned before treatment, the images are read into the computer planning computer and the planning is performed on the phantom. Fiducial positioning markers and
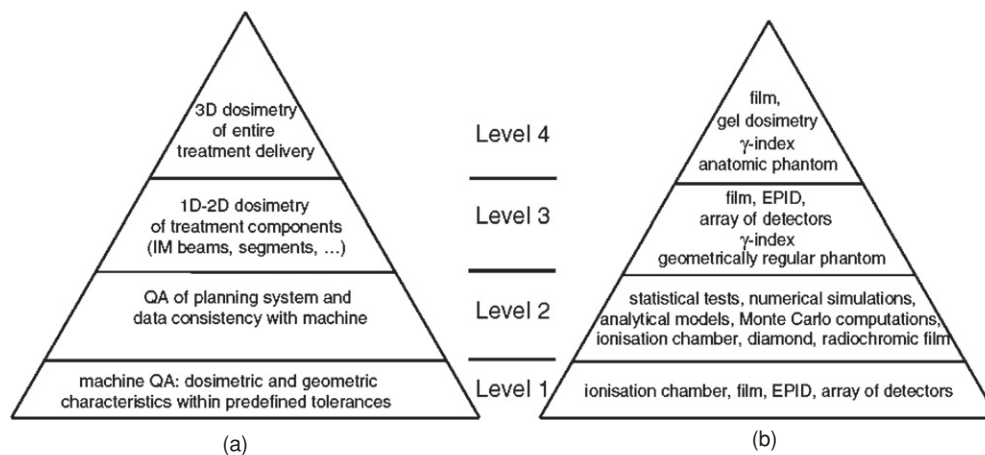
Figure 22. (a) Top-down model of dosimetric quality assurance (QA) in intensity-modulated radiotherapy. In the conceptual pyramid, each level of QA is based on the stability of the underlying levels. The two lower levels can be part of period equipment QA. For QA of a clinical class solution, one may start at the top by applying 3D dosimetry of an entire treatment. One descends the pyramid to the lower levels if the 3D dosimetry reveals intolerable discrepancies with treatment planning. (b) Methodology and tools appropriate for each of the levels. EPID stands for 'electronic portal imaging' (De Wagter *et al* 2004). Reproduced with permission.

isocenter lines may be put on the phantom beforehand. After treatment, the calculated dose maps are compared to the gel derived dose maps. The sensitivity of a treatment to positioning errors can also be investigated by gel dosimetry. In that respect, organ movements during treatment can be simulated (Månsson *et al* 2006).

Preliminary studies comparing gel dose distributions of conformal radiotherapy treatments with dose maps obtained with other dosimetry techniques have revealed average dose deviations of more than 10% relative to the maximum dose in low-dose regions (Ibbott *et al* 1997, Oldham *et al* 1998, De Deene *et al* 1998a, Cosgrove *et al* 2000). It should be noted that a comparison of published feasibility studies is limited by different authors using different quantities to evaluate the performance of polymer gel dosimeters (see table 10). Also the investigated volume and spatial resolution differs significantly amongst different studies. It has to be recognized that although gel dosimetry has been promoted as a 3D method to acquire dose distributions, most of the early studies showed only 2D dose maps (at most in three orthogonal planes). The first experimental study in which more than 20 gel dose maps have been acquired was performed by De Deene *et al* (2000c). In this study, each gel dosimetry acquired dose map was compared with dose maps obtained in a stack of radiographic film and with the dose distribution calculated with treatment planning software.

Structural and stochastic root-mean-square differences (RMSD) between gel measured dose maps and corresponding 2D film measured dose maps of the same experiment are shown in figure 23. It is noted that the largest deviations are seen in regions where dose gradients in the slice recording direction (perpendicular to the image plane) are highest. The stochastic deviations are mainly attributed to noise in the gel measured dose maps and are independent of slice position.

Slightly higher structural RMSD between gel measured dose maps and corresponding treatment planning slices (in the order of 5%) were found in a later study of a dose verification of an intensity-modulated arc therapy (IMAT) treatment (Vergote *et al* 2004b). In this study,

Table 10. Papers presenting gel dosimetry treatment verifications together with the gel type, the volume of the volumetric gel phantom, the spatial resolution (voxel size), the dimension of the gel measured dose distribution, the comparison dosimeter and the evaluation quantity. For the treatment modality, 'IMRT' stands for intensity-modulated radiation therapy, 'SRS' stands for stereotactic radiosurgery and 'IMAT' stands for intensity-modulated arc therapy. For the comparison dosimeters, 'TPS' stands for treatment planning system, 'TLD' stands for thermoluminescence dosimeter, 'IC' stands for ionization chamber, 'DD' stands for diamond detector and 'OPT' stands for optical-CT. With the evaluation quantities, 'DTA' stands for distance-to-agreement, 'PAVD' stands for percentage average dose deviation, 'sys dev' stands for systematic deviation, 'rmsd' stands for root-mean-square deviation, 'gamma' stands for the gamma index. The values in brackets next to the DTA represent the isodose levels for which the DTA was calculated.

| Author	Treatment	Gel type	Volume	Resolution	Dim.	Comp.	Evaluation quantity
Ibbott *et al* (1997)	Gamma knife	BANG-2	–	$1.9 \times 0.95 \times 3$ mm^3	2D	TPS	DTA
Oldham *et al* (1998)	IMRT	PAG	0.66 l	$0.8 \times 0.8 \times 5$ mm^3	2D	TPS	DTA ($D = 50\%, 90\%$)
De Deene *et al* (1998)	IMRT	PAG	3 l	$1.6 \times 1.6 \times 5$ mm^3	2D	Film	PAVD
Low *et al* (1999)	IMRT	BANG	2 l	$1 \times 1 \times 3$ mm^3	2D	TPS, TLD	Gamma
Cosgrove *et al* (2000)	Conformal	BANG-1	0.5 l	$1 \times 1 \times 5$ mm^3	2D	TPS	sys dev
Ertl *et al* (2000)	Gamma knife	BANG-1	0.03 l	$0.23 \times 0.23 \times 1$ mm^3	2D	TPS, film	–
De Deene *et al* (2000)	IMRT	PAG	3 l	$0.47 \times 0.47 \times 5$ mm^3	3D	TPS, film	DTA, rmsd
Grebe *et al* (2001)	SRS	BANG	2.2 l	$0.78 \times 0.78 \times 3$ mm^3	2D	TPS, IC	DTA ($D = 90\%$), rmsd
Oldham *et al* (2001)	SRS	BANG-3	0.3 l	$1 \times 1 \times 2$ mm^3	2D	TPS, OPT	–
Pappas *et al* (2001)	SRS	VIPAR	0.06 l	$0.27 \times 0.27 \times 5$ mm^3	1D	TPS, film, IC	–
Audet *et al* (2002)	SRS	PAG	0.8 l	sl. th. $= 3$ mm	2D	TPS	DTA ($D = 50\%, 80\%$)
Novotny *et al* (2002)	SRS	PAG-2	0.05 l	$0.5 \times 0.5 \times 2$ mm^3	2D	TPS	sys dev
Watanabe *et al* (2002)	SRS	BANG-3	2.2 l	$0.95 \times 0.95 \times 3$ mm^3	2D	TPS	Shift
Scheib and Gianolini (2002)	Gamma knife	BANG	0.04 l	$1.13 \times 1.13 \times 1.1$ mm^3	2D	TPS	–
Vergote *et al* (2003)	IMRT	PAG	2.4 l	$1 \times 1 \times 6$ mm^3	3D	TPS, DD	Gamma, rmsd
Duthoy *et al* (2003)	IMAT	PAG	9.5 l	$2.5 \times 2.5 \times 5$ mm^3	3D	TPS	Gamma
Love *et al* (2003)	IMRT	PAG	2.8 l	$1 \times 1 \times 5$ mm^3	2D	TPS	–
Gustavsson *et al* (2003)	IMRT	MAGIC	1.5 l	$1 \times 1 \times 3$ mm^3	3D	TPS	Gamma
Vergote *et al* (2004b)	IMAT	PAG	10 l	$2.5 \times 2.5 \times 5$ mm^3	3D	TPS	Gamma
Duthoy *et al* (2004)	IMAT	PAG	10 l	$2.5 \times 2.5 \times 5$ mm^3	3D	TPS	Gamma
Sandilos *et al* (2004)	IMRT	VIPAR	1.6 l	$0.75 \times 0.75 \times 3$ mm^3	3D	TPS	–
Papagiannis *et al* (2005)	Gamma knife	PABIG	0.17 l	$1 \times 1 \times 1$ mm^3	3D	TPS	–
Karaiskos *et al* (2005)	Gamma knife	VIPAR	0.17 l	$1 \times 1 \times 1$ mm^3	3D	TPS	–
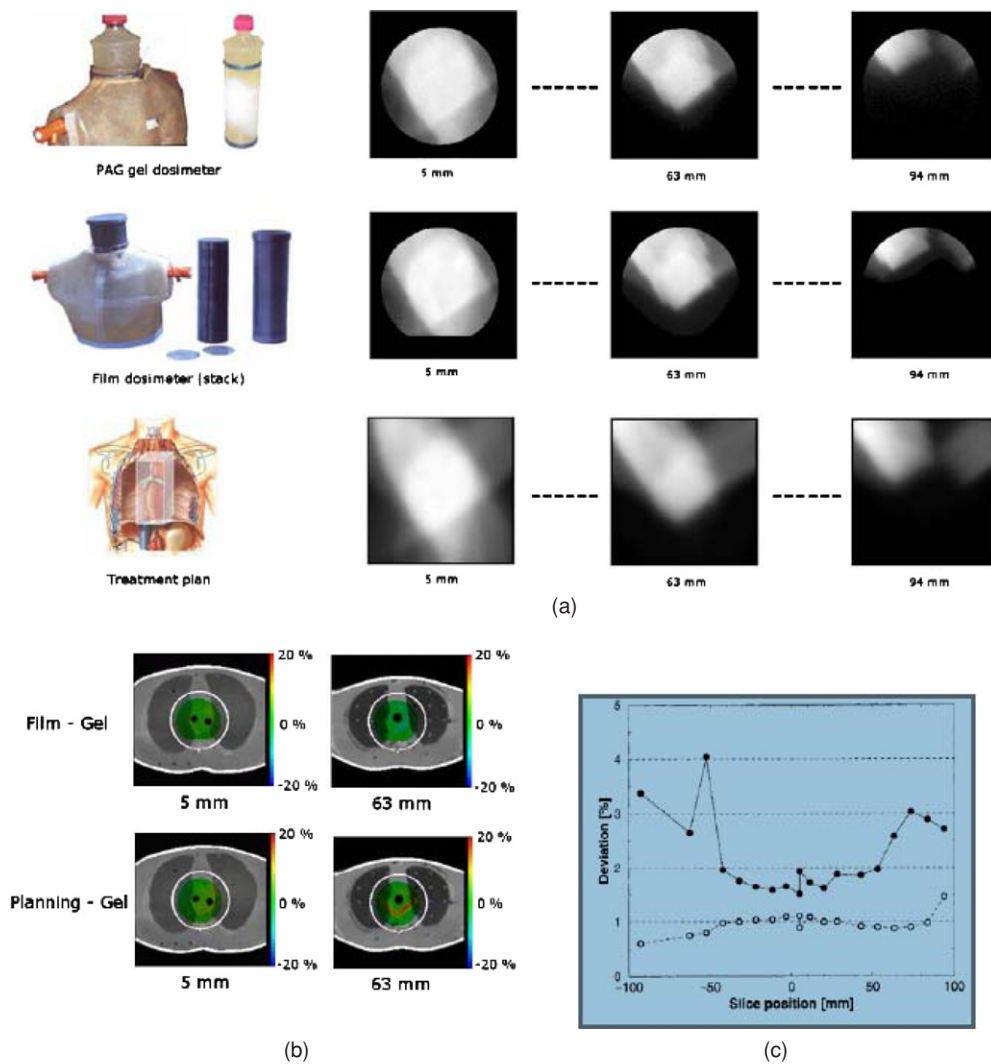
Figure 23. (a) Stack of corresponding dose maps obtained by three different dosimetry techniques: gel dosimetry, film dosimetry and computer planning. (b) Color-washed difference images superimposed onto anatomical CT-images. (c) Mean structural root-mean-square difference (closed symbols) and stochastic root-mean-square difference (open symbols) in corresponding dose maps obtained with gel dosimetry and film dosimetry (De Deene *et al* 2000c). Reproduced with permission.

a much larger volumetric gel phantom was scanned and rf field non-uniformity corrections were applied.

The large deviations encountered in these preliminary studies have been attributed to a variety of factors. With the anoxic polymer gel dosimeters that were used in these studies, oxygen was expelled during fabrication by bubbling nitrogen through the solution. Residues of oxygen in the gel will result in an inhibition in the low-dose region. Also the phantom cast material should be impermeable to oxygen. A study on the oxygen permeability of different materials that can be heat folded to obtain an anthropomorphic shaped cast showed that Barex® had the best characteristics (Bonnett *et al* 1999). Also
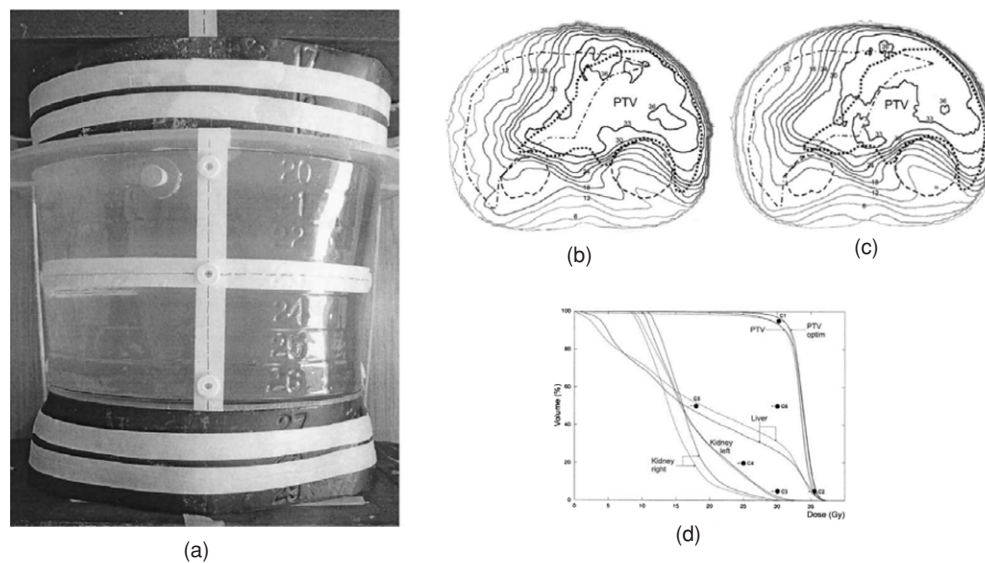
Figure 24. Dose verification of an IMAT treatment using polymer gel dosimetry. (a) A 10 l Barex cast was filled with PAG. At each side of the phantom, three slices of the anthropomorphic Rando phantom were added in the cranio-caudal direction to obtain full scatter conditions. Dose distributions in the middle transverse plane of the phantom as calculated with a collapsed cone convolution/superposition algorithm (b) and measured with polymer gel dosimetry (c). Corresponding dose–volume histograms for PTV, liver and kidneys are also shown (d) (Duthoy *et al* 2003). Reproduced with permission.

the inlets and outlets of the phantom should be sealed properly. When fabricating the cast of the phantom special attention has to be paid to the choice of the glue to join different parts together as some glues may initiate polymerization in the gel (Oldham *et al* 1998). To some extent the deviations seen in the early studies were also attributed to MRI artifacts such as susceptibility artifacts (Ibbott *et al* 1997, Oldham *et al* 1998) and B_1 field inhomogeneities (De Deene *et al* 2000b, Ertl *et al* 2000). Several MR imaging artifacts have been isolated and investigated quantitatively and compensation strategies have been proposed (De Deene *et al* 2000a, 2000b, 2001a, De Deene and De Wagter 2001, Lepage *et al* 2001b). Also, chemical instabilities were not recognized and quantified until 2000 (De Deene *et al* 2000d). Compensation of all these error contributions has resulted in far better outcomes. Further optimization of imaging sequence parameters has also aided in acquiring 3D dose distributions within a feasible time span (Vergote *et al* 2003, 2004a, Duthoy *et al* 2003, 2004, Gustavsson *et al* 2003, Sandilos *et al* 2004, Papagiannis *et al* 2005, Karaiskos *et al* 2005). An example of a large volume dose verification gel dosimetry experiment is shown in figure 24.

The effect of air cavities on the dose distribution after conformal radiation treatment has also been investigated (Vergote *et al* 2003).

6.2. Brachytherapy

That gel dosimetry is able to visualize steep dose gradients in 3D makes it very attractive for acquiring the dose distributions of brachytherapy sources obtained with both low dose rate (LDR) and high dose rate sources (HDR) (see table 8). Moreover, gel dosimeters integrate
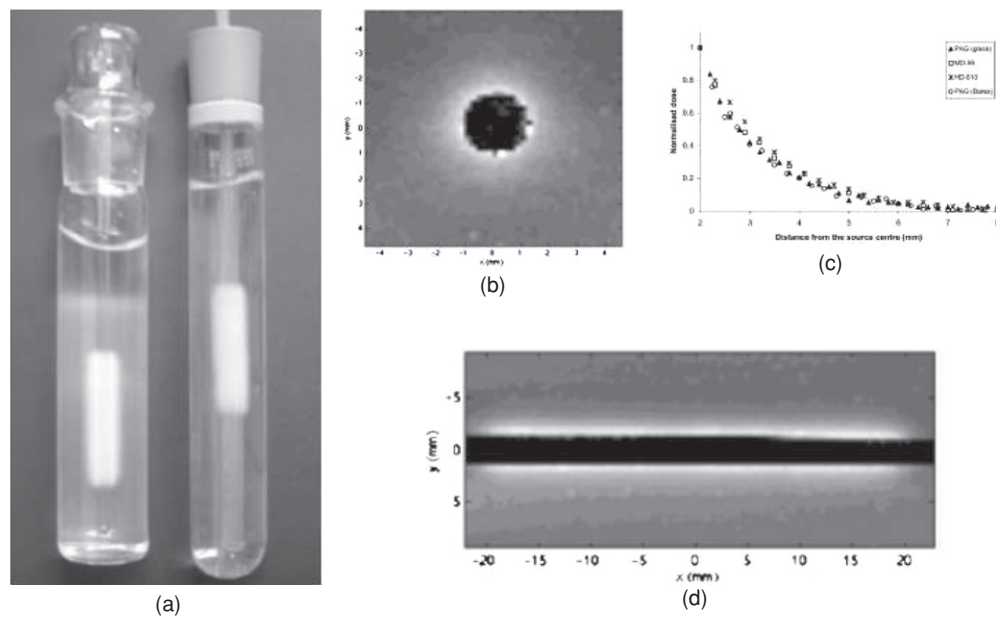
Figure 25. (a) PAG irradiated after irradiation with a source consisting of a train of 16 90Sr/90Y pellets inserted in glass (left) and Barex tubes (right). (b) Axial $R2$ image with an in-plane resolution of 0.2 mm. (c) Relative dose profiles obtained with polymer gel dosimetry and two different radiochromic films. (d) The longitudinal $R2$ image (Amin *et al* 2003). Reproduced with permission.

the dose delivery over time so that the total dose distribution from a moving source can be measured. Different types of sources have been evaluated. An example of a polymer gel dosimetry experiment of an intravascular radiation treatment is shown in figure 25.

Although polymer gel dosimetry has been perceived as a suitable dosimeter for dose verification in brachytherapy, some additional difficulties may be encountered that are related to the insertion of applicators or catheters into the polymer gel. Significant dose deviations near the catheter wall have been noted (McJury *et al* 1999, Hurley *et al* 2003). In polymer gel dosimeters, oxygen diffusion through the wall of the cavity may contaminate the gel and result in an underestimation of absorbed dose (Farajollahi *et al* 1999). The inhibition of oxygen passing through the catheter wall of a HDR ^{192}Ir source has been analyzed quantitatively by De Deene *et al* (2001a). Other sources of dose deviations related to the high dose gradients encountered with HDR point sources and measured with MRI have also been established. The influence of magnetic field distortions related to magnetic susceptibility differences between the gel and catheter has been studied extensively and compensation strategies have been proposed (De Deene *et al* 2001a). A mathematical model for diffusion of monomers during irradiation resulting in loss of spatial integrity has been established and the influence of partial volume effects was also investigated (De Deene *et al* 2001a). For some applications such as endovascular brachytherapy and β emitters, sub-millimeter dose maps are required. With MRI, an increase in image resolution is accomplished by using stronger imaging magnetic field gradients. It is found that the measured R_2 becomes dependent on the image resolution as a result of molecular self-diffusion of water within these magnetic field gradients (Hurley *et al* 2003). Therefore much attention should be paid to the calibration procedure. It should be noted that until now, the energy dependence for low energies and other radiation sources has not been experimentally verified.
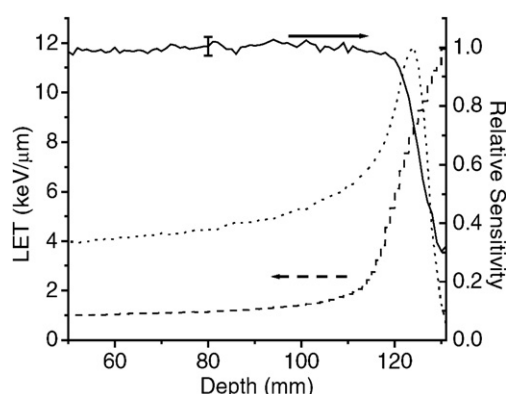
Figure 26. The variation in LET as a function of depth for a 133 MeV proton beam (dashed curve, left-hand side) and the measured relative sensitivity normalized to the measured dose at a depth of 60 mm (solid curve, right-hand side). Also shown is the corresponding depth–dose curve normalized to 100% at the Bragg peak (Gustavsson *et al* 2004). Reproduced with permission.

6.3. High LET particle irradiation

The very sharp delivery of dose in the absence of exit dose and minimum lateral scattering has increased the interest for using hadrons for radiation treatment. The sharp dose distributions encountered with hadron treatments requires a 3D dose verification method. Several attempts have been made to use polymer gel dosimetry for measuring three dimensional dose distributions of proton (Heufelder *et al* 2003, Gustavsson *et al* 2004) and heavy ion beams (Ramm *et al* 2000). However, in all studies it was found that the dose sensitivity for protons or heavy ions was significantly smaller than for high-energy photons. Theoretical track structure calculations and FT Raman spectroscopic measurements have been used to calculate the effect of LET on the dose response in proton beams (Jirasek and Duzenli 2002). It was found that the gel effectiveness decreases with increasing proton LET (figure 26).

The decreased sensitivity of polymer gels close to the proton track may be attributed to a larger density of polymer radical chains that favors a faster termination of the polymerization reactions. Alternatively, at high LET, radical recombination leads to the formation of molecular products (e.g. H_2O_2), decreasing the amount of radicals that can inititate a polymerization reaction. In order to describe the difference in dose response of the gel dosimeter for hadrons as compared to photons, the property 'relative effectiveness' (RE) is introduced. The RE is defined as the ratio of hadron to x-ray dose sensitivity of the dosimeter. As the LET is not constant along the particle track, the dose sensitivity becomes depth dependent (Jirasek and Duzenli 2002, Heufelder *et al* 2003, Gustavsson *et al* 2004). An increase in dose sensitivity was found for increasing projectile energies of $^{12}C^{6+}$ ion energies in both BANG-1(tm) and BANG-3(tm) polymer gel dosimeters in accordance with a decrease in LET for increasing projectile energies (Ramm *et al* 2000).

6.4. Boron neutron capture therapy (BNCT)

In BNCT boron-10 is administered and accumulated in the tumor by a tumor-specific boron carrier. Subsequently, the tumor and surrounding tissues are irradiated with epithermal neutrons. Neutrons undergo a nuclear reaction with boron with the formation of ^7Li and an alpha particle. Also some gamma-radiation (480 keV) is released. Neutrons may also
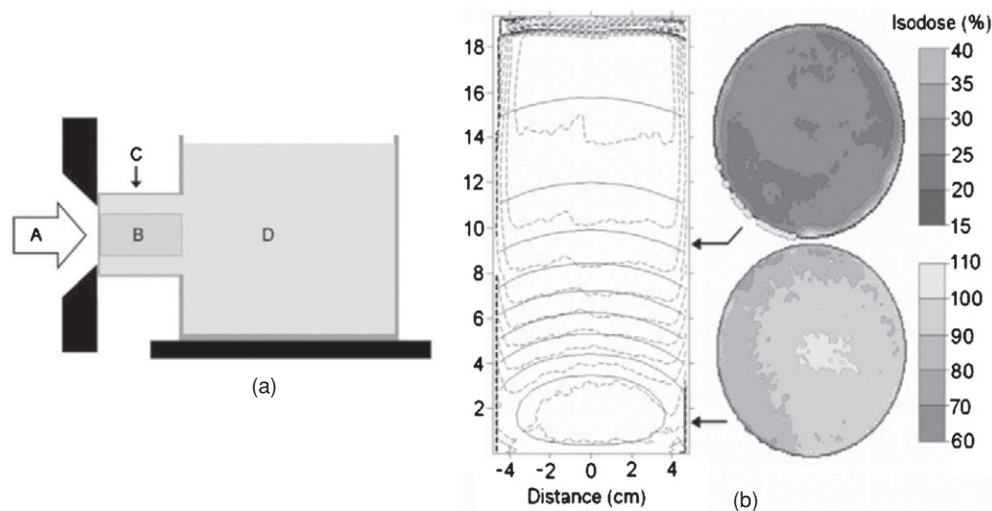
Figure 27. (a) Neutron irradiation setup: the epithermal neutron beam is incident from the left through a circular beam aperture (A); cylindrical gel phantom (B) is inserted into a cylindrical extension (C) of the water phantom (D); (b) calculated (solid line) and measured (dashed line) isodoses (10% intervals, starting from the 90% isodose) in the central cross-section of the cylindrical gel phantom. Also shown are two axial cross-sections (Uusi-Simola *et al* 2007).

interact with other atoms present in the subject. Farajollahi *et al* (2000) showed an increase in dose response in a PAG doped with boron as compared to an undoped PAG. The trend was found to be in accordance with Monte Carlo calculations. Monte Carlo simulations were also performed to investigate the dose contributions from different particles in a neutron beam (Wojnecki and Green 2001). From this study, it is concluded that PAG provides a good simulation of radiation transport in the brain and is very similar to water. In a study of the relative dose–response of BANG-3 polymer gel dosimeters in epithermal neutron irradiation, a good correspondence was found between the measured dose distribution and the calculated dose distribution obtained with a two-dimensional discrete ordinate radiation transport code (DORT) (Uusi-Simola *et al* 2003). This demonstrates that for the BANG-3 polymer gel, there is no significant change in dose sensitivity due to differences in LET that may occur in this epithermal neutron beam. A fair correspondence was also found between the gel measured and the Monte Carlo calculated dose distribution for a MAGIC-type polymer gel (Uusi-Simola *et al* 2007) (figure 27).

6.5. Radionuclide dosimetry

Polymer gel dosimetry experiments have been undertaken to investigate the dosimetry of unsealed therapy radionuclides I-131 (Courbon *et al* 2006, Gear *et al* 2007) and P-32 (Gear *et al* 2006) and the unsealed diagnostic radionuclide Tc-99 m (Braun *et al* 2007, 2009). The use of polymer gels has shown promise with the potential for measurement of non-uniform uptake of therapy and diagnostic radionuclides in normoxic polymer gel dosimeters.

6.6. Diagnostic dosimetry

Polymer gel dosimetry has been evaluated for measuring quality assurance parameters of diagnostic CT scanners with respect to the exposure of patient dose (figure 28) (Hill *et al*
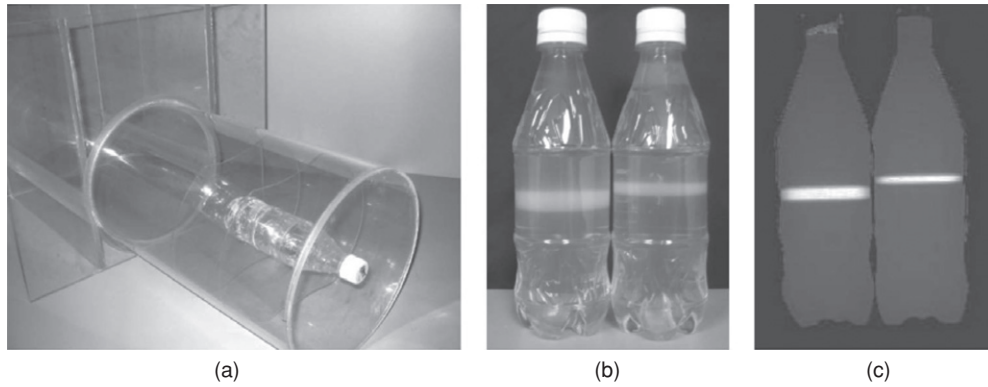
Figure 28. (a) Water phantom with a normoxic polymer gel dosimeter centrally positioned for diagnostic CT-dose profiles and CTDI determination; (b) normoxic polymer gel dosimeter phantoms; (c) corresponding $R2$ image after exposure to x-rays from a CT scanner. The accumulated dose is from 50 accumulated single transaxial CT slices for 8 and 5 2020 mm slice widths (140 kVp, 400 mAs) (Hill *et al* 2005b). Reproduced with permission.

2005b, 2008, Sarabipour *et al* 2006). Important parameters that can be extracted from a polymer gel dosimetry experiment are the computer tomography dose index (CTDI) and the slice width dose profile (SWDP). The CTDI is defined as the integral of the dose profile ($D(z)$) along a line perpendicular to the tomographic plane divided by the product of the nominal tomographic section thickness (T) and the number of tomograms (n) produced in a single axial scan:

$$\text{CTDI}_{100} = \frac{1}{nT} \int_{-50\,\text{mm}}^{50\,\text{mm}} D(z)\,dx.$$ (28)

The SWDP cannot be measured by an ionization chamber but is usually measured with either thermoluminescent dosimetry (TLD) or film. Gel dosimetry enables the recording of the whole 3D dose distribution and can be performed in an anthropomorphic phantom. This is particularly important for helical CT scanners.

7. Summary of previous criticisms of gel dosimetry and their rebuttals

In a previous review paper in this journal, MacDougall *et al* (2002) employed a 'systematic review' technique to assess the complete body of literature on gel dosimetry found by the authors. Their conclusion was that 'there [was] only sparse, or absent, evidence of sufficient quality for the accuracy and precision parameters for polymer and Fricke gels'. This assessment on the then state-of-the-art was strongly disputed by *inter alia* two of the authors of this article (De Deene *et al* 2003, Baldock 2009) for the following reasons.

 (i) Whilst a systematic review to answer a very tightly defined set of questions is a laudable objective in a mature field, the exclusion criteria laid down by McDougall *et al* were so restrictive that, for example, of the 115 gel dosimetry references found, only one prior publication was allowed to contribute to their conclusion on accuracy.
 (ii) The 'ultra-focused' questions being asked were not useful ones, with the evaluation criteria being unsuitable for 3D dosimeters.
(iii) The exclusion criteria were not appropriate, requiring, for example, comparison to be made with an ionization chamber for the publication to be admissible. For many of the

Table 11. Papers presenting gel dosimetry treatment verifications together with the gel type, the volume of the volumetric gel phantom, the spatial resolution (voxel size), the dimension of the gel measured dose distribution, the comparison dosimeter and the evaluation quantity. With the evaluation quantities, 'PAVD' stands for percentage average dose deviation, 'rmsd' stands for root-mean-square deviation and 'gamma' stands for the gamma index. 'Visual' means that the dose distributions are plotted on top of each other allowing visual inspection.

Author	Treatment	Polymer type	Resolution	Dim.	Comp.	Evaluation quality
Farajollahi et al (1999)	^{137}Cs LDR source	BANG	$0.8 \times 0.8 \times 3$ mm^3	2D	TLD, TPS (Helax)	rmsd
McJury et al (1999)	^{192}Ir HDR source	PAG	$1 \times 1 \times 5$ mm^3	2D	TPS (NPS)	Visual
Hafeli et al (2000)	^{188}W-^{188}Re β line source	BANG	$0.1 \times 0.1 \times 2$ mm^3	1D	MC	PAVD
De Deene et al (2001a)	^{192}Ir HDR source	PAG	$0.8 \times 0.8 \times 2$ mm^3	2D	MC	Visual
Papagiannis et al (2001)	^{192}Ir HDR source	VIPAR	$0.4 \times 0.4 \times 3$ mm^3	2D	MC	Visual
Chan et al (2001)	^{106}Ru ophthalmological applicator	BANG	$0.3 \times 0.3 \times 3$ mm^3	–	–	
Kipouros et al (2003)	^{192}Ir HDR source	VIPAR	$0.8 \times 0.8 \times 1.5$ mm^3	2D	TPS (Plato, Swift)	Gamma
Amin et al (2003)	^{90}S–^{90}Y source	PAG	$0.2 \times 0.2 \times 0.5$ mm^3	1D	RC Film	PAVD
Fragoso et al (2004)	^{137}Cs intracavitary applicator	PAG	$1 \times 1 \times 5$ mm^3	2D	TPS (Plato), MC	Visual
Pantelis et al (2004)	^{125}I isoseed	PABIG	$0.5 \times 0.5 \times 0.5$ mm^3	1D	MC	Visual
Baras et al (2005)	^{192}Ir HDR source	PABIG	$0.8 \times 0.8 \times 0.8$ mm^3	1D	TPS (Gammaplan)	Visual
Hurley et al (2006)	^{192}Ir HDR source	MAGIC	$0.1 \times 0.1 \times 2$ mm^3	2D	TPS (Plato), MC	Visual
Sandilos et al (2006)	^{192}Ir HDR source	PABIG	$0.8 \times 0.8 \times 0.8$ mm^3	2D	TPS (Gammaplan)	Visual

scenarios in which gel dosimetry is most useful, an ionization chamber does not produce data of acceptable accuracy.

(iv) The analysis of the literature was incomplete, with numerous examples missed by the authors. Perhaps the inclusion of experts in polymer gel dosimetry should have been considered.

(v) Given the strictly limited nature of the assessment, the conclusion quoted above was poorly worded and could too easily have been taken out of context to apply to the field of gel dosimetry as a whole.

3D radiation dosimetry is an example of an area that requires considerable experience in three separate fields: polymer chemistry, radiation physics and the quantitative use of an imaging technique such as MRI or optical-CT. There are thus significant pitfalls in sample preparation and handling, in the design of the irradiation and experimental protocols and in the analysis of quantitative data. In some publications, there have been large deviations between the dose distributions measured by gels and the results of film or the planning system. We emphasize that it is necessary before reporting such results to ensure that the optimum 3D dosimetry protocol has been followed. This might include, for example,

(i) taking appropriate precautions against oxygen inhibition;

(ii) monitoring or controlling the temperature at which irradiation, post-irradiation polymerization and scanning take place, then making appropriate corrections;

(iii) performing any calibration in an appropriate sized vessel and being generally aware of vessel size and vessel wall effects;

(iv) controlling for dose-rate or fractionation-dependent effects;

(v) if using MRI as a readout, employing the optimal measurement sequence—for example, when a single slice is required, a 32-echo sequence can give five times the signal-to-noise of a single-echo sequence;

(vi) if using MRI, being aware of the potential sources of systematic error: geometric distortions, eddy currents, stimulated echoes, B_1 field inhomogeneities and molecular diffusion and the consequences that these have on quantitative measurements;

(vii) if using optical-CT, understanding the origins and required corrections for ring, container wall and refractive index inhomogeneity artifacts;

(viii) using the correct functional form to fit calibration curves (normally a mono- or bi-exponential curve not a polynomial, which will have inappropriate behavior extrapolated outside its region of support) based on the underpinning physical model of reaction kinetics;

(ix) use of the gamma function (Low and Dempsey 2003) only where relevant clinically and then only as an adjunct to the presentation of simple dose difference and distance-to-agreement maps.

8. Conclusions and future perspectives

The ultimate goal of polymer gel dosimetry is to verify radiation dose distributions in 3D. The major challenge in gel dosimetry is to achieve a spatial and dose accuracy and precision that satisfy the requirements for 3D dose verification of radiation treatments that are performed in the radiation hospital. As there exists no other experimental 3D dosimeter that can serve as a 'gold standard', a measure for both the spatial and dose accuracy is difficult to define. In addition, as a 3D dosimeter, gel dosimeters have to accomplish specific dosimetric requirements in terms of stability, spatial integrity, temperature insensitivity, dose rate and energy independence and tissue equivalence.

Research in the field of polymer gel dosimetry covers many different aspects. Several studies have been conducted on the chemistry of the polymer gel and different gel compositions have been proposed. A better understanding of the physical and chemical interactions within the polymer gel dosimeter can help in optimizing the composition to obtain a gel that fulfills the dosimetric criteria and achieves high dose sensitivity. Research in the field of gel dosimetry includes also the development and optimization of quantitative scan techniques. The most promising scan techniques are magnetic resonance imaging and x-ray and optical computerized tomography. For different scan techniques, different optimal gel dosimeters can be found. Optimal gel systems for magnetic resonance imaging display a significant change in NMR relaxation time or magnetization transfer. For x-ray CT, the dose sensitivity is determined by the density change.

Polymer non-gel dosimeters containing radiation sensitive dyes may be more suitable for optical imaging than polymer gel dosimeters as the latter are characterized by a high amount of light scatter which may deteriorate the measured optical density (Adamovics and Maryanski 2006, Sakhalkar and Oldham 2008, Brown *et al* 2008). These dosimeters however are not suitable for imaging with either MRI or x-ray CT.

Currently, research is conducted to make gel dosimetry more user-friendly and less toxic. Specific MRI QA protocols can help in benchmarking the accuracy of MR imaging sequences. Optical-CT techniques and x-ray CT scanning are becoming an interesting alternative for the less cost-effective and less accessible NMR readout technique. The authors emphasize the importance of determining the overall accuracy of the total 3D dosimetry technique including both the gel dosimeter and the readout system. Each gel dosimeter should meet a series of dosimetric properties such as stability, spatial integrity, temperature insensitivity, dose rate and energy independence and tissue equivalence.

References

Adamovics J and Maryanski M J 2006 Characterisation of PRESAGE: a new 3-D radiochromic solid polymer dosemeter for ionising radiation *Radiat. Prot. Dosim.* **120** 107–12

Alexander P, Charlesby A and Ross M 1954 The degradation of solid polymethylmethacrylate by ionizing radiations *Proc. R. Soc.* A **223** 392

Amin M N, Horsfield M A, Bonnett D E, Dunn M J, Poulton M and Harding P F 2003 A comparison of polyacrylamide gels and radiochromic film for source measurements in intravascular brachytherapy *Br. J. Radiol.* **76** 824–31

Andrews H L, Murphy R E and LeBrun E J 1957 Gel dosimeter for depth dose measurements *Rev. Sci. Instrum.* **28** 329–32

Audet C, Hilts M, Jirasek A and Duzenli C 2002 CT gel dosimetry technique: comparison of a planned and measured 3D stereotactic dose volume *J. Appl. Clin. Med. Phys.* **3** 110–8

Babic S and Schreiner L J 2006 An NMR relaxometry and gravimetric study of gelatin-free aqueous polyacrylamide dosimeters *Phys. Med. Biol.* **51** 4171–87

Baldock C 2006 Historical overview of the development of gel dosimetry *J. Phys.: Conf. Ser.* **56** 14–22

Baldock C 2009 Historical overview of the development of gel dosimetry: another personal perspective *J. Phys.: Conf. Ser.* **164** 012002

Baldock C, Burford R P, Billingham N, Wagner G S, Patval S, Badawi R D and Keevil S F 1998a Experimental procedure for the manufacture and calibration of polyacrylamide gel (PAG) for magnetic resonance imaging (MRI) radiation dosimetry *Phys. Med. Biol.* **43** 695–702

Baldock C, Harris P J, Piercy A R and Healy B 2001a Experimental determination of the diffusion coefficient in two-dimensions in ferrous sulphate gels using the finite element method *Australas. Phys. Eng. Sci. Med.* **24** 19–30

Baldock C, Hasler C D, Keevil S F, Greener A G, Billingham N C and Burford R P 1996 A dosimetry phantom for external beam radiation therapy of the breast using radiation-sensitive polymer gels and MRI *Med. Phys.* **23** 1490

Baldock C, Lepage M, Back S A J, Murry P J, Jayasekera P M, Porter D and Kron T 2001b Dose resolution in radiotherapy polymer gel dosimetry: effect of echo spacing in MRI pulse sequence *Phys. Med. Biol.* **46** 449–60

Baldock C, Rintoul L, Keevil S F, Pope J M and George G A 1998b Fourier transform Raman spectroscopy of polyacrylamide gel (PAGs) for radiation dosimetry *Phys. Med. Biol.* **43** 3617–27

Baldock C and Watson S 1999 Risk assessment for the manufacture of radiation dosimetry polymer gels *Proc. 1st Int. Workshop on Radiation Therapy Gel Dosimetry (Lexington, KY, USA)* ed L J Schreiner and C Audet pp 154–6

Bankamp A and Schad L R 2003 Comparison of TSE, TGSE, and CPMG measurement techniques for MR polymer gel dosimetry *Magn. Reson. Imaging* **21** 929–39

Baras P, Seimenis I, Sandilos P, Vlahos L, Bieganski T, Georgiou E, Pantelis E, Papagiannis P and Sakelliou L 2005 An evaluation of the TSE MR sequence for time efficient data acquisition in polymer gel dosimetry of applications involving high doses and steep dose gradients *Med. Phys.* **32** 3339–45

Baselga J, Hernández-Fuentes I, Piérola I F and Llorente M A 1987 Elastic properties of highly cross-linked polyacrylamide gels *Macromolecules* **20** 3060–65

Baselga J, Llorente M A, Hernández-Fuentes I and Piérola I F 1989 Polyacrylamide networks. Process of network formation *Eur. Polym. J.* **25** 477–80

Baselga J, Llorente M A, Nieto J L, Hernández-Fuentes I and Piérola I F 1988 Polyacrylamide networks. Sequence distribution of crosslinker *Eur. Polym. J.* **2** 161–5

Bausert I C, Oldham M, Smith T A D, Hayes C, Webb S and Leach M O 2000 Optimized MR imaging for polyacrylamide gel dosimetry *Phys. Med. Biol.* **45** 847–58

Baxter P, Jirasek A and Hilts M 2007 X-ray CT dose in normoxic polyacrylamide gel dosimetry *Med. Phys.* **34** 1934–43

Bayreder C, Georg D, Moser E and Berg A 2006 Basic investigations on the performance of a normoxic polymer gel with tetrakis-hydroxy-methyl-phosphonium chloride as an oxygen scavenger: reproducibility, accuracy, stability and dose rate dependence *Med. Phys.* **33** 2506–18

Bloembergen N, Purcell E M and Pound V 1948 Relaxation effects in nuclear magnetic resonance absorption *Phys. Rev.* **73** 679–712

Bohidar H B, Jena S S, Maity S and Saxena A 1998 Dielectric behaviour of gelatin solutions and gels *Colloid Polym. Sci.* **276** 81–6

Boni A L 1961 A polyacrylamide gamma dosimeter *Radiat. Res.* **14** 374–80

Bonnett D E, Farajollahi A J and Harding F P 1999 *Proc. 1st Int. Workshop on Radiation Therapy Gel Dosimetry (Lexington, KY, USA)* ed L J Schreiner and C Audet pp 142–5

Bosi S, Naseri P, Puran A, Davis J and Baldock C 2007 Initial investigation of a novel light-scattering gel phantom for evaluation of optical-CT scanners for radiotherapy gel dosimetry *Phys. Med. Biol.* **52** 2893–903

Bosi S G, Brown S, Sarabipour S, De Deene Y and Baldock C 2009a Modelling optical scattering artefacts for varying pathlength in a gel dosimeter phantom *Phys. Med. Biol.* **54** 275–83

Bosi S, Naseri P and Baldock C 2009b Light-scattering-induced artifacts in a complex polymer gel dosimetry phantom *Appl. Opt.* **48** 2427–34

Boudou C, Briston M C, Corde S, Adam J F, Ferrero C, Esteve F and Elleaume H 2004 Synchrotron stereotactic radiotherapy: dosimetry by Fricke gel and Monte Carlo simulations *Phys. Med. Biol.* **49** 5135–44

Bozena R 1999 A percolation approach to dye fluorescence quenching during the gelation process *J. Phys. B: At. Mol. Opt. Phys.* **32** 3463–8

Brandrup J, Immergut E H and Grulke E A 1999 *Polymer Handbook* 4th edn (New York: Wiley)

Braun K, Bailey D, Hill B and Baldock C 2009 Preliminary investigation of PAGAT polymer gel radionuclide dosimetry of Tc-99m *J. Phys.: Conf. Ser.* **164** 012050

Braun K, Brown S, Hill B, Bailey D and Baldock C 2007 Use of polymer gels for radionuclide dosimetry *Australas. Phys. Eng. Sci. Med.* **30** 63

Brindha S, Venning A J, Hill B and Baldock C 2004 Experimental study of attenuation properties of normoxic polymer gel dosimeters *Phys. Med. Biol.* **49** N353–61

Brown S, Venning A, De Deene Y, Vial P, Oliver L, Adamovics J and Baldock C 2008 Radiological properties of the PRESAGE and PAGAT polymer dosimeters *Appl. Radiat. Isot.* **66** 1970–4

Buxton G V, Greenstock C L, Helman W P and Ross A B 1988 Critical review of rate constants for reactions of hydrated electrons, hydrogen atoms and hydroxyl radicals ($^\bullet$OH/$^\bullet$O$^-$) in aqueous-solution *J. Phys. Chem. Ref. Data* **17** 513–886

Ceckler T L, Wolff S D, Yip V, Simon S A and Balaban R S 1992 Dynamic and chemical factors affecting water proton relaxation by macromolecules *J. Magn. Reson.* **98** 637–45

Chan M, Fung A Y C, Hu Y-C, Chui C-S, Amols H, Zaider M and Abramson D 2001 The measurement of three dimensional dose distribution of a ruthenium-106 ophthalmological applicator using magnetic resonance imaging of BANG polymer gels *J. Appl. Clin. Med. Phys.* **2** 85–9

Chapiro A 1962 *Radiation Chemistry of Polymeric Systems* (New York: Wiley)

Chernyshev A V, Soini A E, Surovtsev I V, Maltsev V P and Soini E 1997 A mathematical model of dispersion radical polymerization kinetics *J. Polym. Sci.* A **35** 1799–807

Conklin J, Deshpande R, Battista J and Jordan K 2008 Fast laser optical CT scanner with rotating mirror and Fresnel lenses *J. Phys.: Conf. Ser.* **56** 211–3

Cosgrove V P, Murphy P S, McJury M, Adams E J, Warrington A P, Leach M O and Webb S 2000 The reproducibility of polyacrylamide gel dosimetry applied to stereotactic conformal radiotherapy *Phys. Med. Biol.* **45** 1195–210

Courbon F, Love P, Chittenden S, Flux G, Ravel P and Cook G 2006 Preparation and use of I-131 MAGIC gel as a dosimeter for targeted radionuclide therapy *Cancer Biother. Radiopharm.* **21** 427–36

Crescenti R A, Bamber J C, Partridge M, Bush N L and Webb S 2007 Characterization of the ultrasonic attenuation coefficient and its frequency dependence in a polymer gel dosimeter *Phys. Med. Biol.* **52** 6747–59

Daoud 1987 Polymerization and aggregation during gelation *Kinetics of Nonhomogeneous Processes* ed G R Freeman (Alberta: Wiley) pp 651–723

Day M J and Stein G 1950 Chemical effects of ionizing radiation in some gels *Nature* **166** 146–7

De Deene Y 2002 Gel dosimetry for the dose verification of intensity modulated radiotherapy treatments *Med. Phys.* **12** 77–88

De Deene Y 2004a Fundamentals of MRI measurements for gel dosimetry *J. Phys.: Conf. Ser.* **3** 87–114

De Deene Y 2004b Essential characteristics of polymer gel dosimeters *J. Phys.: Conf. Ser.* **3** 34–57

De Deene Y 2006 On the accuracy and precision of gel dosimetry *J. Phys.: Conf. Ser.* **56** 72–85

De Deene Y and Baldock C 2002 Optimization of multiple spin–echo sequences for 3D polymer gel dosimetry *Phys. Med. Biol.* **47** 3117–41

De Deene Y and De Wagter C 2001 Artifacts in multi-echo T2 imaging for high-precision gel dosimetry: III. Effects of temperature drift during scanning *Phys. Med. Biol.* **46** 2697–711

De Deene Y, De Wagter C and Baldock C 2003 Comment on 'A systematic review of the precision and accuracy of dose measurements in photon radiotherapy using polymer and Fricke MRI gel dosimetry' *Phys. Med. Biol.* **48** L15–8

De Deene Y, De Wagter C, De Neve W and Achten E 2000a Artifacts in multi-echo T2 imaging for high-precision gel dosimetry: I. Analysis and compensation of eddy currents *Phys. Med. Biol.* **45** 1807–23

De Deene Y, De Wagter C and De Neve W 2000b Artifacts in multi-echo T2 imaging for high-precision gel dosimetry: II. Analysis of B1 field inhomogeneity *Phys. Med. Biol.* **45** 1825–39

De Deene Y, De Wagter C, Van Duyse B, Derycke S, De Neve W and Achten E 1998a Three-dimensional dosimetry using polymer gel and magnetic resonance imaging applied to the verification of conformal radiation therapy in head-and-neck cancer *Radiother. Oncol.* **48** 283–91

De Deene Y, De Wagter C, Van Duyse B, Derycke S, Mersseman B, De Gersem W, Voet T, Achten E and De Neve W 2000c Validation of MR-based polymer gel dosimetry as a preclinical three-dimensional verification tool in conformal radiotherapy *Magn. Reson. Med.* **43** 116–25

De Deene Y, Hanselaer P, De Wagter C, Achten E and De Neve W 2000d An investigation of the chemical stability of a monomer/polymer gel dosimeter *Phys. Med. Biol.* **45** 859–78

De Deene Y, Hurley C, Venning A, Vergote K, Mather M, Healy B J and Baldock C 2002a A basic study of some normoxic polymer gel dosimeters *Phys. Med. Biol.* **47** 3441–63

De Deene Y, Reynaert N and De Wagter C 2001a On the accuracy of monomer/polymer gel dosimetry in the proximity of a high-dose-rate ^{192}Ir source *Phys. Med. Biol.* **46** 2801–25

De Deene Y, Pittomvils G and Visalatchi S 2007a On the influence of the cooling rate at the accuracy of normoxic polymer gel dosimeters *Phys. Med. Biol.* **52** 2719–28

De Deene Y, Van de Walle R, Achten E and De Wagter C 1998b Mathematical analysis and experimental investigation of noise in quantitative magnetic resonance imaging applied in polymer gel dosimetry *Signal Process.* **70** 85–101

De Deene Y, Venning A, Hurley C, Healy B J and Baldock C 2002b Dose–response stability and integrity of the dose distribution of various polymer gel dosimeters *Phys. Med. Biol.* **47** 2459–70

De Deene Y, Vergote K, Claeys C and De Wagter C 2006a The fundamental radiation properties of normoxic polymer gel dosimeters: a comparison between a methacrylic acid based gel and acrylamide based gels *Phys. Med. Biol.* **51** 653–73

De Deene Y, Vergote K, Claeys C and De Wagter C 2006b Three dimensional radiation dosimetry in lung-equivalent regions by use of a radiation sensitive gel foam: proof of principle *Med. Phys.* **33** 2586–97

Del Gado E, de Arcangelis L and Coniglio A 1998 A percolation dynamic approach to the sol–gel transition *J. Phys. A: Math. Gen.* **31** 1901–10

De Wagter C 2004 The ideal dosimeter for intensity modulated radiation therapy (IMRT): what is required? *J. Phys.: Conf. Ser.* **3** 4–8

Doran S J 2008 The history and principles of optical computed tomography for scanning 3-D radiation dosimeters: 2008 update *DOSGEL 2008 5th Int. Conf. on Radiotherapy Gel Dosimetry (Hersonissos, Crete)*

Doran S J, Koerkamp K K, Bero M A, Jenneson P, Morton E J and Gilboy W B 2001 A CCD-based optical-CT scanner for high-resolution 3D-imaging of radiation dose distributions: equipment specifications, optical simulations and preliminary results *Phys. Med. Biol.* **46** 3191–213

Doran S J and Krstajic N 2006 The history and principles of optical computed tomography for scanning 3-D radiation dosimeters *J. Phys.: Conf. Ser.* **56** 45–57

DOSGEL 1999 *Proc. 1st Int. Workshop on Radiation Therapy Gel Dosimetry (Canadian Organization of Medical Physicists, Lexington, KY)* ed L J Schreiner and C Audet

DOSGEL 2001 *Proc. 2nd Int. Conf. on Radiation Therapy Gel Dosimetry (Queensland University of Technology, Brisbane, Australia)* ed C Baldock and Y De Deene

DOSGEL 2004 *Proc. 3rd Int. Conf. on Radiation Therapy Gel Dosimetry (Ghent University, Ghent, Belgium)* ed Y De Deene and C Baldock

DOSGEL 2006 *Proc. 4th Int. Conf. on Radiation Therapy Gel Dosimetry (Université de Sherbrooke, Sherbrooke, Canada)* ed M Lepage, A Jirasek and L J Schreiner

DOSGEL 2008 *Proc. 5th Int. Conf. on Radiation Therapy Gel Dosimetry (University of Crete, Greece)* ed T G Maris and E Pappas

Dumas E, Leclerc G and Lepage M 2006 Effect of container size on the accuracy of polymer gel dosimetry *J. Phys.: Conf. Ser.* **56** 239–41

Duthoy W, De Gersem W, Vergote K, Boterberg T, Derie C, Smeets P, De Wagter C and De Neve W 2004 Clinical implementation of intensity-modulated arc therapy (IMAT) for rectal cancer *Int. J. Radiat. Oncol. Biol. Phys.* **60** 794–806

Duthoy W, De Gersem W, Vergote K, Coghe M, Boterberg T, De Deene Y, De Wagter C, Van Belle S and De Neve W 2003 Whole abdominopelvic radiotherapy (WAPRT) using intensity-modulated arc therapy (IMAT): first clinical experience *Int. J. Radiat. Oncol. Biol. Phys.* **57** 1019–32

Edzes H T and Samulski E T 1978 The measurement of cross-relaxation effects in the proton NMR spin–lattice relaxation of water in biological systems: hydrated collagen and muscle *J. Magn. Reson.* **31** 207–29

Ertl A, Berg A, Zehetmayer M and Frigo P 2000 High-resolution dose profile studies based on MR imaging with polymer BANG gels in stereotactic radiation techniques *Magn. Reson. Imaging* **18** 343–9

Farajollahi A R, Bonnett D E, Ratcliffe A J, Aukett R J and Mills J A 1999 An investigation into the use of polymer gel dosimetry in low dose rate brachytherapy *Br. J. Radiol.* **72** 1085–92

Farajollahi A R, Bonnett D E, Tattam D and Green S 2000 The potential use of polymer gel dosimetry in boron neutron capture therapy *Phys. Med. Biol.* **45** N9-14

Fong P M, Keil D C, Does M D and Gore J C 2001 Polymer gels for magnetic resonance imaging of radiation dose distributions at normal room atmosphere *Phys. Med. Biol.* **46** 3105–13

Fragoso M, Love P A, Verhaegen F, Nalder C, Bidmead A M, Leach M and Webb S 2004 The dose distribution of low dose rate Cs-137 in intracavitary brachytherapy: comparison of Monte Carlo simulation, treatment planning calculation and polymer gel measurement *Phys. Med. Biol.* **49** 5459–74

Fricke H and Morse S 1927 The chemical action of Roentgen rays on dilute ferrous sulphate solutions as a measure of radiation dose *Am. J. Roentgenol. Radium Ther. Nucl. Med.* **18** 430–2

Fuxman A M, McAuley K B and Schreiner L J 2003 Modeling of free-radical crosslinking copolymerization of acrylamide and *N,N'*-methylene bis (acrylamide) for radiation dosimetry *Macromol. Theory Simul.* **12** 647–62

Fuxman A M, McAuley K B and Schreiner L J 2005 Modeling of polyacrylamide gel dosimeters with spatially non-uniform radiation dose distributions *Chem. Eng. Sci.* **60** 1277–93

Gambarini G, Collia, Gaya S, Petrovichc C, Pirolaa L and Rosid G 2004 In-phantom imaging of all dose components in boron neutron capture therapy by means of gel dosimeters *Appl. Radiat. Isot.* **61** 759–63

Gear J I, Charles-Edwards E, Partridge M and Flux G D 2007 A quality-control method for SPECT-based dosimetry in targeted radionuclide therapy *Cancer Biother. Radiopharm.* **22** 166–74

Gear J I, Flux G D, Charles-Edwards E, Partridge M, Cook G and Ott R J 2006 The application of polymer gel dosimeters to dosimetry for targeted radionuclide therapy *Phys. Med. Biol.* **51** 3503–16

Gelfi C and Righetti P G 1981a Polymerization kinetics of polyacrylamide gels: I. Effect of different cross-linkers *Electrophoresis* **2** 213–9

Gelfi C and Righetti P G 1981b Polymerization kinetics of polyacrylamide gels: I. Effect of temperature *Electrophoresis* **2** 220–8

Gochberg D F, Fong P M and Gore J C 2001 Studies of magnetization transfer and relaxation in irradiated polymer gels—interpretation of MRI-based dosimetry *Phys. Med. Biol.* **46** 799–811

Gochberg D F, Kennan R P, Maryanski M J and Gore J C 1998 The role of specific side groups and pH in magnetization transfer in polymers *J. Magn. Reson.* **131** 191–8

Gore J C, Kang Y S and Schulz R J 1984 Measurement of radiation dose distributions by nuclear magnetic resonance (NMR) imaging *Phys. Med. Biol.* **29** 1189–97

Gore J C, Ranade M, Maryanski M J and Schulz R J 1996 Radiation dose distributions in three dimensions from tomographic optical density scanning of polymer gels: I. Development of an optical scanner *Phys. Med. Biol.* **41** 2695–704

Grebe G, Pfaender M, Roll M and Luedemann L 2001 Dynamic arc radiosurgery and radiotherapy: commissioning and verification of dose distributions *Int. J. Radiat. Oncol. Biol. Phys.* **49** 1451–60

Gustavsson H, Bäck S Å J, Medin J, Grusell E and Olsson L E 2004 Linear energy transfer dependence of a normoxic polymer gel dosimeter investigated using proton beam absorbed dose measurements *Phys. Med. Biol.* **49** 3847–55

Gustavsson H, Karlsson A, Bäck S Å J, Olsson L E, Haraldsson P, Engström P and Nyström H 2003 MAGIC-type polymer gel for three-dimensional dosimetry: intensity-modulated radiation therapy verification *Med. Phys.* **30** 1264–71

Hafeli U O, Roberts W K, Meier D S, Ciezki J P, Pauer G J, Lee E J and Weinhous M S 2000 Dosimetry of a W-188/Re-188 beta line source for endovascular brachytherapy *Med. Phys.* **27** 668–75

Haraldsson P, Bäck S Å J, Magnusson P and Olsson L E 2000 Dose response characteristics and basic dose distribution data for a polymerization-based dosimeter gel evaluated using MR *Br. J. Radiol.* **73** 58–65

Harris P J, Piercy A R and Baldock C 1996 A method for determining the diffusion coefficient in Fe(II/III) radiation dosimetry gels using finite elements *Phys. Med. Biol.* **41** 1745–53

Heufelder J, Stiefel S, Pfaender M, Lüdemann L, Grebe G and Heese J 2003 Use of BANG polymer gel for dose measurements in a 68 MeV proton beam *Med. Phys.* **30** 1235–40

Hill B, Venning A J and Baldock C 2005a The dose response of normoxic polymer gel dosimeters measured using X-ray CT *Br. J. Radiol* **78** 623–30

Hill B, Venning A J and Baldock C 2005b A preliminary study of the novel application of normoxic polymer gel dosimeters for the measurement of CTDI on diagnostic x-ray CT scanners *Med. Phys.* **32** 1589–97

Hill B, Venning A J and Baldock C 2008 Polymer gel dosimetry on a multislice computed tomography scanner: effect of changing parameters on CTDI *Physica Medica* **24** 149–58

Hilts M 2006 X-ray computed tomography imaging of polymer gel dosimeters *J. Phys.: Conf. Ser.* **56** 95–107

Hilts M, Audet C, Duzenli C and Jirasek A 2000 Polymer gel dosimetry using x-ray computed tomography: a feasibility study *Phys. Med. Biol.* **45** 2559–71

Hilts M and Duzenli C 2004 Image filtering for improved dose resolution in CT polymer gel dosimetry *Med. Phys.* **31** 39–49

Hilts M and Jirasek A 2008 Adaptive mean filtering for noise reduction in CT polymer gel dosimetry *Med. Phys.* **35** 344–55

Hilts M, Jirasek A and Duzenli C 2004 Effects of gel composition on the radiation induced density change in PAG polymer gel dosimeters: a model and experimental investigations *Phys. Med. Biol.* **49** 2477–90

Hilts M, Jirasek A and Duzenli C 2005 Technical considerations for implementation of x-ray CT polymer gel dosimetry *Phys. Med. Biol.* **50** 1727–45

Hsieh J 2003 *Computed Tomography: Principles, Design, Artifacts and Recent Advances* (Bellingham, WA: SPIE Optical Engineering Press) p 387

Hoecker F E and Watkins I W 1958 Radiation polymerization dosimetry *Int. J. Appl. Radiat. Isot.* **3** 31–5

Huang H and Sorensen C M 1996 Shear effects during the gelation of aqueous gelatine *Phys. Rev.* E **53** 5075–8

Hurley C, De Deene Y, Meder R, Pope M J and Baldock C 2003 The effect of water molecular self-diffusion on quantitative high-resolution MRI polymer gel dosimetry *Phys. Med. Biol.* **48** 3043–58

Hurley C, McLucas C, Pedrazzini G and Baldock C 2006 High-resolution gel dosimetry of a HDR brachytherapy source using normoxic polymer gel dosimeters: preliminary study *Nucl. Instrum. Methods Phys. Res.* A **565** 801–11

Hurley C, Venning A and Baldock C 2005 A study of a normoxic polymer gel dosimeter comprising methacrylic acid, gelatin and tetraxis (hydroxymethyl) phosphonium chloride (MAGAT) *Appl. Radiat Isot.* **63** 443–56

Ibbott G S, Maryanski M J, Eastman P, Holcomb S D, Zhang Y, Avison R G, Sanders M and Gore J C 1997 Three-dimensional visualization and measurement of conformal dose distributions using magnetic resonance imaging of BANG polymer gel dosimeters *Int. J. Radiat. Oncol. Biol. Phys.* **38** 1097–103

ICRU 1987 Use of Computers in External Bean Radiotherapy Procedures with High-Energy Photons and Electrons *ICRU Report No 42* (Bethesda, MD: ICRU)

Islam K T S, Dempsey J F, Ranade M, Maryanski M J and Low D A 2003 Initial evaluation of commercial optical-CT-based 3D gel dosimeter *Med. Phys.* **30** 2159–68

Jiang S B, Sharp G C, Neicu T, Berbeco R I, Flampouri S and Bortfeld T 2006 On dose distribution comparison *Phys. Med. Biol.* **51** 759–76

Jirasek A I, Duzenli C, Audet C and Eldridge J 2001a Characterization of monomer/crosslinker consumption and polymer formation observed in FT-Raman spectra of irradiated polyacrylamide gels *Phys. Med. Biol.* **46** 151–65

Jirasek A I and Duzenli C 2001b Effects of crosslinker fraction in polymer gel dosimeters using FT Raman spectroscopy *Phys. Med. Biol.* **46** 1949–61

Jirasek A I and Duzenli C 2002 Relative effectiveness of polyacrylamide gel dosimeters applied to proton beams: Fourier transform Raman observations and track structure calculations *Med. Phys.* **29** 569–77

Jirasek A, Hilts M, Berman A and McAuley K B 2009 Effects of glycerol co-solvent on the rate and form of polymer gel dose response *Phys. Med. Biol.* **54** 907–18

Jirasek A, Hilts M, Shaw C and Baxter P 2006a Investigation of tetrakis hydroxymethyl phosphonium chloride as an antioxidant for use in x-ray computed tomography polyacrylamide gel dosimetry *Phys. Med. Biol.* **51** 1891–906

Jirasek A, Matthews Q, Hilts M, Schulze G, Blades M W and Turner R F B 2006b Investigation of a 2D two-point maximum entropy regularization method for signal-to-noise ratio enhancement: application to CT polymer gel dosimetry *Phys. Med. Biol.* **51** 2599–617

Karaiskos P *et al* 2005 Dose verification of single shot gamma knife applications using VIPAR polymer gel and MRI *Phys. Med. Biol.* **50** 1235–50

Karlsson A, Gustavsson H, Månsson S, McAuley K B and Bäck S Å J 2007 Dose integration characteristics in normoxic polymer gel dosimetry investigated using sequential beam irradiation *Phys. Med. Biol.* **52** 4697–706

Keall P J and Baldock C 1999 A theoretical study of the radiological properties and water equivalence of Fricke and polymer gels used for radiation dosimetry *Australas. Phys. Eng. Sci. Med.* **22** 85–91

Keles H, Celik M, Sacak M and Aksu L 1999 Graft copolymerization of methyl methacrylate upon gelatin initiated by benzoyl peroxide in aqueous medium *J. Appl. Polym. Sci.* **74** 1547–56

Kelly R G, Jordan K J and Battista J J 1998 Optical-CT reconstruction of 3D dose distributions using the ferrous-benzoic-xylenol (FBX) gel dosimeter *Med. Phys.* **25** 1741–50

Kennan R P, Maryanski M J, Zhong J and Gore J C 1992 Hydrodynamic effects and cross relaxation in cross linked polymer gels *Proc. Int. Soc. for Magnetic Resonance in Medicine (New York)*

Kennan R P, Richardson K A, Zhong J, Maryanski M J and Gore J C 1996 The effects of cross-link density and chemical exchange on magnetization transfer in polyacrylamide gels *J. Magn. Reson.* B **110** 267–77

Kim C J and Hamielec A E 1984 Polymerization of acrylamide with diffusion-controlled termination *Polymer* **25** 845–9

Kipouros P, Papagiannis P, Sakelliou L, Karaiskos P, Sandilos P, Baras P, Seimenis I, Kozicki M, Anagnostopoulos G and Baras D 2003 3D dose verification in Ir-192 HDR prostate monotherapy using polymer gels and MRI *Med. Phys.* **30** 2031–9

Koeva V I, Csaszar E S, Senden R J, McAuley K B and Schreiner L J 2008 Polymer gel dosimeters with increased solubility: a preliminary investigation of the NMR and optical dose–response using different crosslinkers and co-solvents *Macromol. Symp.* **261** 157–66

Koeva V I, Olding T, Jirasek A, Schreiner L J and McAuley K B 2009 Preliminary investigation of the NMR, optical and x-ray CT dose–response of polymer gel dosimeters incorporating cosolvents to improve dose sensitivity *Phys. Med. Biol.* **54** 2779–90

Kozicki M, Filipczak K and Rosiak J M 2003 Reactions of hydroxyl radicals, H atoms and hydrated electrons with Bis in aqueous solution: a pulse radiolysis study *Radiat. Phys. Chem.* **68** 827–35

Kozicki M, Kujawa P and Rosiak J M 2002 Pulse radiolysis study of diacrylate macromonomer in aqueous solution *Radiat. Phys. Chem.* **65** 133–9

Kron T, Jonas D and Pope J 1997 Fast T1 imaging of gel samples for diffusion measurements in NMR dosimetry gels *Magn. Reson. Imaging* **15** 211–21

Krstajic N and Doran S 2006 Focusing optics of a parallel beam CCD optical tomography apparatus for 3D radiation gel dosimetry *Phys. Med. Biol.* **51** 2055–75

Krstajic N and Doran S 2007 Fast laser scanning optical-CT apparatus for 3D radiation dosimetry *Phys. Med. Biol.* **52** N257–63

Lepage M, Jayasakera P M, Back S A and Baldock C 2001a Dose resolution optimization of polymer gel dosimeters using different monomers *Phys. Med. Biol.* **46** 2665–80

Lepage M, McMahon K, Galloway G J, De Deene Y, Back S A J and Baldock C 2002 Magnetization transfer imaging for polymer gel dosimetry *Phys. Med. Biol.* **47** 1881–90

Lepage M, Tofts P S, Bäck S A J, Jayasekera P M and Baldock C 2001b Simple methods for the correction of T2 maps of phantoms *Magn. Reson. Med.* **46** 1123–9

Lepage M, Whittaker A K, Rintoul L, Back S A and Baldock C 2001c The relationship between radiation-induced chemical processes and transverse relaxation times in polymer gel dosimeters *Phys. Med. Biol.* **46** 1061–74

Lepage M, Whittaker A K, Rintoul L and Baldock C 2001d 13C-NMR, 1H-NMR, and FT-Raman study of radiation-induced modifications in radiation dosimetry polymer gels *J. Appl. Polym. Sci.* **79** 1572–81

Lepage M, Whittaker A K, Rintoul L, Bäck S A J and Baldock C 2001e Modelling of post-irradiation events in polymer gel dosimeters *Phys. Med. Biol.* **46** 2827–39

Lopatiuk-Tirpak O, Langen K M, Meeks S L, Kupelian P A, Zeidan O A and Maryanski M J 2008 Performance evaluation of an improved optical computed tomography polymer gel dosimeter system for 3D dose verification of static and dynamic phantom deliveries *Med. Phys.* **35** 3447–59

Love P A, Evans P M, Leach M O and Webb S 2003 Polymer gel measurement of dose homogeneity in the breast: comparing MLC intensity modulation with standard wedged delivery *Phys. Med. Biol.* **48** 1065–74

Low D A and Dempsey J F 2003 Evaluation of the gamma dose distribution comparison method *Med. Phys.* **30** 2455–64

Low D A, Dempsey J F, Venkatesan R, Mutic S, Markman J, Haacke E M and Purdy J A 1999 Evaluation of polymer gels and MRI as a 3-D dosimeter for intensity-modulated radiation therapy *Med. Phys.* **26** 1542–51

Low D A, Harms W B, Mutic S and Purdy J A 1998 A technique for the quantitative evaluation of dose distributions *Med. Phys.* **25** 656–61

MacDougall N D, Pitchford W G and Smith M A 2002 A systematic review of the precision and accuracy of dose measurements in photon radiotherapy using polymer and Fricke MRI gel dosimetry *Phys. Med. Biol.* **47** R107–21

Mackie A R, Gunning A P, Ridout M J and Morris V J 1998 Gelation of gelatin observation in the bulk and in the air–water interface *Biopolymers* **46** 245–52

Magee J L and Chatterjee A 1987 Track reactions of radiation chemistry *Kinetics of Nonhomogeneous Processes* ed G R Freeman (New York: Wiley) chapter 4

Månsson S, Karlsson A, Gustavsson H, Christensson J and Bäck S Å J 2006 Dosimetric verification of breathing adapted radiotherapy using polymer gel *J. Phys.: Conf. Ser.* **56** 300–3

Maquet J, Théveneau H, Djabourov M, Leblond J and Papon P 1986 State of water in gelatin solutions and gels: an ^{1}H NMR investigation *Polymer* **27** 1103–10

Maryanski M J, Audet C and Gore J C 1997 Effects of crosslinking and temperature on the dose response of a BANG polymer gel dosimeter *Phys. Med. Biol.* **42** 303–11

Maryanski M J, Gore J C, Kennan R P and Schulz R J 1993 NMR relaxation enhancement in gels polymerized and cross-linked by ionizing radiation: a new approach to 3D dosimetry by MRI *Magn. Reson. Imaging* **11** 253–8

Maryanski M J, Gore J C and Schulz R J 1992 3-D radiation dosimetry by MRI: solvent proton relaxation enhancement by radiation-controlled polymerisation and cross-linking in gels *Proc. Int. Soc. for Magnetic Resonance in Medicine (New York)*

Maryanski M J, Schulz R J and Gore J C 1994a Three dimensional detection, dosimetry and imaging of an energy field by formation of a polymer in a gel *US Patent* No. 5,321,357

Maryanski M J, Schulz R J, Ibbott G S, Gatenby J C, Xie J, Horton D and Gore J C 1994b Magnetic resonance imaging of radiation dose distributions using a polymer-gel dosimeter *Phys. Med. Biol.* **39** 1437–55

Maryanski M J, Zastavker Y Z and Gore J C 1996 Radiation dose distributions in three dimensions from tomographic optical density scanning of polymer gels: II. Optical properties of the BANG polymer gel *Phys. Med. Biol.* **41** 2705–17

Mather M L and Baldock C 2003 Ultrasound tomography imaging of radiation dose distributions in polymer gel dosimeters: preliminary study *Med. Phys.* **30** 2140–8

Mather M L, Charles P H and Baldock C 2003a Measurement of ultrasonic attenuation coefficient in polymer gel dosimeters *Phys. Med. Biol.* **48** N269–75

Mather M L, Collings A F, Bajenov N, Whittaker A K and Baldock C 2003b Ultrasonic absorption in polymer gel dosimeters *Ultrasonics* **41** 551–9

Mather M L, De Deene Y, Whitakker A K, Simon G P, Rutgers R and Baldock C 2002a Investigation of ultrasonic properties of PAG and MAGIC polymer gel dosimeters *Phys. Med. Biol.* **47** 4397–409

Mather M L, Whitakker A K and Baldock C 2002b Ultrasound evaluation of polymer gel dosimeters *Phys. Med. Biol.* **47** 1449–58

McJury M, Oldham M, Cosgrove V P, Murphy P S, Doran S, Leach M O and Webb S 2000 Radiation dosimetry using polymer gels: methods and applications *Br. J. Radiol.* **73** 919–29

McJury M, Tapper P D, Cosgrove V P, Murphy P S, Griffin S, Leach M O, Webb S and Oldham M 1999 Experimental 3D dosimetry around a high-dose-rate clinical ^{192}Ir source using a polyacrylamide gel (PAG) dosimeter *Phys. Med. Biol.* **44** 2431–44

Meeks S L, Bova F J, Maryanski M J, Kendrick L A, Ranade M K, Buatti J M and Friedman W A 1999 Image registration of BANG gel dose maps for quantitative dosimetry verification *Int. J. Radiat. Oncol. Biol. Phys.* **43** 1135–41

Michael G J, Henderson C J, Nitschke K and Baldock C 2000 Effects of glass and backscatter on measurement of absorbed dose in polyacrylamide gel (PAG) dosimeters *Phys. Med. Biol.* **45** N133–8

Narten A H, Danford M D and Levy H A 1967 X-ray diffraction study of liquid water in the temperature range 4–200 °C *Faraday Discuss.* **43** 97–107

Nieto J L, Baselga J, Hernandez-Fuentes I, Llorente M A and Piérola I F 1987 Polyacrylamide networks: kinetic and structural studies by high-field ^{1}H-NMR with polymerization *in situ Eur. Polym. J.* **23** 551–5

Novotny J Jr, Dvorak P, Spevacek V, Tintera J, Novotny J, Cechak T and Liscak R 2002 Quality control of the stereotactic radiosurgery procedure with the polymer-gel dosimetry *Radiother. Oncol.* **63** 223–30

Novotny J Jr, Spevacek V, Dvorak P, Novotny J and Cechak T 2001 Energy and dose rate dependence of BANG-2 polymer-gel dosimeters *Med. Phys.* **28** 2379–86

Okay O, Naghash H J and Capek I 1995 Free-radical crosslinking copolymerization: effect of cyclization on diffusion-controlled termination at low conversion *Polymer* **36** 2413–9

Oldham M 2006 Optical CT 3D dosimetry by optical-CT scanning *J. Phys.: Conf. Ser.* **56** 58–71

Oldham M, Baustert I, Lord C, Smith T A D, McJury M, Warrington A P, Leach M O and Webb S 1998 An investigation into the dosimetry of a nine-field tomotherapy irradiation using BANG-gel dosimetry *Phys. Med. Biol.* **43** 1113–32

Oldham M and Kim L 2004 Optical-CT-gel dosimetry: II. Optical artifacts and geometric distortion *Med. Phys.* **31** 1093–104

Oldham M, Siewerdsen J H, Kumar S, Wong J and Jaffray D A 2003 Optical-CT gel dosimetry I: basic investigations *Med. Phys.* **30** 623–34

Oldham M, Siewerdsen J H, Shetty A and Jaffray D A 2001 High resolution gel-dosimetry by optical-CT and MR scanning *Med. Phys.* **28** 1436–45

Olsson L E, Fransson A, Ericsson A and Mattsson S 1990 MR imaging of absorbed dose distributions for radiotherapy using ferrous sulphate gels *Phys. Med. Biol.* **35** 1623–31

Olsson L E, Westrin B A, Fransson A and Nordell B 1992 Diffusion of ferric ions in agarose dosimeter gels *Phys. Med. Biol.* **37** 2243–52

Panajkar M S, Guha S N and Copinathan C 1995 Reactions of hydrated electron with *N,N′*-methylenebisacrylamide in aqueous solution—a pulse radiolysis study *J. Macromol. Sci.* A **32** 143–56

Pantelis E, Karlis A K, Kozicki M, Papagiannis P, Sakelliou L and Rosiak J M 2004 Polymer gel water equivalence and relative energy response with emphasis on low photon energy dosimetry in brachytherapy *Phys. Med. Biol.* **49** 3495–514

Papagiannis P, Karaiskos P, Kozicki M, Rosiak J M, Sakelliou L, Sandilos P, Seimenis I and Torrens M 2005 Three-dimensional dose verification of the clinical application of gamma knife stereotactic radiosurgery using polymer gel and MRI *Phys. Med. Biol.* **50** 1979–90

Papagiannis P, Pappas E, Kipouros P, Angelopoulos A, Sakelliou L, Baras P, Karaiskos P, Seimenis I, Sandilos P and Baltas D 2001 Dosimetry close to an Ir-192 HDR source using *N*-vinylpyrrolidone based polymer gels and magnetic resonance imaging *Med. Phys.* **28** 1416–26

Pappas E, Maris T G, Angelopoulos A, Paparigopoulou M, Sakelliou L, Sandilos P, Voyiatzi S and Vlachos L 1999 A new polymer gel for magnetic resonance imaging (MRI) radiation dosimetry *Phys. Med. Biol.* **44** 2677–84

Pappas E, Seimenis I, Angelopoulos A, Georgolopoulou P, Kamariotaki Paparigopoulou M, Maris T, Sakelliou L, Sandilos P and Vlachos L 2001 Narrow stereotactic beam profile measurements using *N*-vinylpyrrolidone based polymer gels and magnetic resonance imaging *Phys. Med. Biol.* **46** 783–97

Ramm U, Weber U, Bock M, Kramer M, Bankamp A, Damrau M, Thilmann C, Bottcher H D, Schad L R and Kraft G 2000 Three-dimensional BANG gel dosimetry in conformal carbon ion radiotherapy *Phys. Med. Biol.* **45** N95–102

Rintoul L, Lepage M and Baldock C 2003 Radiation dose distribution in polymer gels by Raman spectroscopy *Appl. Spectrosc.* **57** 51–7

Safrani M and Wojnarovits L 1993 Radiolysis of hydroxyl ethylacrylate in dilute aqueous solutions *Radiat. Phys. Chem.* **41** 531–7

Sakhalkar H, Adamovics J, Ibbott G and Oldham M 2009 A comprehensive evaluation of the PRESAGE/optical-CT 3D dosimetry system *Med. Phys.* **36** 71–82

Sakhalkar H S and Oldham M 2008 Fast, high-resolution 3D dosimetry utilizing a novel optical-CT scanner incorporating tertiary telecentric collimation *Med. Phys.* **35** 101–11

Salomons G J, Park S P, McAuley K B and Schreiner L J 2002 Temperature increases associated with polymerization of irradiated PAG dosimeters *Phys. Med. Biol.* **47** 1435–48

Sandilos P *et al* 2004 Dose verification in clinical IMRT prostate incidents *Int. J. Radiation Oncology Biol. Phys.* **59** 1540–7

Sandilos P, Baras P, Georgiou E, Dardoufas K, Karaiskos P, Papagiannis P, Paschalis T, Tatsis E, Torrens M and Vlahos L 2006 Fast, three-dimensional, MR imaging for polymer gel dosimetric applications involving high-dose and steep dose gradients *Nucl. Instrum. Methods Phys. Res.* A **569** 572–6

Sarabipour S, Bosi S, Hill B and Baldock C 2006 A preliminary study of the measurement of slice-width dose profiles (SWDP) on diagnostic x-ray CT scanners using PAGAT polymer gel dosimeters with optical CT read-out *J. Phys.: Conf. Ser.* **56** 280–2

Scheib S G and Gianolini S 2002 Three-dimensional dose verification using BANG gel: a clinical example *J. Neurosurg.* **97** 582–7

Schreiner L J 2006 Dosimetry in modern radiation therapy: limitations and needs *J. Phys.: Conf. Ser.* **56** 1–13

Senden R J, De Jean P, McAuley K B and Schreiner L J 2006 Polymer gel dosimeters with reduced toxicity: a preliminary investigation of the NMR and optical dose–response using different monomers *Phys. Med. Biol.* **51** 3301–14

Spevacek V, Novotny J Jr, Dvorak P, Novotny J, Vymazal J and Cechak T 2001 Temperature dependence of polymer-gel dosimeter nuclear magnetic resonance response *Med. Phys.* **28** 2370–8

Spinks J W T and Woods R J 1964 *An Introduction to Radiation Chemistry* (New York: Wiley)

Stejskal J, Strakova D and Kratochvil P 1988 Grafting of gelatin during polymerization of methyl methacrylate in aqueous medium *J. Appl. Polym. Sci.* **36** 215–27

Swallow A J 1973 *Radiation Chemistry: An Introduction* (London: Longman)

Tarte B and van Doorn T 1993 Optical scanning of ferrous sulphate gels for radiotherapy treatment dosimetry *Proc. ACPSEM/BECON 93*

Tarte B and van Doorn T 1995 Laser base tomographic scanning of gel volumes for applications in ionising radiation dosimetry *Proc. 10th Conf. of Australian Optical Society*

Tobita H and Hamielec A E 1990 Crosslinking kinetics in polyacrylamide networks *Polymer* **31** 1546–52

Tobita H and Hamielec A E 1992 Control of network structure in free radical crosslinking copolymerization *Polymer* **33** 3647–57

Trapp J V, Back S A J, Lepage M, Michael G and Baldock C 2001a An experimental study of the dose response of polymer gel dosimeters imaged with x-ray computed tomography *Phys. Med. Biol.* **46** 2939–51

Trapp J V, Michael G and Baldock C 2001b Theoretical considerations of scan parameters appropriate for CT imaging of polymer gel dosimeters *DOSGEL 2001 Proc. 2nd Int. Conf. on Radiation Therapy Gel Dosimetry (Queensland University of Technology, Brisbane, Australia)* ed C Baldock and Y De Deene

Trapp J V, Michael G, De Deene Y and Baldock C 2002 Attenuation of diagnostic energy photons by polymer gel dosimeters *Phys. Med. Biol.* **47** 4247–58

Uusi-Simola J, Heikkinen S, Kotiluoto P, Serén T, Seppälä T, Auterinen L and Savolainen S 2007 MAGIC polymer gel dosimetric verification in boron neutron capture therapy *J. Appl. Clin. Med. Phys.* **8** 114–23

Uusi-Simola J et al 2003 Study of the relative dose–response of BANG-3® polymer gel dosimeters in epithermal neutron irradiation *Phys. Med. Biol.* **48** 2895–906

Van Doorn T, Bhat M, Rutten T P, Tran T and Costanzo A 2005 A fast, high spatial resolution optical tomographic scanner for measurement of absorption in gel dosimetry *Australas. Phys. Eng. Sci. Med.* **28** 76–85

Wai P, Adamovics J, Krstajic N, Ismail A, Nisbet A and Doran S 2009 Dosimetry of the microSelection-HRD Ir-192 source using PRESAGE™ and optical CT *Appl. Radiat. Isotopes* **67** 419–22

Venning A J, Healy B J, Nitschke K N and Baldock C 2005b Investigation of the MAGAS polymer gel dosimeter with Pyrex glass walls for clinical radiotherapy dosimetry *Nucl. Instrum. Methods Phys. Res.* A **555** 396–402

Venning A J, Hill B, Brindha S, Healy B J and Baldock C 2005a Investigation of the PAGAT polymer gel dosimeter using magnetic resonance imaging *Phys. Med. Biol.* **50** 3875–88

Venning A J, Nitschke K N, Keall P J and Baldock C 2005c Radiological properties of normoxic polymer gel dosimeters *Med. Phys.* **32** 1047–52

Vergote K, De Deene Y, Claus F, De Gersem W, Van Duyse B, Paelinck L, Achten E, De Neve W and De Wagter C 2003 Application of monomer/polymer gel dosimetry to study the effects of tissue inhomogeneities on intensity-modulated radiation therapy (IMRT) dose distributions *Radiother. Oncol.* **67** 119–28

Vergote K, De Deene Y, Duthoy W, De Gersem W, De Neve W and Achten E 2004a Validation and application of polymer gel dosimetry for the dose verification of an intensity-modulated arc therapy (IMAT) treatment *Phys. Med. Biol.* **49** 287–305

Vergote K, De Deene Y, Vanden Bussche E and De Wagter C 2004b On the relation between the spatial dose integrity and the temporal instability of polymer gel dosimeters *Phys. Med. Biol.* **49** 4507–22

Venning A, Brindha S, Hill B and Boldeck C 2004 Study of a normoxic PAG gel dosimeter with tetrakis (hydroxymethyl) phosphonium chloride as an anti-oxidant *Med. Phys.* **31** (*46th Ann. Meeting of the AAPM*) 1918

Ward A G 1977 *The Science and Technology of Gelatin* (London: Academic)

Watanabe Y, Perera G M and Mooij R B 2002 Image distortion in MRI-based polymer gel dosimetry of Gamma Knife stereotactic radiosurgery systems *Med. Phys.* **29** 797–802

Weiss N and Silberberg A 1977 Inhomogeneity of polyacrylamide gel structure from permeability and viscoelasticity *Br. Polym. J.* 144–50

Whitney H M, Gochberg D F and Gore J C 2008 Magnetization transfer proportion: a simplified measure of dose response for polymer gel dosimetry *Phys. Med. Biol.* **53** 7107–24

Whittaker A K 2001 A discussion of the factors influencing the polymerization processes in polymer gel dosimeters *Proc. 2nd Int. Conf. on Radiotherapy Gel Dosimetry (QUT, Brisbane, Australia)* ed C Baldock and Y De Deene pp 23–30

Woessner D E 1962 Nuclear spin relaxation in ellipsoids undergoing rotational Brownian motion *J. Chem. Phys.* **37** 647–54

Wojnecki C and Green S 2001 A computational study into the use of polyacrylamide gel and A-150 plastic as brain substitutes for boron neutron capture therapy *Phys. Med. Biol.* **46** 1399–405

Wolodzko J G, Marsden C and Appleby A 1999 CCD imaging for optical tomography of gel radiation dosimeters *Med. Phys.* **26** 2508–13

Wuu C-S, Schiff P, Maryanski M J, Liu T, Borzillary S and Weinberger J 2003 Dosimetry study of Re-188 liquid balloon for intravascular brachytherapy using polymer gel dosimeters and laser-beam optical-CT scanner *Med. Phys.* **30** 132–7

Xu Y and Wuu C-S 2004 Performance of a commercial optical-CT scanner and polymer gel dosimeters for 3D dose verification *Med. Phys.* **31** 3024–33

Xu Y, Wuu C S and Maryanski M J 2003 Determining optimal gel sensitivity in optical-CT scanning of gel dosimeters *Med. Phys.* **30** 2257–63

Zimmerman J R and Brittin W E 1957 Nuclear magnetic resonance studies in multiple phase systems: lifetime of a water molecule in an adsorbing phase on silica gel *J. Phys. Chem.* **61** 1328